POLITECNICO
MILANO 1863

SCUOLA DI INGEGNERIA INDUSTRIALE
E DELL'INFORMAZIONE

Innovative SMA actuator for space applications: study of torsional antagonistic configuration

TESI DI LAUREA MAGISTRALE IN
SPACE ENGINEERING - INGEGNERIA SPAZIALE

Author: **Luisa Gaddi**

Student ID: 10863364
Advisor: Paolo Bettini
Co-advisor: Elena Villa
Tiziana Biasutti
Emanuele Casciaro
Academic Year: 2022-23

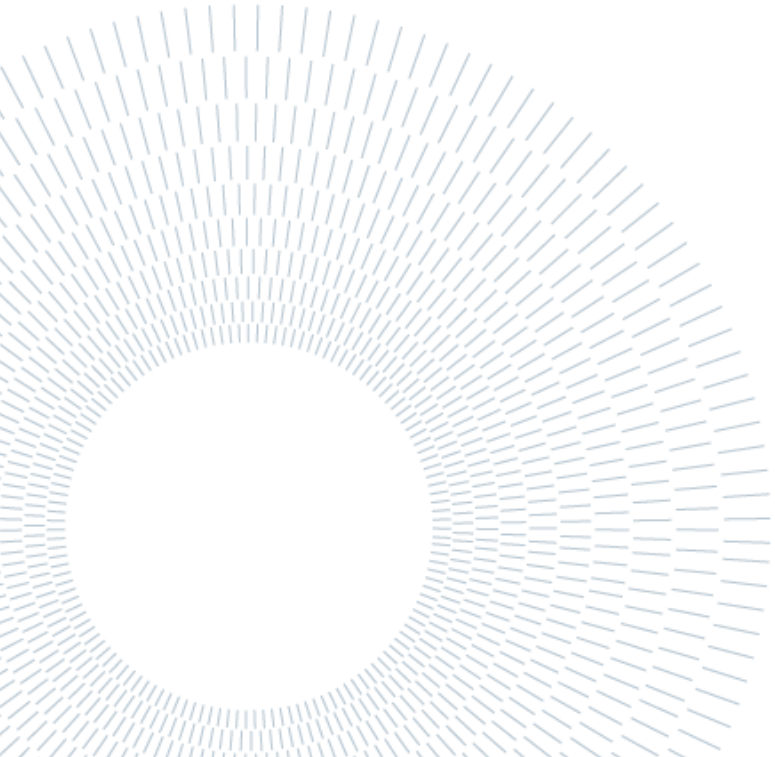

Ai miei nonni.

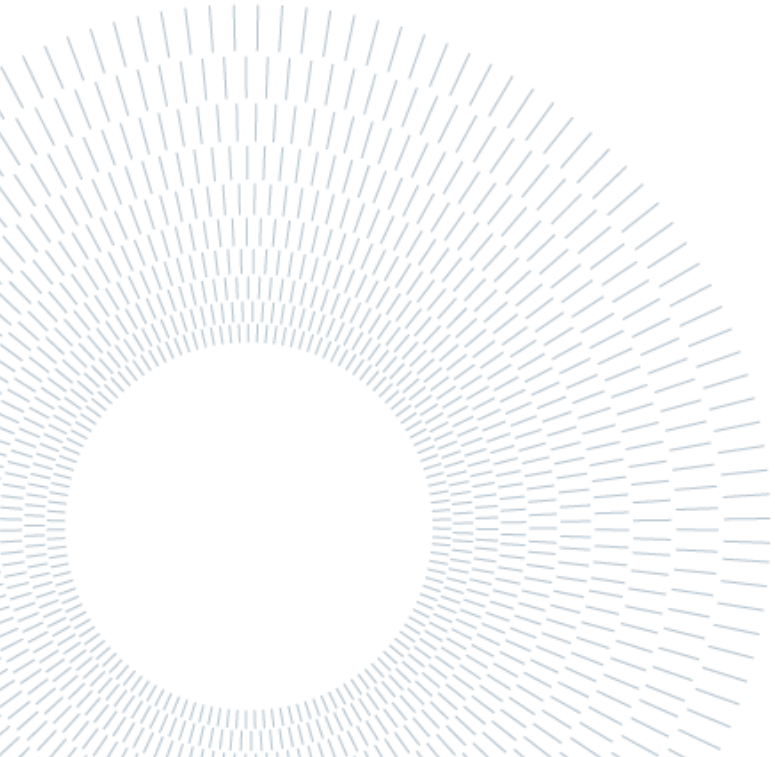

Abstract

The trend in the space sector to increasingly reduce the size and mass of satellites and their subsystems has led to the exploration and adoption of innovative solutions and the use of materials different from those commonly employed in space, including Shape Memory Alloys (SMAs). Considering the ongoing research into new SMA applications in space, this thesis aims at designing a torsional actuator that utilizes antagonism as a rearming method through two SMA tubes. By activating one of the two tubes, this recovers a previously imposed rotation, thereby arming the other tube, to which it is appropriately connected. Antagonism guarantees tubes' reciprocal rearm, thus multiple actuation: this makes the actuator suitable for actual use in a space application, such as a hinge for a CubeSat panel. The development of the thesis can be divided into four main phases: initial theoretical study on the material's properties followed by the conception of the actuator; experimental torsional characterization, particularly significative given the scarse presence of such studies in existing literature; design and implementation of the experimental setup; test campaign and analysis of the results. In the final experiment, the whole setup has been cooled in the MTS enviromental chamber, and the tubes have been alternatively heated through Joule effect. The cycling has been carried out for a considerable amount of cycles to monitor the trend in the recovered rotation, and to demonstrate the validity of the torsional antagonistic rearm.

Key-words: Shape Memory Alloys, torsional actuator, antagonistic characterization, SMA tubes, CubeSat

Sommario

La tendenza in ambito spaziale a ridurre in modo sempre più decisivo la dimensione e la massa dei satelliti e dei loro sottosistemi, ha condotto verso la ricerca l'adozione di soluzioni innovative e l'utilizzo di materiali diversi da quelli comunemente utilizzati in ambito spaziale, tra cui le Leghe a Memoria di Forma. Considerando la continua ricerca di nuove applicazioni SMA in ambito spaziale, questa tesi si pone l'obiettivo di ideare un attuatore torsionale che sfrutti l'antagonismo come metodo di riarmo utilizzando due tubi SMA. Attivando uno dei due tubi, questo recupera una rotazione precedentemente imposta, armando di conseguenza l'altro tubo, al quale è appropriatamente connesso. L'antagonismo garantisce il riarmo reciproco dei tubi, consentendo così numerose attuazioni: ciò rende l'attuatore adatto all'uso effettivo in un'applicazione spaziale, come una cerniera per un pannello CubeSat. Lo sviluppo della tesi può essere suddiviso in quattro fasi principali: studio teorico iniziale sulle caratteristiche del materiale seguito dalla concezione dell'idea di attuatore; caratterizzazione sperimentale torsionale, particolarmente significativa data la scarsa presenza di tali studi in letteratura; ideazione e realizzazione del setup sperimentale; test sperimentali e analisi dei risultati. Nell'esperimento finale, l'intero setup è stato raffreddato nella camera ambientale MTS, e i tubi sono stati riscaldati alternativamente mediante effetto Joule. Il ciclaggio è stato eseguito per un considerevole numero di cicli per monitorare la tendenza nella rotazione recuperata e dimostrare la validità del riarmo torsionale antagonista.

Parole chiave: Leghe a memoria di forma, Attuatore torsionale, Caratterizzazione in antagonismo, Tubi SMA, CubeSat

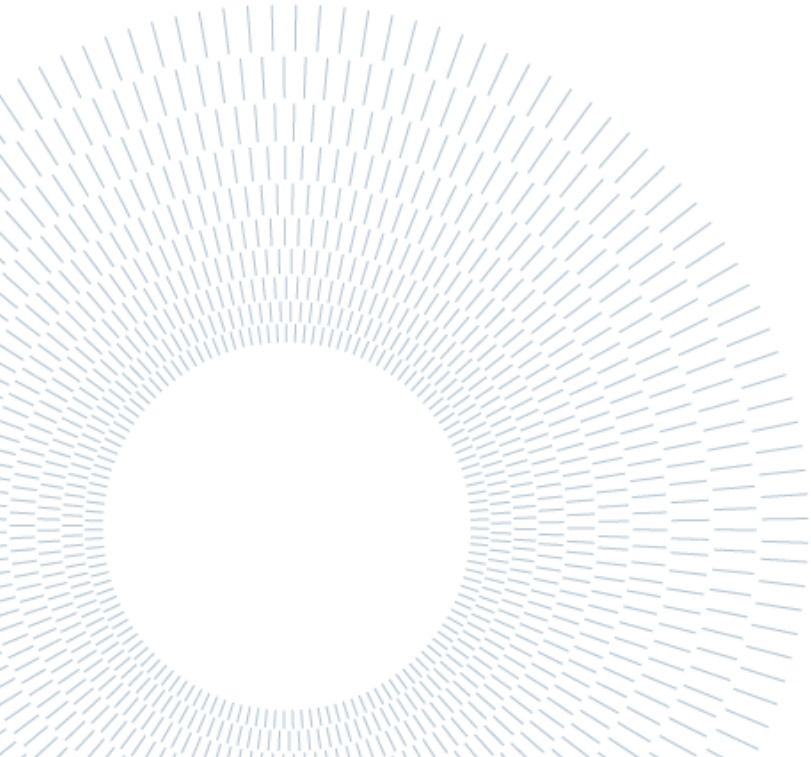

Contents

Introduction

The analysis of the development that the space sector experienced in the last years makes it evident that a broader range of entities came in contact and enter the space industry, guiding its effort in making space more accessible, cost-effective and flexible in terms of application. To meet these new necessities, the satellites' design has gradually changed, following a trend known as "miniaturization", whose main objective is reducing as much as possible satellites' size and mass: examples of this process are often referred to as "nanosatellites" or "CubeSats". The cost-effectiveness in realizing these types of satellite results from the possibility of using standardized modules, which also reduces the development time. Moreover, increased and more flexible launch options become available. Obviously, this process requires advancements in technology and new solutions to be found, to deal with risk of failure and performance's standards: that is why developing compact, yet powerful devices has become a research driver.

The "miniaturization" trend experienced by satellites, then, logically transfers to the satellites' components: innovative ways to save volume and mass on board must be found, to keep up the pace with the current requirements and expectation which characterize modern space missions. Miniaturization of electronic components has already been achieved, but the tendency to reduce volumes and masses affects also all the other spacecraft's components. This also explains why the interest for new materials is increasing, as it is the case for Shape Memory Alloys, whose use until now has been more frequently used for Earth's applications, with some exception for the aeronautical sector. The high energy densities, small dimensions, volumes and weights obtainable with this material, but most of all the fact that the actuation is a

consequence of the change in the crystallographic structure, are worthy reasons for investigating the SMAs. This last characteristic, in particular, is of great importance because it would allow to remove most of the components that are necessary to transmit a mechanical motion in a common actuator, thus greatly reducing the risk of failure of the whole device.

This thesis is under the collaboration agreement between Politecnico di Milano and Agenzia Spaziale Italiana (n. 2018-5-HH.0 "Attività di ricerca e innovazione" of the framework agreement n. 2016-27-H.0), aiming at designing shape memory alloy actuation systems for aerospace applications.

The desire of exploring possible ways to exploit Shape Memory Alloys as actuators in a space environment has led to the investigation of the most interesting shapes and configurations for a practical implementation. Torsional actuators turned out to be a newsworthy field in which to investigate, since they are particularly promising in terms of respecting the compacteness requirements always present in space missions, especially when CubeSats are involved. The choice of studying and realizing a SMA torsional actuator was also encouraged by the quite limited research carried out until now in previous literature's studies, which gives this thesis the possibility to take a step forward in the characterization of this material. The desire of realizing an actuator working in torsion has led to the choice of a tube as the main subject of this thesis: this guarantees different design approaches regarding both the geometrical configuration of the actuator and the activation strategy to be adopted. The concept of SMA actuator for a space application cannot be completed if a rearm mechanism is not provided already from the very beginning of the design process, and antagonism proves to be the most interesting rearm strategy to be tested and validated. Based on these initial goals, the material's characterization has been carried out on different samples thanks to the collaboration with the CNR Laboratory in Lecco. This tests campaign allowed to gather all the information needed for deciding which type of design was worth to investigate. The final decision has been

about focusing the effort in characterizing the antagonism behavior of two equal tubes, and putting them in series represented an essential step to obtain a meaningful characterization. To validate the working principle, an ad hoc experimental setup has been designed and realized, and a measurements apparatus has been selected among the possibilities which met the experiment's working condition and the desired outputs.

In order to better follow the workflow of the thesis, a brief overview of each chapter is given.

- **Chapter 1** starts with the fundamental concepts necessary to describe the Shape Memory Alloys' behaviour and characteristics and provides some application examples present in previous literature studies. The reasons behind the choice of studying torsional SMA actuators and their rearm strategies during this thesis have also been investigated and clarified. An example of a practical application of the studied actuator has been finally proposed, with the aim of confirming the potentialities of such a device.
- **Chapter 2** represents the first part of the practical activity, dedicated to the material properties characterization. The thermal treatments and mechanical tests performed at the CNR Laboratories have been described, followed by their subsequent analysis, which constitute the basis of the following work.
- **Chapter 3** portrays the second part of practical activity, related to the design and realization of the experimental setup aimed at validating the conceptual design of torsional antagonistic actuator. Every aspect related to the measurements and configuration of the experimental phase has been analysed, providing justifications and, in some cases, possible alternative solutions. The chapter is completed by the final experiment's description and results.
- **Chapter 4** is the conclusive chapter, where a summary of what has been done is reported, analizing which are possible future developments of this project.

1 Shape Memory Alloys

Shape Memory Alloys are an example of the so-called "smart materials" and represent viable option to substitute mechanical systems commonly used for actuation purposes. They are simple, light, small, and have the capacity to work in some cases without the need of an electric power supplement. An increment of temperature is sufficient to trigger a phase transformation, during which a shape recovery takes place, even under high loading conditions. This results in the highest actuation energy densities among active materials (in the order of $10^3\,J/kg$)[1].The phase transformation happens between two crystalline structures: austenite and martensite. As said, temperature plays a fundamental role in determining which crystalline structure is present in SMA material. The transformation from one structure to the other is not immediate, but rather gradual, and it proceeds along with temperature. Four characteristic temperatures can be identified, and they define the temperature ranges in which the crystalline change happens. Starting from a material in martensite, temperature needs to be increased in order to promote the transition to austenite, which happens between a temperature called Austenite Start (A_s) and another one, higher, called Austenite Finish (A_f). From this point, to go back to the martensite structure, temperature needs to be reduced, so from A_f it will reach A_s without any change to the structure, and then, by decreasing the temperature, the Martensite Start temperature will be reached (M_s). The transformation is completed at a lower a temperature called Martensite Finish (M_f). If temperature decreases again falling behind M_f, no change will occur, and the structure will remain martensitic.

The austenite structure is called the "parent phase" andfor NiTi alloys it is characterized by a body centred B2 cubic structure, and it is the stable phase at high temperatures. As the alloy cools down, the structure collapses in a tetragonal shape, a monoclinic B19' structure, which is characteristic of the martensite (twinned) phase, also known as "product phase": this is typical at lower temperatures, where it can also exist in an alternative form, the martensite detwinned, obtained if an external stress is applied. The martensite twinned structure, indeed, is characterized by couples made of two crystals, which can be oriented in 24 different ways. When a stress is applied, the couple is deformed and the two crystals are oriented in the same direction, according to the applied stress. The martensite detwinned can be also obtained directly starting from austenite and applying a stress: in this case, we talk about stress-induced martensite.

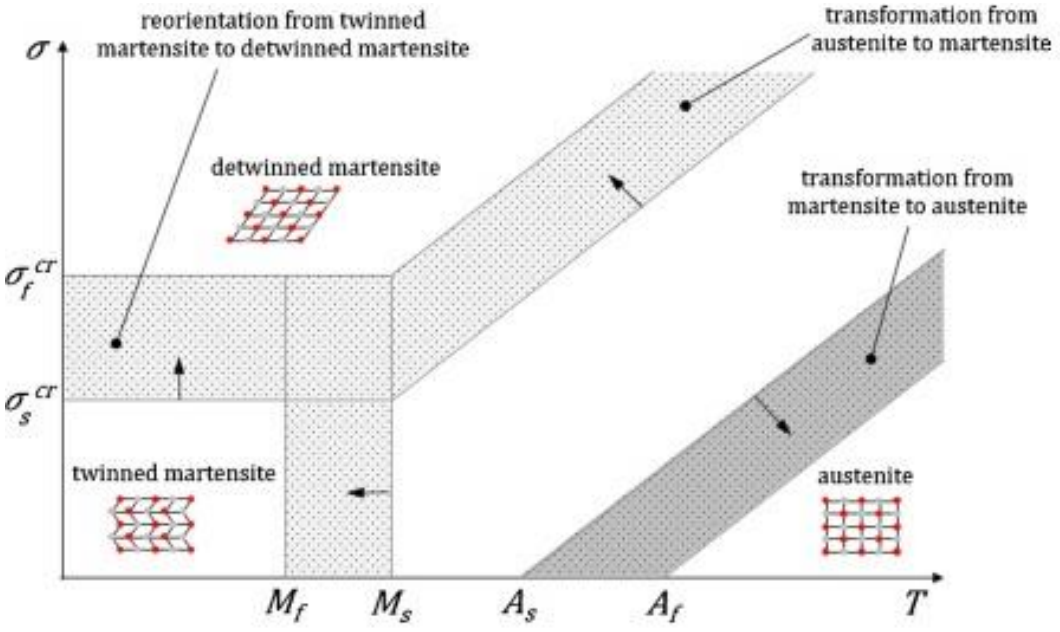

Figure 1.1 Transformations shown on phase diagram [2]

As it is clear from the phase diagram, the two most influencing factors in determining SMA phase transformations are, as seen, are temperature and stress. A relationship between transformation temperatures and applied stresses can be established through the use of Clausius Clapeyron coefficients, c_M and c_A.

$$M_{s(\sigma)} = M_{s0} + \frac{\sigma}{c_M}$$

$$M_{f(\sigma)} = M_{f0} + \frac{\sigma}{c_M}$$

$$A_{s(\sigma)} = A_{s0} + \frac{\sigma}{c_A}$$

$$A_{f(\sigma)} = A_{f0} + \frac{\sigma}{c_A}$$

As these relationships show, the transformation temperatures ($M_{s(\sigma)}, M_{f(\sigma)}, A_{s(\sigma)}, A_{f(\sigma)}$) increase as the applied load (σ) increases as well. The coefficients must be experimentally determined (2.5.1) and are graphically represented by the slope of the curves in the phase diagram.

A third, intermediate state, known as the R-phase or rombohedral phase [3], can be found during the cooling segmentas an intermediate martensite before the formation of the martensite B19', because of the defects related to some specific thermal treatments performed on the material.

Finally, since the martensitic transformation is a thermo-elastic reversible transformation, a backword transformation is also possible. The crystallographic reversibility is given by enucleation and localized propagation of microscopic mobile planes between the phases, also called habit planes, and the driving force for this process is the Gibb's free energy. The austenite cubic crystalline structure (as well as the shape associated to it) can be recovered starting from martensite twinned if heat is applied, or starting from martensite detwinned in two conditions: if heat is applied, or if the stress is removed (when $T>A_f$). During both the phase transformations, respectively the martensitic transformation (or "direct" transformation, A-M) and the "reverse" transformation (M-A), the resistivity of the material changes, giving feedback of the ongoing phase change.

The transformation from martensite to austenite, with the associated shape recovery, is exactly what produces the actuation stress/force that makes the SMA so appealing in numerous fields, and it is called Shape Memory Effect.

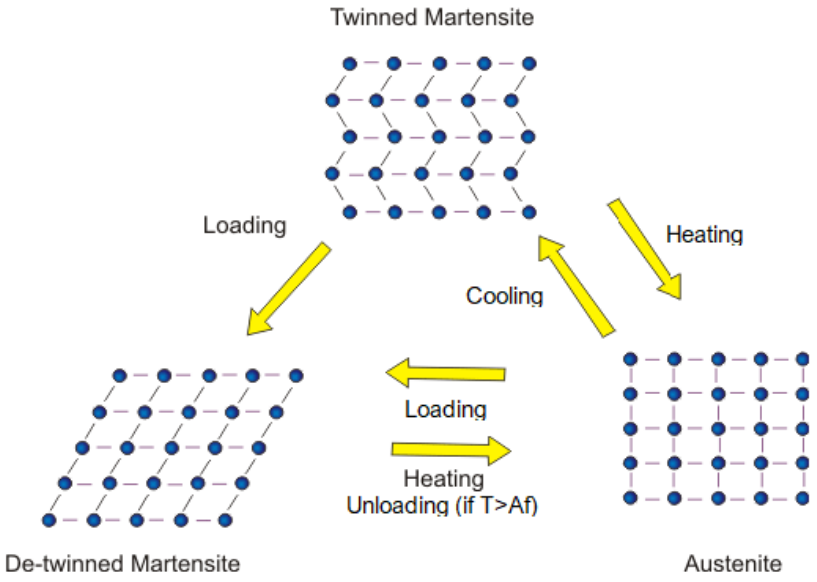

Figure 1.2 Phase transformation processes

Two different SME can be distinguished: the One-Way SME and Two-Ways SME. In the One-Way SME the alloy can remember one single shape, in the austenite phase. Despite undergoing different deformations while being in the martensite phase, as soon as the austenite transformation temperature is reached, the original austenite shape is re-established. The representative steps of this behaviour are visible on the right part of Figure 1.4, showing the Stress-Strain-Temperature diagram of a SMAat T<M_f. At this temperature the material can be largely deformed applying a load until a permanent deformation is produced, visible even when the load is removed. This deformation can be fully recovered by increasing the temperature over A_f (the recovery process starts at $A_s$and ends at A_f).

In order to exploit the Two-Way SME the alloy shall undergo a "training" consisting in a thermomechanical cycle along a specific loading path, in order to induce changes and defects in the microstructure: these allow the alloy to "remember" two shapes, one at lower temperatures in the martensite phase, and one at higher temperatures in the austenite phase. The training can be carried out in different ways: one example consists in a sequence that must be performed for at least 10 times. The sample must be heated until a temperature T>$A_f$to transform the material in austenite then a load

must be applied to obtain a maximum strain of 6%, generating stress-induced martensite. Keeping the same load applied, a cooling must be performed until temperature reaches a value T<M_f. The last step is heating again the sample to restore the original undeformed shape. Nevertheless, the smaller strains obtainable, the unknown long-term fatigue behaviour, and the fact that a slight overheat is sufficient to remove the SME form the Two-Way alloys, make their use extremely limited.

A shape setting must be performed also to obtain the One-Way SME: the procedure starts by giving the desired final shape to the material; then a thermal treatment must be performed so that the material lattice recrystallizes and settles in a configuration associated to the applied macroscopic shape.

Finally, immediately after the thermal treatment a quick quenching is required to maintain the microstructure obtained during the thermal treatment. This corresponds to a microscopic change only, while macroscopically the shape is the same.

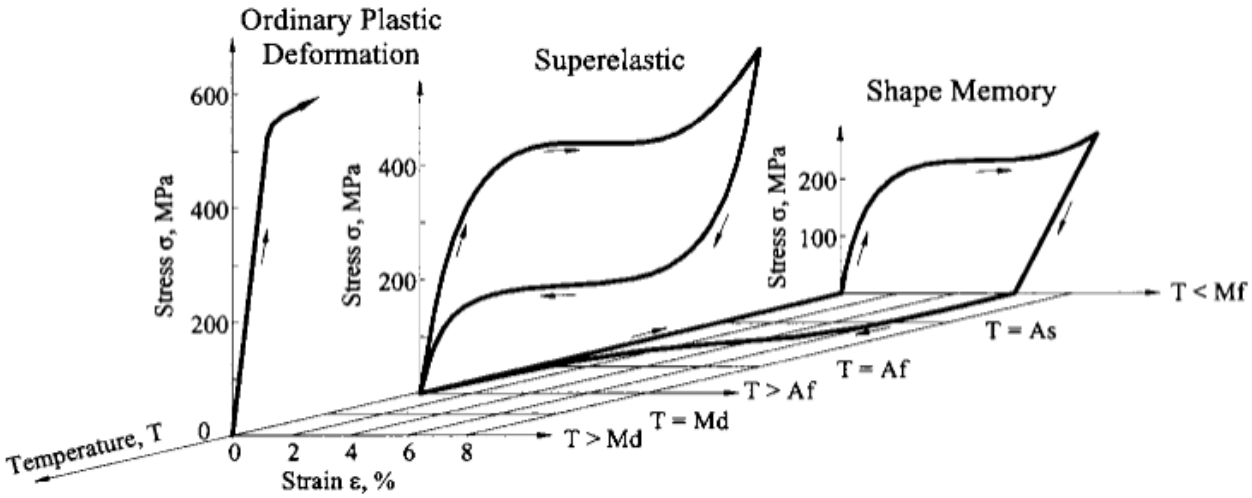

Figure 1.3 Superelastic behavior for T>A_f

SMA also show a super-elastic behaviour, known as pseudo-elasticity, possible thanks to the formation of stress-induced martensite (SIM), which reverts

immediately to austenite as soon as the load is removed. This happens when the material is at temperatures higher then A_f: thanks to this behaviour the alloy can be deformed largely without entering the plastic domain, and thus recovering the original shape immediatelywith no residual strain. A mechanical hysteretic behaviour can be observed in the stress-strain diagram, due to the different paths followed during loading and unloading phases, thus revealing a dissipation of energy.

1.1. Space applications of Shape Memory Alloys

1.1.1. Low-shock release mechanisms

Shape memory alloys find a great field of applications in the low-shock release mechanisms production, as they make it possible to avoid the generation of shocks able to propagate inside the structure of the satellite, which can turn out to be particularly problematic and dangerous. Most of the aborted missions, indeed, are due to the malfunctioning of the explosive release devices, which do not explode, or do not explode in the designed way, often non in a synchronized way.

The use of low-shock release mechanisms actuated by SMA is particularly suited for micro-satellites, where the possibility for miniaturization is a fundamental research driver.

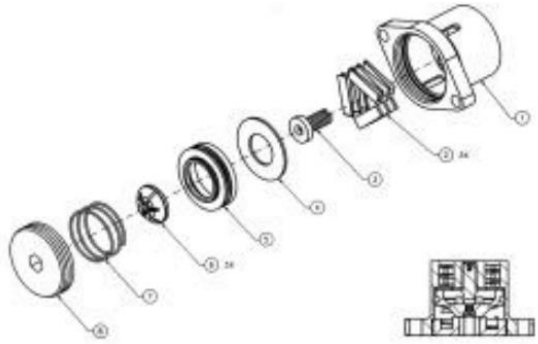

Figure 1.4 Mini separation nut assembly

Figure 1.5 Mini separation nut mechanism

Mini and micro separation nut have been designed where the segmented nut is constrained by the collar in a nut shape, allowing a bolt to be tighten. The collar is kept in place by a compression spring, from which it is driven in opposition when a shape memory alloy element is heated. This causes the segmented nut to separate, thus releasing the bolt [4].

Non-explosive release actuators can be developed using SMA wires: the trigger operation for the bolt release here is performed by the contraction of the SMA wire when it is heated using a power source. By contracting, the wire causes the upward movement of the trigger block, which thanks to a simple mechanism exploiting balls and rollers to allow translation and encastre, generates the upward movements of the locking sleeve. The segmented nuts get separated and the bolt is released [5].

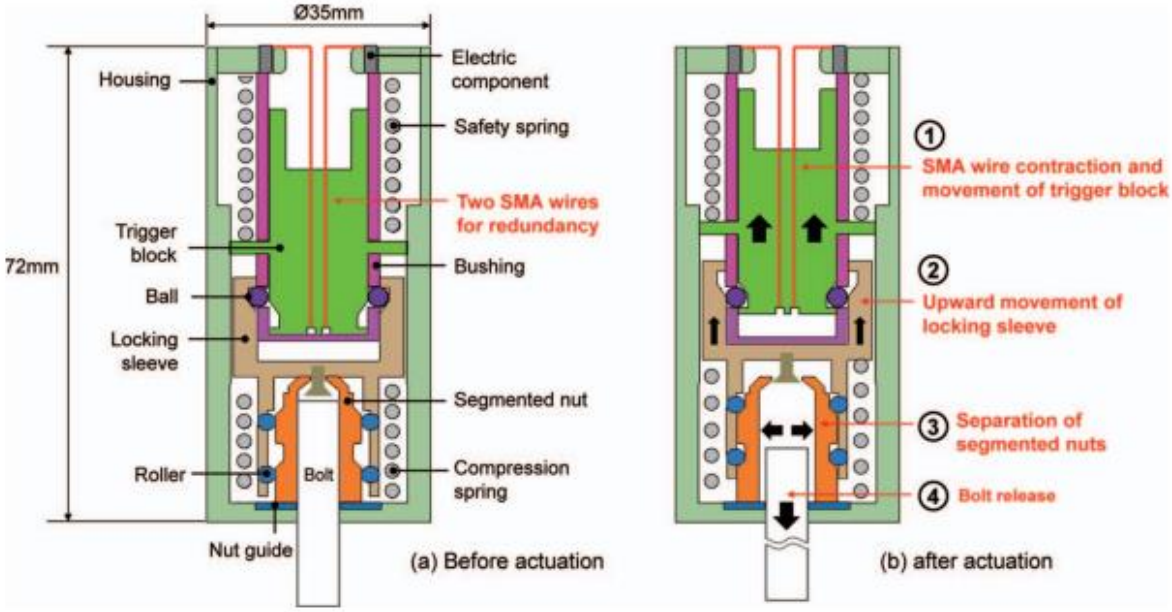

Figure 1.6 Configuration of low shock release device

1.1.2. Solar sails deployment mechanism

Because of their big size, solar sails must be packed during launch and then deployed gradually, following a predetermined sequence. SMA wires have been studied for this type of application, and they have been used in a rolled configuration to obtain ribbons of rectangular cross section, used as resistances in an electric circuit arranged

on the solar sail. The transformation takes place when the transformation temperature is reached thanks to the heat transferred by Joule effect [6].

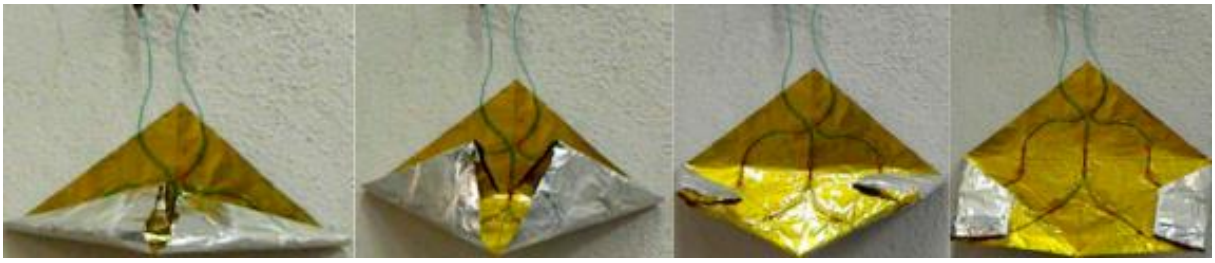

Figure 1.7 Solar sail deployment sequence

1.1.3. Solar panels deployment mechanism

Two antagonistic SMA wires have been integrated in a 4D-printed active compliant hinge with a selected variable stiffness to allow a 90° orientation of a 6U CubeSat solar panel. Two Shape Memory Polymers were used to realize multi-material 3D printed components, such that the reduction in stiffness is limited only to the central region of the hinge. The variation in bending stiffness is achieved by applying a thermal input to heat the central region of the hinge, which in turn allows its bending through a SMA spring. The hinge is then kept in the desired position by the spring while the temperature goes down, restoring the initial stiffness of the hinge: in this way it is possible to keep the hinge fixed in the final position without powering the SMA spring.

An analogous process is performed to bring the hinge back to the original configuration, this time exploiting the antagonistic spring. The central region of the hinge is heated again, in order to reduce its stiffness, while the spring on the other side of the hinge is activated.

This spring, indeed, has been armed during the first movement of the hinge which put it under a tensile condition: when it is activated, it recovers its deformation, allowing the hinge to change its shape, and thus, orientation [7].

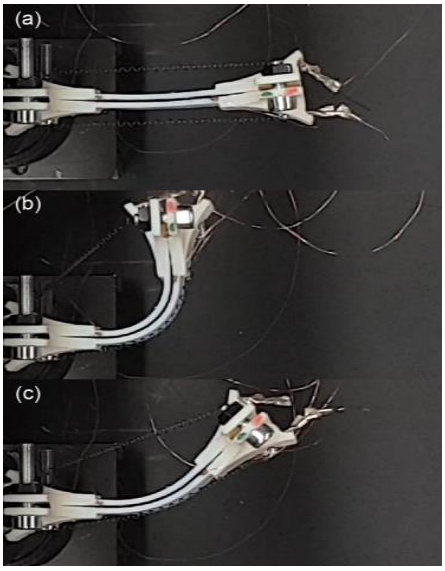

Figure 1.8 (a) Original position (b) Bending (c) Locking at 45°

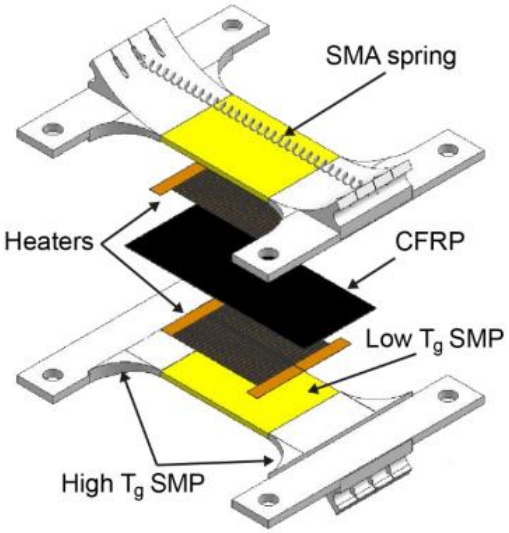

Figure 1.9 Hinge configuration

Another application of SMA as hinges is represented in the "Lightweight solar array experiment", where the hinges are deployed by means of heaters powered by the spacecraft 28V bus. The use of internally connected, pliable nichrome heaters to apply heat causes the shape memory alloy to transform into its austenitic phase, resulting in a smooth and shock-free deployment of the hinge [8].

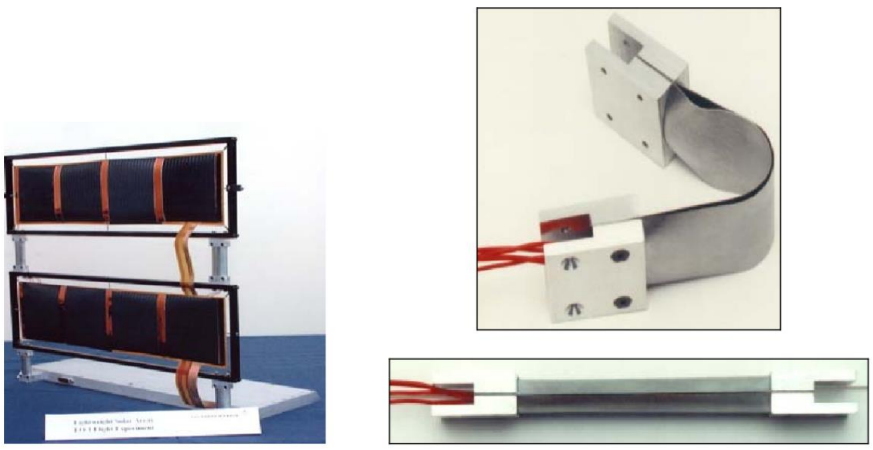

Figure 1.10 Solar panel hinge

1.1.4. Morphing radiator actuation mechanism

SMA can be used as actuation and control mechanisms for morphing radiators. These radiators exhibit exceptional turndown ratios due to their capacity to alter their configuration, thereby adjusting the rate at which they emit heat into the surrounding space. A morphing radiator comprises the following elements: a flow tube for conveying the thermal working fluid from the spacecraft cabin to the radiator; an array of cylindrical panels with high thermal conductivity that dissipate heat from the flow tube and emit it into space; SMA actuators fixed to the exterior of the conductive panels, enabling them to expand when warmer and contract when cooler; terminal blocks serving as structural anchors for the SMA, transforming their tensile force into applied moments and compressive forces at the panel's free edges. In deep space the SMA is in the martensitic phase, allowing a closed configuration where the inside view factor approaches zero, and the radiative heat rejection is dependent on the emissivity of the convex surface, which is coated to ensure low emissivity. When the ambient temperature or the heat load supplied via the flow tube increases, the SMA components transform toward the austenite phase and contract circumferentially, opening the radiator toward a semicircular shape [9].

1.1.5. Rotating arm

The rotating arm of the Mars Pathfinder mission is aimed at covering/uncovering a solar array with a cover glass, in order to discover the impact that the settling dust has on energy production. The arm is attached to an axle which is free to rotate while a SMA wire is anchored to the axle and to a stationary point. The NiTiNOL wire is heated resistively by passing a DC current through the wire, which undergoes heating, and leads to its contraction: in this way it exerts a force on the axle, resulting in the rotation of both the arm and the cover glass. When the current to the wire is shut off, the wire expands and is returned to the rest position by a flat spring [10].

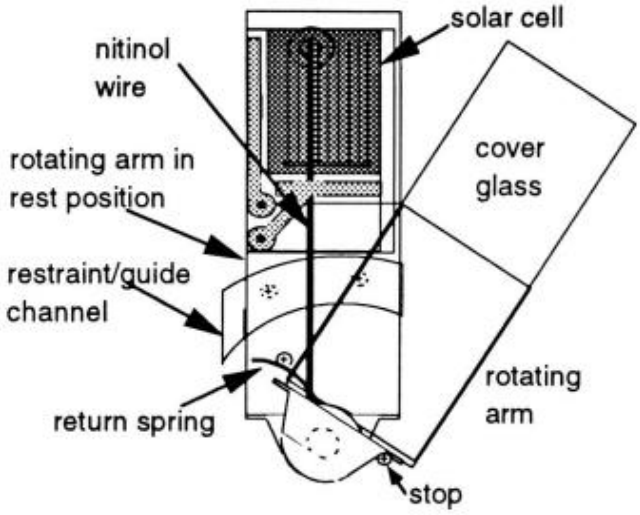

Figure 1.11 Arm configuration [10]

1.1.6. Torsional actuators

The great majority of torsional actuators exploiting SMA make use of SMA wires, converting their linear motion in a rotational one. One example of such an actuator is the rotational driving mechanism which converts the expansion and contraction of the SMA wires into the bidirectional rotary motion with high torque. The mechanism comprises a rotor and a wobbler, both supported by three crankshafts.

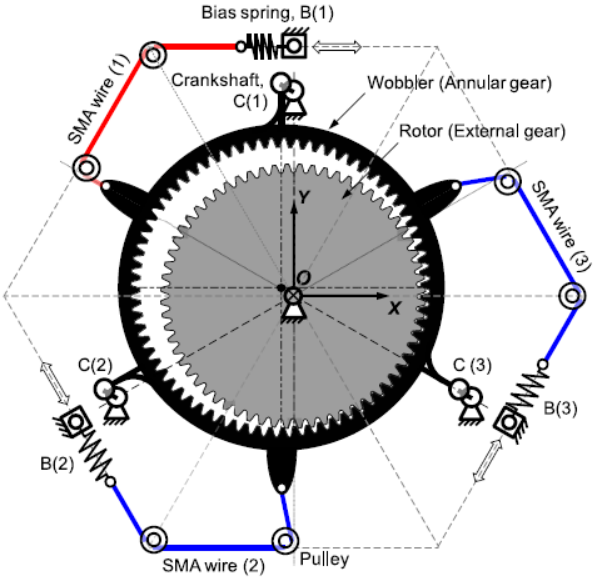

Figure 1.12 Kinematic configuration of the actuator [10]

The rotor is firmly attached at the center of the driving mechanism, while the wobbler is eccentrically located relative to the rotor. To achieve clockwise (1-2-3) or counterclockwise (1-3-2) rotation of the annular gear, three SMA wires, connected in series and equipped with bias springs, are activated sequentially [11].

A different kind of application is represented by the preliminary design in [12], where the final part of a plane wing is composed of flexible ribs. Each rib is composed of three distinct tubes that are linked to the structure through an electromechanical clutch, capable of disconnecting the other two tubes when one of them is activated. This actuation is achieved by heating SMA actuator tubes using patches of electric resistors embedded in a plastic adhesive film. The utilization of SMAs has been extensively researched and applied in the aeronautical sector, particularly for wing shape control. Variable leading/trailing-edge camber adjustments can significantly reduce drag, while local variations in wing-surface contour are employed to mitigate shock intensity and the propensity for boundary layer separation in transonic aircraft.

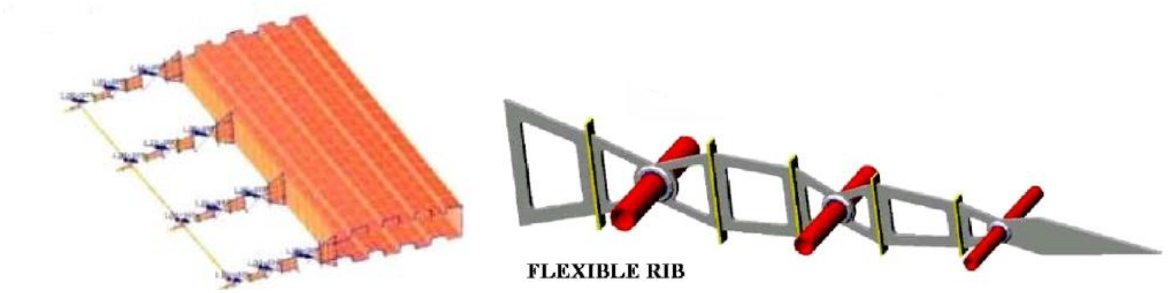

Figure 1.13 SMA actuator tubes used in a plane wing

1.2. Why SMA torsional actuators?

SMA actuators are obviously not the only ones capable of providing a rotational motion to mechanical systems, as it can be obtained also through pneumatic and hydraulic rotary actuators as well as electrical motors. Pneumatic and hydraulic actuators convert fluid pressure into rotational motion, exploiting three possible basic designs: gear motors, vane motors, and rack and pinion. The first two employ a direct rotational actuation approach, while the third one converts axial motion to rotation. Hydraulic and pneumatic actuators, though powerful, are not suited for applications where operational space is limited. Moreover, they are bulky, heavy, and labor intensive as regards maintenance. As regards electrical motors they use pole brushless motors to generate continuous rotation, but the drawbacks consist in offering low torque if compared with pneumatic and hydraulic actuators, being loud, producing vibrations and often experiencing problems with heat management.

The use of SMA in designing actuators represents one of the most compact and vibrationless possible options to supply rotational motion under load. Two primary approaches can be identified: direct rotational actuation, and linear actuation converted to rotational motion, and an example of both has been provided in Section 1.1.6.

While axial SMA actuation (using wires) is highly common, SMA torsional actuation is less discussed and developed in existing literature. Despite this, rotational actuators utilizing linear SMA elements are typically low torque and low frequency, they tend to be very complex and occupy a large operating volume. Direct rotational motion can be achieved in a more straightforward way using SMA torque tubesand rods twisted about their long axis. These types of actuators are extremely compact, easy to maintain and replace. Direct rotational transformation results in an higher torque output than the linear-to-rotational SMA counterparts: indeed, SMA torque tubes produce extremely high torque per unit volume as compared to all types of

rotary actuators. This happens because the actuation mechanism arises directly from the material response and it is not the result of a mechanical interaction.

Considering the constraints of space applications, tubes offer performance advantages in component design. A wide range of torques and angular rotation magnitudes can be provided by SMA torque tubes of various sizes and, as a result of a solid-to-solid phase transformation, tubes can generate up to 7% shear strain across a range of stress values [13]. The limiting factors in using SMA torque tubes as actuators are high input power requirements and low frequency of actuation. These two aspects generate most of the thermal management challenges, especially in cooling, as all the heat supplied must be dissipated into the surrounding environment. For this reason, the local efficiency of a given SMA actuator may be very low, but globally, the system-level efficiency generally benefits from the use of SMA actuators [14].

1.3. Which rearm strategy?

The interest in designing a SMA torsional actuator is justified by what has been said until now, but when talking about Shape Memory Alloys application, the concept of rearm is of central importance because it is what allows for multiple actuations. The rearm mechanism should be capable of restoring the original configuration of the actuator, the one characterizing it before the actuation: without it, a SMA actuator could work only once, and it would require an interruption of the activity to permit a manual reset of it.

Torsional spring

The most intuitive way to perform a rearm is to use a spring: in this case a torsional spring would have been required. Nevertheless, constraining the spring to the structure and around the SMA sample, considering that it must perform a torsion, may represents complications in the configuration. It would not allow a real compact

actuator's design, which is one of the main objectives of this thesis, so this option was soon ruled out.

Pseudo elastic rod

The possibility of realizing an actuator using a NiTiNOL tube, suggested the idea of trying to obtain the rearm by exploiting a thin rod of pseudo elastic material inserted inside the tube. This elegant solution would allow to exploit the same material exploiting both the shape memory effect of the tube, and the super-elasticity of the internal, coaxial rod. The working principle of such integrated device can be summarized in two steps: the tube is activated, generatinga torque that would cause the rotation of the rod of pseudo elastic material, which is forced to follow the movement of the actuator inside which it is allocated, by realizing specific constraints. Then, when the tube starts cooling, the torsional force exerted by the pseudo elastic rod prevails, driving the tube back to the original position.
The pseudo elastic rod would almost work like a spring, with the advantage of being integrated in a unique device. The main difficulty consists in inserting the rod in the tube and constraining it to the tube in such a way that they are free to rotate, but at the same time to rearm each other.

Two-ways shape memory effect

A possible solution was to exploit the two-way shape memory effect, thus training the material to remember two angular positions: one at low temperatures, one at high temperatures. Nevertheless, the smaller strains obtainable, the unknown long-term fatigue behaviour, and the fact that a slight overheat is sufficient to remove the SME form the Two-Way alloys, make their use extremely limited.

Antagonistic SMA

One way of obtaining a compact and integrated actuator, capable of performing a rearm, is exploiting two SMA actuators working in torsion, but producing torque in

opposite directions: by activating them in different moments, the torque produced by a SMA sample would be capable of arming the other one. Using two samples which stays at different temperatures undoubdtedly leads to the necessity of insulation. Moreover, the interaction between the samples must be carefully studied in order to understand which are proper working conditions and the optimal configuration for the actuator.

1.3.1. Selected solution

The use of antagonism as rearm mechanism has been considered the most promising and the most interesting option to investigate, as it leads to the possibility to follow different approaches in the design. It allows the satisfaction of the compactness requirement, typical for any item designed for a space application, given the possibility of exploiting a coaxial configuration. Indeed, the two SMAs could consist of two tubes with different diameters, or a tube and a rod, coaxial and one inside the other. The activation strategies can be different: the intern tube can be activated by a hot fluid flowing in a circuit, while the bigger tube can be activated by Joule effect provided by an electric wire located on its external surface. Alternatively, they can be both activated through Joule effect, or be integrated in two different circuits. The space between the two coaxial elements can be useful in case an insulant material is needed in order the keep the tubes at different temperatures, thus ensuring the optimal functioning.

Since in the literature torsional behavior of shape memory alloys is not yet completely studied, let alone torsional antagonism, this thesis aims to move the first steps in characterizing it. Before considering a compact configuration, it could be worth checking the behavior of the actuator in an “open” configuration, thus putting the two elements in series. Moreover,choosing two equal tubes as the two elements to be but in series, would provide a reference for future studies on the compact

configuration, and it would allow a complete characterization both of the torsional behaviour of SMA tubes, and their relative rearm through antagonism.

1.4. Space Application

The possible applications of such an actuator can be different due to its characteristics. The capacity of working in torsion without all the components typical of an electrical motor makes it a simpler actuator with a reduced need for maintenance and a reduced risk of failure as well as lower mass and occupied volume. Moreover, the possibility of realizing a compact actuator has been demonstrated, using a coaxial rod and a tube. Different types of applications are also possible thanks to the possibility of exploiting different sources of energy to activate it: electrical energy produced by Joule effect like in the experimental demonstrator can be used, oralternativerly, the tubes can be integrated in a circuit in which a fluid is able to circulate. In this way, different areas of a satellite can be thermally connected: the hot fluid coming from a hot region can activate the SMA tubes when passing through them, dissipating its energy.

Thanks to the reduced mass and the simplicity of such an actuator, it can be adopted for a CubeSat application. CubeSats represent a growing sector in the space industry and there are still many challenging aspects to consider when designing them. One of the principal problems to solve, is represented by the themal management, which is extremely challenging considering the small dimensions of such satellites. What is commonly done, is relying on a passive solution for thermal management, adopting a radiative panel. The actuator decribed until now could be used as the hinge of such radiating panel, allowing its opening and closing. One tube can be activated to open the panel when heat needs to be dissipated, thus arming the other tube, or rod, depending on the configuration. On the other hand, when the panel needs to be closed, the activation of the second tube (already armed) happens. This second activation would lead to the re-arm of the first tube, and the sequence can restart

once the panel needs to be opened again. In the next paragraphs an overview of CubeSat characteristics, the orbit in which they are more used, and the characteristics of such orbit, is given. The intention is defining a possible operating framework of the actuator, demonstrating that its characteristics, with particular attention to actuation frequency, can meet the working conditions of an operating satellite.

1.4.1. CubeSat

When it comes to describing what a CubeSat is, the word “standardized” reveals the winning concept that makes it so appealing in the space field both from an engineering and commercial point of view. A CubeSat is a type of very small satellite which is based on a standardized unit of volume and mass, respectively 10x10x10 cm, and 1,33 kg. CubSat units can be combined exploiting the modularity concept that lies behind their developement. Due to the standardized dimensions of CubeSats, they commonly adhere to uniform requirements and constraints. As a result, a variety of standardized functional modules, such as power systems and communication systems, have been designed. The utilization of readily available, off-the-shelf components is a factor which facilitates the rapid and cost-efficient development of CubeSats. Typically, CubeSats are launched into space enclosed within deployers as part of containerized payloads. This approach streamlines the launch campaign's complexity and associated costs. CubeSat missions frequently incorporate non-space components as part of a cost-effective and expeditious strategy. This, in conjunction with the fact that most CubeSat missions operate within Low Earth Orbit (LEO) with relatively short lifespans, allows for a greater degree of tolerance for technical risk [15]. CubeSats are remarkably adaptable and serve a multitude of mission types. They can be employed for technology demonstrations, validating the readiness of novel instruments or materials for future space missions (TRL8). Alternatively, they can carry compact scientific instruments for data acquisition and experimentation in space. CubeSats are also harnessed for

commercial purposes, such as providing telecommunication services and Earth monitoring through imaging. Furthermore, their diminutive size and cost-effectiveness make CubeSats well-suited for educational projects.

1.4.2. LEO

“Low-Earth Orbit (often known as LEO) encompasses Earth-centered orbits with an altitude of 2000 km or less. Low-Earth orbit is considered the area in Earth orbit near enough to Earth for convenient transportation, communication, observation and resupply. This is the area where the International Space Station currently orbits and where many proposed future platforms will be located” [16]. As the NASA definition of Low-Earth orbit states, LEO is the most usedorbit for satellite imaging, as being near the surface allows both to take images of higher resolution, and, given the high speed of satellites in a low orbit, to circle Earth multiple times per day. Owing to the rapid movement, substantial efforts are necessary for tracking low Earth orbit (LEO) satellites from ground stations. Consequently, communication satellites in LEO frequently function as components of extensive constellations. Unlike geostationary (GEO) satellites, which must adhere to the equatorial orbit, LEO satellites are not confined to a fixed path around Earth. Their orbits can be inclined, providing more diverse trajectories, which contributes to the widespread use of LEO. Nonetheless, numerous factors disrupt satellite orbital motion, beginning at launch and continuing throughout their operational lifespan. These disturbances can be categorized into gravitational and non-gravitational perturbations. Gravitational perturbations comprise the gravitational pull of Earth, Earth's oblateness, sectorial spherical harmonics, and the gravitational effects of the Sun and Moon. Non-gravitational perturbations encompass the dominant atmospheric drag force in LEO, solar radiation pressure, particularly affecting geosynchronous satellites, and magnetic forces arising from the interaction between a satellite's dipole moment and Earth's magnetic field. Atmospheric drag poses the most complex challenge in dealing with

LEO satellites [17], which do not orbit below 160 km: within 120 to 160 km of Earth's surface, indeed, atmospheric drag leads to rapid orbital decay, culminating in disintegration around 80 km (the lowest orbiting satellite, the Japanese satellite Tsubame, orbited at 167.4 km [18]). An additional concern is the relatively short lifespan of LEO satellites, given their constant exposure to solar and other radiation sources. While launch costs are reduced due to lower altitudes, the limited lifespan (5-10 years), higher power requirements for orbit maintenance to counteract atmospheric drag, and the prevalence of atmospheric effects necessitating robust guidance, navigation, and control (GNC) systems make LEO satellite missions costly. In LEO orbits, one of the most significant hazards is atomic oxygen, a highly reactive form of oxygen. Solar ultraviolet light splits oxygen molecules, releasing oxygen atoms, which, despite their lower thermal velocity compared to spacecraft, can instigate chemical and physical reactions on satellite surfaces, causing material degradation. The extent of damage varies based on several factors, such as spacecraft altitude, orientation, orbital inclination, mission duration, and solar activity fluctuations. The presence of space debris worsen these effects, as even small projectiles can inflict structural damage and surface vulnerabilities, exposing materials to atomic oxygen, vacuum-ultraviolet radiation, and setting the stage for future failures.

1.4.3. LEO thermal environment

The analysis of the thermal environment is vital to characterise the thermal control problem, and to solve it through the thermal system design. The thermal system allows to keep the spacecraft's component within their operative temperature ranges, thus making it possible to successfully completing the mission. It must be immediately clarified that also the ground environment and the launch environment must be carefully accounted for, but commonly the thermal control system is designed to achieve temperature requirements in the environment encountered on-

orbit, while compatibility with ground operations and launch ascent condition is assured by controlling the environment or limiting the spacecraft's exposure to it. During the satellite's operative life, the main sources of environmental heat are direct sunlight, albedo and infrared energy emitted from a planet's atmosphere or surface [19]. The spectral distribution of solar irradiation is approximated by a blackbody at 5762 K, while the intensity of Sun radiation varies both depending on Sun-Earth distance and wavelength. The solar radiation absorbed by a flat surface of area A, whose normal vector forms an angle $\theta$with the solar rays, considering the intensity of the solar radiation at Earth's mean distance from the Sun, G_s, to be $1367\frac{\mathrm{W}}{\mathrm{m}^2}$, α being the solar absorbance of the surface, is given by [20]:

$$Q_{sun} = \alpha G_s A \cos\theta \qquad 1.1$$

Albedo is the percentage of sunlight reflected by a planet. It can be calculated considering that a is the planetary albedo coefficient, Gs the solar constant, ϕ is the solar zenith angle and $F_{sc_p}$the view factor between the surface and the planet.

$$Q_{alb} = a G_s A \, F_{sc\_p} \cos\phi \qquad 1.2$$

The view factor is greater over land than over oceans and it commonly increases when solar elevation angles decreases, or cloud coverage increases as well as when latitude increases because of the greater presence of snow and ice.

Inclination [deg]	Angle of Sun out of orbit plane [deg]	Emitted radiation $[W/m^2]$		Albedo [%]	
		Min	Max	Min	Max
0-30	0	228	275	18	28
	90	228	275	45	55
30-60	0	218	257	23	30
	90	218	257	50	57
60-90	0	218	244	23	30
	90	218	244	50	57

Figure 1.14 Albedo values [20]

As regards the Earth IR radiation, its intensity is function of different parameters, such as the local surface temperature and the amount of cloud coverage. It must be noted that the IR energy emitted by the Earth is almost of the same wavelength as that emitted by a spacecraft. For this reason, Earth IR radiations incident on a spacecraft cannot be reflected away from radiator surfaces with thermal control coatings, since the same coatings would prevent the radiation of waste heat away from the spacecraft. Considering T_p as the blackbody temperature of the planet, ε the infrared emissivity of the surface, and σ the Stefan-Boltzmann constant, the planetary infrared thermal load on a spacecraft surface of area A can be calculated as:

$$Q_{IR} = \varepsilon A F_{sc/p} \sigma T_p^{\ 4} \qquad 1.3$$

1.4.4. Feasibility demonstration

An existing CubeSat has been taken into consideration in order to characterize a possible environment found in an application of the described actuator. This thesis aims at demonstrating the working principle and the rearm strategy, while as regard the compact configuration, it has only been described theorically and some preliminary tests have been done to demonstrate its feasibility, but it has not been experimentally validated yet. A compact configuration is desirable for a real application as it is easier to be integrated in the satellite and it allows to exploit the actuator as much as possible. The objective of this chapter, however, is independent from the configuration, as another aspect must be taken into serious consideration when talking about SMA actuator: the actuation frequency. This is a critical parameter to be evaluated for any specific application as the material, after one actuation, meaning after being heated to transform towards austenite, must then be cooled before being ready for another actuation. It shoud be cooled also before being reamed, otherwise, as it can be seen from the phase diagram, a huge stress would be

needed to obtain martensite detwinned and the shape memory effect would not be present.

The time between two subsequent activations, which determines the activation frequency, is dependent from the SMA cooling time. The actuator can be cooled down using an active tecnique, such as exploiting a refrigerating fluid, or forced convention, but in this case only radiative heat dissipation has been considered. This is the simplest technique that can be used in space as it does not need a dedicated circuit or particular working conditions to be verified.

The CubeSat taken into consideration is IceCube [21], a cloud ice observation 3U CubeSat nanosatellite operated by NASA and GSFC (Goddard Space Flight Centre). The satellite was launched on 18 April 2017 and deployed from the ISS on 16 May 2017 and it re-entered the atmosphere in October 2018. IceCube followed a near circular orbit at an altitude of approximately 400 km and an inclination of 51.6°(β angle variation: 0-75º).

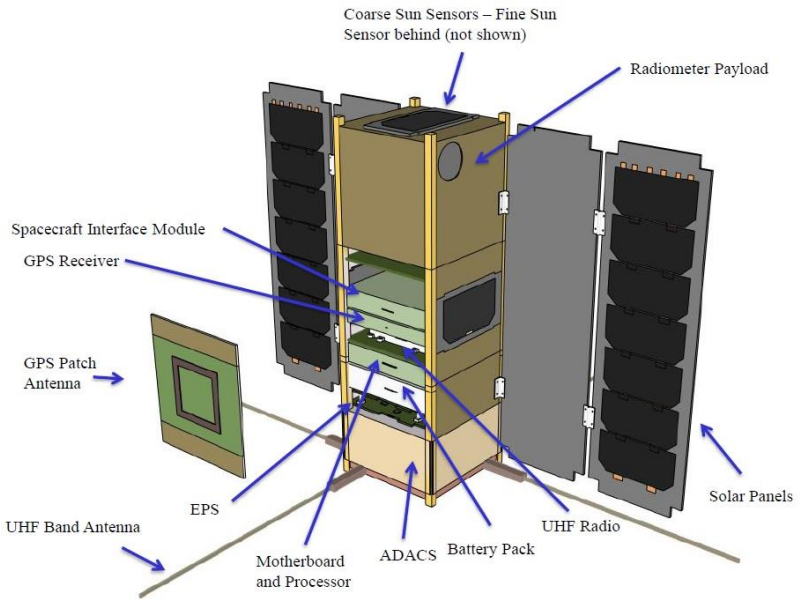

Figure 1.15 IceCube satellite

Knowing the internal heat sources of the satellite and the survailability temperatures of the components [22], the temperature the satellite reaches in the hot case can be computed and compared with the operational temperatures of the components. The

temperature of the hot case is equal to 59.2°C, which is almost equal to the survailability temperature of the battery, and has been found with the equation here reported:

$$T_i = \frac{Q_{hot}}{\varepsilon \cdot A_s \cdot \sigma} = 59.2\ °C \quad 1.4$$

This analysis demonstrates that there is the need of dissipating a certain amount of thermal energy in order for the components to work correctly, as T_i is too close to the limit survailability temperature of the battery, 60°C, chosen as a reference to keep the calculations conservative.

Q_{hot} is the heat of the satellite in the hot case scenario, given by the sum of the heat inputs described in the previous paragraph and Q_i, the satellite internally generated heat.

$$Q_i = Q_{Instrument} + Q_{GNC+OBDH} + Q_{EPS} + Q_{RF+} Q_{TCS} + Q_{battery} = 23.96\ W \quad 1.5$$

$$Q_{hot} = Q_{sun} + Q_{alb} + Q_{IR} + Q_i = 207.19\ W \quad 1.6$$

The objective temperature of the simulation is set to 40°C in order to keep the temperatures of the battery and other electronical components inside the range of their operative, and therefore survival, temperature. The time needed by the surface of the panel to radiate the thermal energy is 1298.3 seconds, slightly more than 21 minutes, so the panels must be kept open for that amount of time.

$$t = \frac{\Delta T \cdot m_{sat} \cdot c_t}{A_s \cdot \varepsilon \cdot \sigma \cdot T_i^4} \quad 1.7$$

Where T_i is 60°C, the temperature at which the satellite is initially, before the heat dissipation starts, and ΔT is the difference between the initial temperature and the objective temperature.

Parameter	Value	Description
$\boldsymbol{\alpha}$	0.84	Solar absorptance of Solar Array Cells
$\mathbf{G_s}$	$1367\ \frac{\mathrm{W}}{\mathrm{m}^2}$	Solar constant
A	$0.15\ \mathrm{m}^2$	Area illuminated by the sun
a	0.525	Albedo constant for β=75°
$\mathbf{F_{sc\_p}}$	0.8855	Viewfactor
cosϕ	0.0506	Solar zenith angle considering Darmstad ground station
eps	0.6	Planet emissivity
σ	$5.67e^{-8}\ \frac{\mathrm{W}}{\mathrm{m}^2\mathrm{K}^4}$	Boltzmanconstant
$\mathbf{Q_{Tp}}$	250K	Blackbody temperature of the planet
$\mathbf{Q_{Instrument}}$	6W	Internal heat due to the instrument
$\mathbf{Q_{GNC+OBDH}}$	4.6 W	Internal heat due to GNC and OBDH subsystems
$\mathbf{Q_{RF}}$	12.06 W	Internal heat due to RF
$\mathbf{Q_{EPS}}$	0.4W	Internal heat due to EPS subsystem
$\mathbf{Q_{battery}}$	0.1W	Internal heat produced by the battery
$\mathbf{Q_{TCS}}$	0.8W	Internal heat due to TCS subsystem
ε	0.8	Satellite emissivity
$\mathbf{A_s}$	$0.45\mathrm{m}^2$	Surface area of the satellite

$\mathbf{T_{objective}}$	40°C	Temperature at which the satellite must be cooled down
$\mathbf{c_t}$	$700\ \frac{J}{kgK}$	Thermal capacity of the satellite
$\mathbf{m_{sat}}$	4kg	Satellite's mass

Table 1.1 Parameters used during the simulation [22],[23]

Considering that the SMA actuator is placed in the hinge of the radiating panels, it would be responsible for their opening and closing, thus regulating the heat dissipation of the satellite. The condition that has to be verified is that the cooling time of the SMA actuator is lower than the time needed by the panels to dissipate the satellite's heat. Obviously, for an actual use of such an actuator, a specific composition of the alloy must be selected already starting from the production process according to the desired range of transformation temperatures and in order to limit the thermal treatments. For this simulation the initial temperature and the objective temperature have been considered the same as the ones used during the experimental phase, namely -20°C and 60°C. The time needed by the tube to dissipate through radiation has been computed with the equation 1.7 (using the tube's parameters reported in Table 1.2 as 25 seconds, which is far less than the time needed by panels to dissipate satellite's heat, thus demonstrating that this kind of application is possible.

Parameter	Value	Description
$\boldsymbol{\varepsilon}$	0.66	Tube's emissivity[24]
m	0.005 kg	Tube's mass
A	$0.0188\ m^2$	Tube's surface area
$\mathbf{c_t}$	$542\ \frac{J}{kgK}$	NiTiNOL thermal capacity

Table 1.2 Parameters used during the simulation

2 Material properties' characterization

Shape Memory Alloys' properties and behaviors are still under investigation and far from being represented by a unique and all-encompassing model: for this reason, several tests must be performed to determine the characteristics of the samples to be used, to exploit them in the best possible way while designing the actuator. This empirical method is characteristic of many of the studies related to SMA present in literature.

There are, nevertheless, mathematical descriptions for the transformation behavior exhibited by SMAs that have been developed since 1976. Many constitutive models have been proposed and they are typically based on either micro-mechanics or on a combination of SMA phenomenology, statistical mechanics, and kinetic methods. In modeling torque tubes and rods, these constitutive models are often adapted to allow their implementation [25]. This models however, are very difficult to manage for a practical application, as they are often suited for a specific SMA with a specific composition. For this reason, in this thesis work an empirical path has been followed for the alloy's characterization, which will be described and analyzed in this chapter. In any case for all the model it is necessary to implement them by experimental precise parameter related to the material developed for application.

The dependence from the composition in determining mechanical properties as well as the characteristic temperatures of the alloys has been explained in the previous chapter. According to the application, transformation temperatures may need to be shifted, making thermal treatments needed: this, as previously explained, produces precipitates, making it even more difficult to monitor the internal composition of the alloy and the distribution of the defects. Therefore, it is unavoidable that a characterization of the material before, but especially after the thermal treatment happens to be not only suggested, but essential. Torque-rotation tests and strain recovery tests will be described and analysed, as they allow to find Clausius-Clapeyron coefficients and to study the pseudoelasticity behavior in different temperature and strain conditions, thus defining the tube's mechanical properties.

2.1. Tubes preparation

As a first step, the tubes have been cut to a length of 14 cm, considering that 2.5 cm for each edge would be used to block the tubes into the machine that performs the following tests. This choice led to an operative length of 9 cm, whose definition is carefully described in paragraph 3.1. The cut has been performed with the Dremel 4000 variable speed rotary tool. While cutting, some distilled water has been added in proximity of the cut region, to cool the tube and prevent overheatingand break of the material which could happen because of the high temperature reached during the cut.

Figure 2.1 Cutting phase instrumentation

The burrs deriving from the cut of the tubes have been removed through an abrasion process, being careful to add water on the abrasive material in order not to generate high temperatures. Having the diameter of the tube clean and free from burrs is necessary to insert a plug in each end of the tube before performing the tests: in this way it is possible to prevent the deformation of the tube when clamped. All the residual water present on the sample must be then carefully dried, using compressed air, both outside and inside to avoid the oxidation of the sample. Before and after suitable thermal treatment to regulate the transformation temperature necessary for applicationthe tubes underwent a DSC analysis, in order to determine their transformation temperatures.

Figure 2.2 Abrasion and drying instrumentation

2.2. DSC Analysis

Differential Scanning Calorimetry, or DSC, is a thermal analysis technique that looks at how a material transfer or absorbs heat in correspondance of phase transition. A sample of known mass is heated and cooled so that the changes in its temperatures are tracked as changes in the heat flow. In a heat flux DSC, the endothermic peaks point down, since the sample absorbs heat, being cooler than the furnace. The reverse logic applies to exothermic events, where energy is released. In case a Shape Memory

Alloy undergoes a DSC analysis, the peaks represent the phase transformations occurring with temperature change. Respectively, the peak pointing downward is the transformation towards austenite (endothermic) obtained while heating, while the peak pointing upwards indicates the transformation towards martensite (esothermic) obtained while cooling. The transformation temperatures are obtained throughthe tangent method, in which the intersection point is found between the tangent at the peak's inflection point and the straight line at the base of the heating-cooling curve. When performing a DSC analysis, a temperature rate must be selected, and generally it is good to chose 10°C/min: higher rates, may provide cleaner enthalpy peaks, but could compromise the accuracy in transformation temperatures due to the thermal lag. The reason why it is called "differential" scanning calorimetry lies in the fact that the small sample introduced in the machine that performs the analysis is put in a pan while another identical pan remains empty and works as a reference: all the measures derives from a comparison and a subtraction of temperature's signal between the full pan and the empty pan. This also allows to cut off from the measurements external disturbances, which affect the two pans in the same way. In order to perform a DSC, a small sample with a maximum weight of 50mg must be obtained.

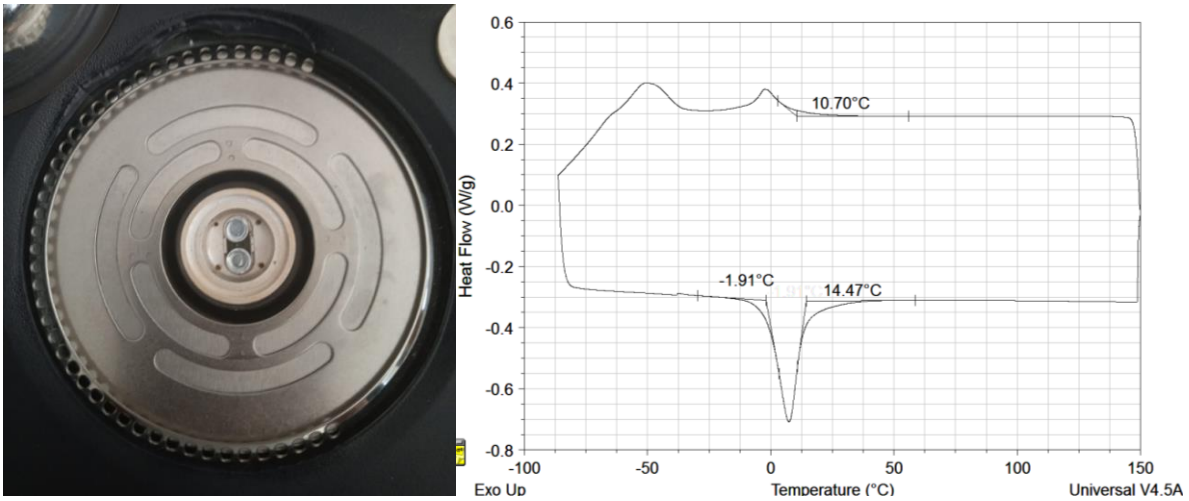

Figure 2.3 DSC of the 6mm-tube sample before thermal treatment

The first DSC analysis was carried out on a sample of the tube with external diameter of 6mm. The limit temperatures were chosen to be -80°C and 150°C. The transformation temperatures of the sample identified through the DSC suggested that a thermal treatment was required, since the martensite temperature is extremely low and already at T=14°C the sample would completely be in austenite, meaning that at room temperature, with $T>A_f$, no actuation would be obtained. From the DSC it is visible the sharp peak of austenite below, in the endothermic region, and two peaks above, in the exothermic region: the second lower peak highlights the presence of the romboedric phase, while the first one, at lower temperatures is the martensite peak.

2.3. Thermal treatment

To perform the thermal treatment a Lenton furnace able to reach a temperature of 1100°C has been used, and the temperature has been chosen according to past experiences where it was discovered that the best results, meaning the sharpest peak visible from a DSC analysis, were obtained leaving the tubes at 570°C for 1 hour and then performing water quenching.

Figure 2.4 Lenton furnace and quenching water

The temperature inside the chamber was monitored by another thermocouple not in contact with the walls. The tubes undergoing the treatment were put on a refractory material, and when the thermal treatment reached its end, the tubes were quickly quenched and a darker color was visible on the surface of the tubes caused by the formation of oxides during the treatment. After the thermal treatment, a little portion of material has been cut in order to perform a DSC analysis and check if the actual shift in temperature has been obtained. As it is evident from the DSC in Figure 2.5, the peaks of the graph are shifted towards higher temperatures and, as it often happens after a thermal treatment, they are not as sharp as in the DSC in Figure 2.3. This is valid especially for the austenite peak and the peak corresponding to the romboedric phase, which after the thermal treatment is merged with the martensite peak. This is due to the formation of precipitates which are the origin of the shift in temperature.

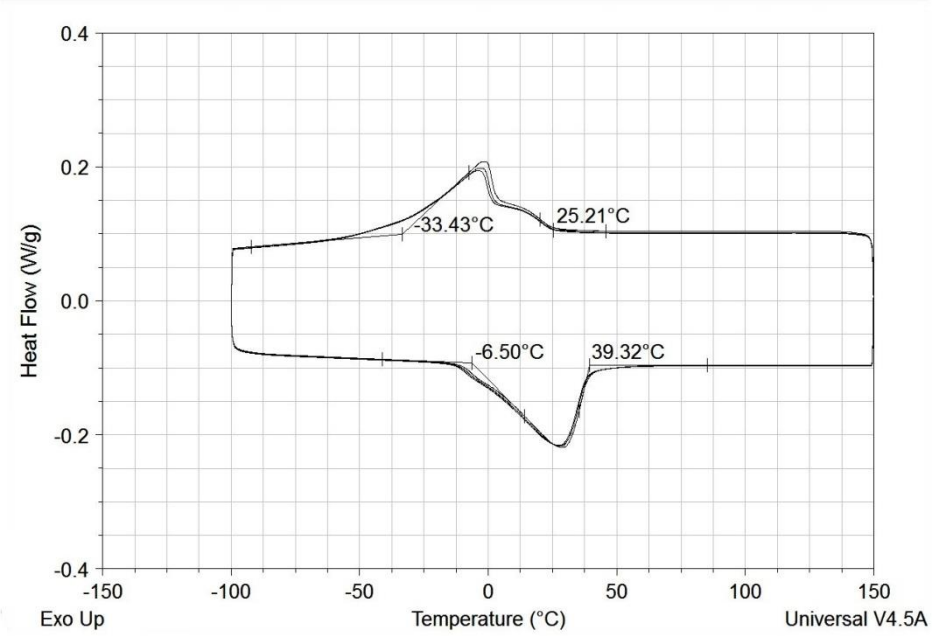

Figure 2.5 DSC of 6mm-tube after thermal treatment

Here the transformation temperatures identified through the tangent method before and after the thermal treatment are reported.

Transformation Temperature	Before Thermal Treatment	After Thermal Treatment
M_f	< -80°C	-33.4°C
M_s	10.7°C	25.2°C
A_s	-1.9°C	-6.5°C
A_f	14.4°C	39.2°C

Table 2.1 Transformation temperatures before and after thermal treatment

2.4. Torque-Rotation test

The Torque-Rotation tests have been the first ones performed for the thermomechanical characterization of Shape Memory Alloy tubes, as they enable to study the behavior of the material and its potentialities. They have been performed using the Instron E3000 mechanical torsional equipment, on which two extensions and two grabs have been mounted to keep the sample in the central region of the thermal chamber. A calibration of this equipment has been performed before and after the placement of the tube. A dynamic calibration has also been performed so that the stiffness of the sample can be computed: this is a parameter used by the Instron to set the controls to be performed during the tests.

The temperatures chosen for performing the torque-rotation test have been decided in such a way to obtain the corresponding curves when the material is completely martensitic, completely austenitic, and in some intermediate phases, in order to follow the behavior of the material by changing the temperature. For this reason, The DSC curve was taken into account in order to identify the two limit temperatures. The tests have been performed starting from -40°C (complete martensite) until arriving at 60°C (complete austenite), with each intermediate test performed every 20°C.

Figure 2.6 Instron E3000 with mounted sample

The setup of the Instron is done using a dedicated software in order to define a precise sequence, accurately defined in order to obtain good results. This sequence is composed of several steps and it starts with Step 1 imposing 3MPa of linear preload, and 0.001 Nm of pre-torsion: this ensures that while the temperature changes to reach the imposed set point, making deformations happen in the material, the Instron's grabs are capable of "following" the tube's deformations, thus keeping the same relative position. In the Step 2 the temperature ramp is imposed to a rate of 5°C/min, while the Step 3 consists in holding the temperature for a certain amount of time: this ensures that the temperature is actually reached in a uniform way in all the chamber and in the sample. This time is longer for very low temperature, so it is set to 30 minutes for the tests at -40°C and -20°C: reaching these temperatures is harder and requires the use of liquid nitrogen, while for higher temperature the holding time can be kept shorter. In the Step 4, also called "Balance", the digital position and the digital rotation are set to zero: this happens because the real measure is going to start, so the current configuration is set as a reference. Finally, the Step 5 starts, imposing the load, which in this case is chosen to be a rotation with a rate of 60°/min.

Once the maximum rotation of 180° is reached, the sample is discharged, completing the Step 6.

Figure 2.7 The use of Nitrogen was required to reach low temperatures

2.4.1. Tube 6mm

The first Torque-Rotation tests have been performed on the tube with 6mm diameter. The first temperature to be tested has been T= 0°C, with an imposed rotation of 180°. This limit to the rotation was imposed to avoid the plastic behavior of the sample and, considering that the application will only require a rotation of 90°, the limit was considered very conservative. After this first test, the temperature has been decreased for the following two tests, respectively to T = -40°C and T= -20°C. It can be noticed that both the tests have been manually interrupted before the rotation reached the limit value of 180°. This was done to avoid the plasticization of the material, which is visible especially in the curve at T=-40°C. After these results, two countermeasures were taken: the former is that a new tube was produced since the one used in the tests was compromised due to the precipitates formed during the plasticization; the latter consists in limiting the imposed rotation to a lower value, chosen to be 120°. This was considered acceptable since it anyway provides a good

margin with respect to the rotation of 90° required for the application. It must be noticed that after every test the sample is affected by a residual deformation, which must be removed by heating the sample itself: this was done using a dedicated hairdryer every time before performing a new test. After producing a new tube with the same process and thermal treatment previously discussed, the tests were performed at temperatures of 20°C, 40°C, and 60°C. The curves at 20°C and 40°C are smooth and with a definite plateau, which shows a different slope with respect to the ones at lower temperatures. This is expected because of the transition to austenite, which is already almost completed at 40°C. At this temperature the residual rotation is 30°, probably due in part to a residual presence of martensite in the structure. For this reason, also in this case it is better to use the hairdryer to transform everything back to austenite. The irregular shape of the plateau obtained during the test at 60°C is due to a slip of the tube which probably was not perfectly blocked in the grabs. The reason of this could rely in the fact that the grabs are not specific for tubes, but for wires, and it is also possible that the hand tightening was not enough when that torques were reached. Nevertheless, the test was considered acceptable since, after every slip, the trend of the curve starts again as expected. It can be assumed that without the slips a slightly higher torque could have been achieved, and a greater rotation recovery could have been visible for this curve. Nevertheless, an even lower residual rotation was expected, so it has been hypothesized that also a continuous slip, not visible clearly from the curves, could have been present. The use of the hairdryer after this test is useless, since the temperature is already above the austenite finish temperature. The residual deformation can no longer be recovered, and it is due to the excessive number of precipitates formed during the thermal treatment that create the defects in the alloy's crystalline lattice. In general in all the curves it is present an initial linear region characteristic of the elastic behavior, which has an higher slope for curves obtained with the sample in austenite phase, as it was expected since in austenite condition the stiffness is higher (2.4.3.1).

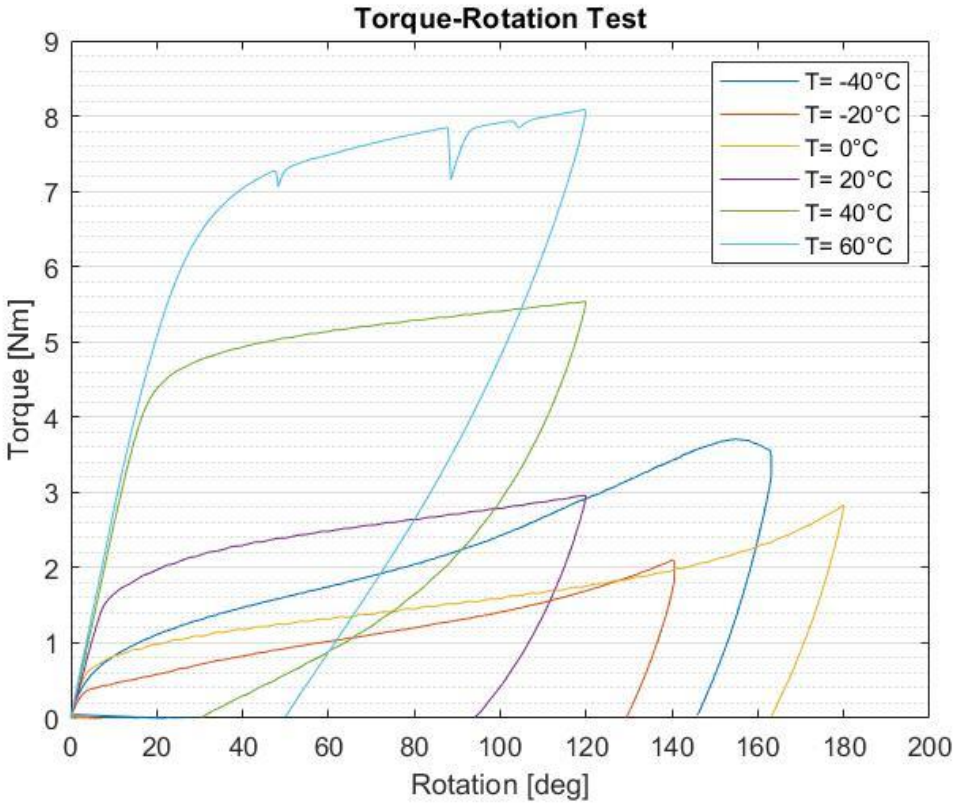

Figure 2.8 Torque-Rotation test of the 6mm-tube

Increasing the torsional load causes then the formation of a plateau: it has a slightly different inclination for martensite and austenite, since in the former case, meaning at lower temperatures, it indicates the detwinning of the martensite, while in the latter case, so at higher temperatures, it represents the formation of stress-induced detwinned martensite. At higher temperature the residual rotation obtained when removing the load is indeed lower with respect to the one obtained in martensite condition, which in turn maintains quite high residual deformations. Overall, it is evident that by increasing the temperature also the austenitic fraction increases inside the alloy, leading to an increased stiffeness, and as a consequence to an increment of critical and maximum stresses.

2.4.2. Tube 3mm

A smaller tube has been tested to see if it could be used to arm the 6mm-tube, in order to design the actuator exploiting one tube inside the other in a coaxial

configuration. A tube with diameter of 3 mm has been tested, starting from the first test performed at T=-40°C with an imposed rotation of 180°. The sample is completely in martensite, as it is evident looking at the DSC done after performing the thermal treatment as the 6mm-tube.

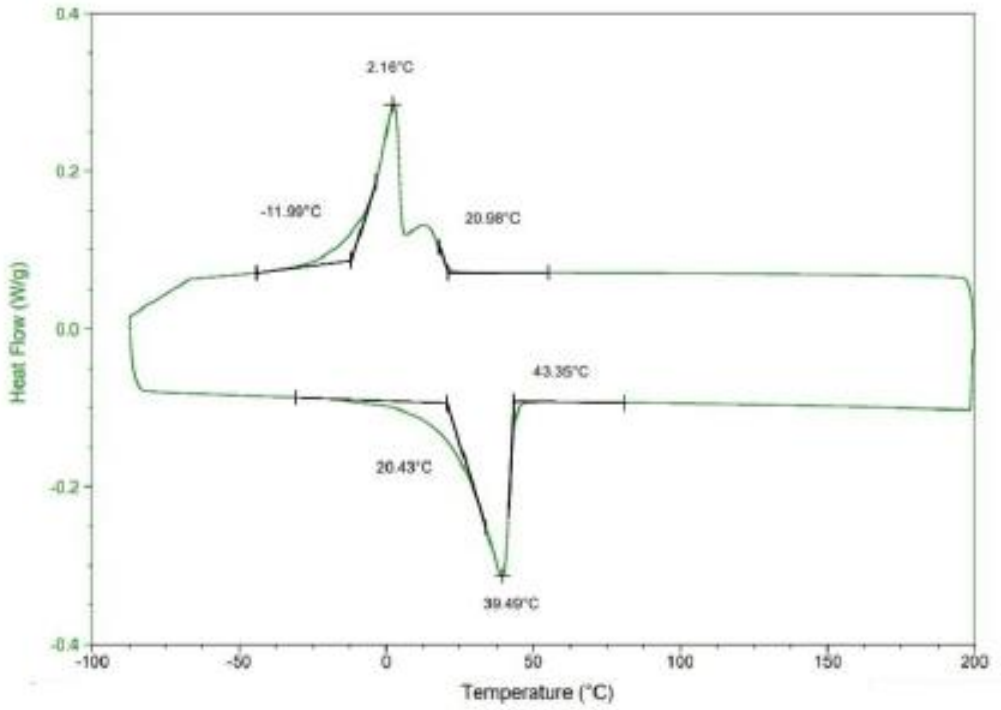

Figure 2.9 DSC of the 3mm-tube

As expected,the reached torque is quite small, as it can be seen in Figure 2.10. In the curve obtained from the test at T=-20°C it can be immediately noted that the curve has no more a perfectly definite plateau, but it presents an oscillatory behavior due to a not so stable blocking process during the measure. The fact that the unloading does not end at torque equal to zero, can be due to the sensitivity of the load cell. Comparing the results obtained in the first two tests with the results obtained in a previous thesis [26], where the same test was performed on a tube with the same diameter and which underwent the same thermal treatment, it has been noticed that the values of critical stress and maximum torque were very similar: it has been hypothesized that similar results, at least same order of magnitude, could have been

expected also for the other tests. From this simple consideration it came out that the tube with smaller diameter couldn't be strong enough to arm the 6mm-diameter tube, which requires torques of approximately 2.8 Nm to perform a 90° rotation at room temperature.

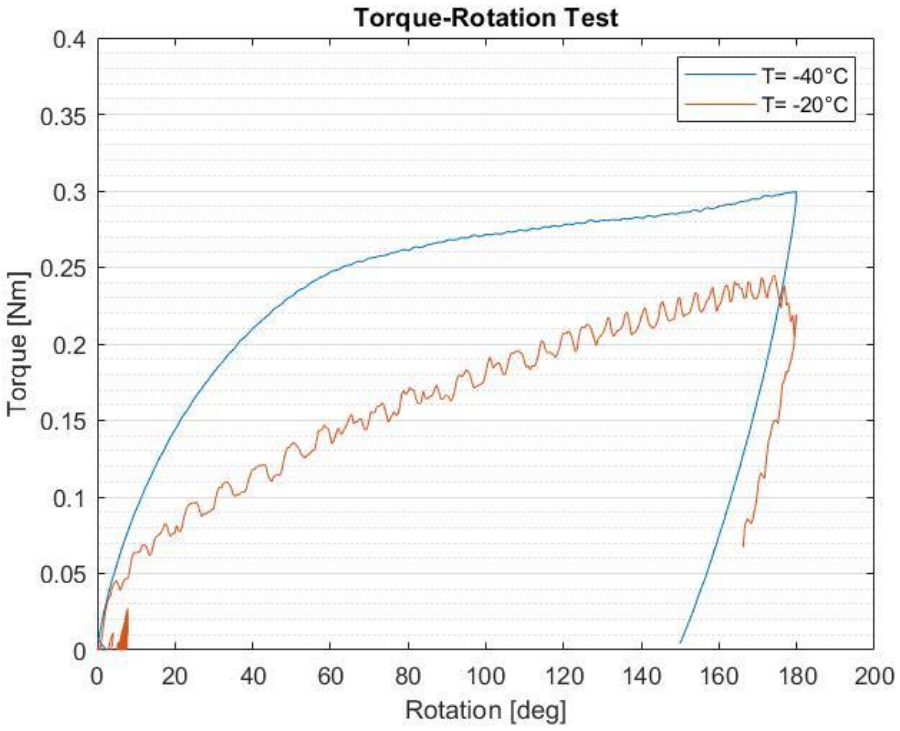

Figure 2.10 Torque-Rotation test of the 3mm-tube

2.4.3. Bar 3mm

As a consequence, a bar of 3 mm diameter was considered for the application since it has a working section (7.07 mm^2) comparable with the one of the 6mm-tube (8.64 mm^2), and it allows to keep the same compact final configuration for the actuator. Being the bar superelastic, as the 6mm-tube, it underwent the same thermal treatment to shift the transformation temperatures for the material to show the shape memory effect instead of superelasticity in the temperature ranges of the application. The result of the DSC analysis after performing the thermal treatment at 570°C for 1 hour and then water quenching can be seen in Figure 2.11.

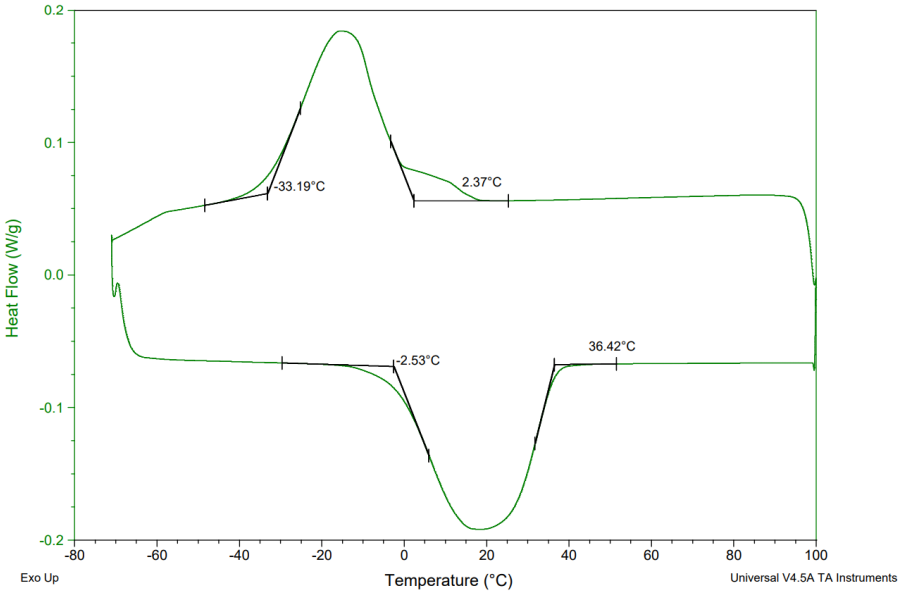

Figure 2.11 DSC of 3mm-bar

The torque-rotation tests were then performed also for this sample at temperatures of -20°C, 20°C, 65°C to show the behavior of the alloy in complete martensite phase, intermediate phase, complete austenite phase respectively. From the curves it is evident that at high temperatures the rod can produce a torque near to the one actually needed to produce a torsion of 90° in the 6mm-tube.

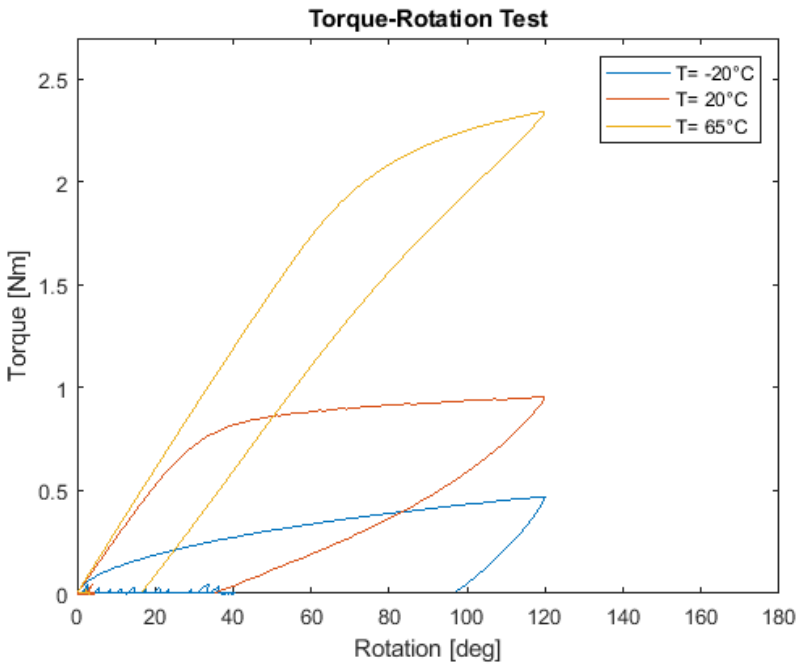

Figure 2.12 Torque-Rotation test of the 3mm-bar

2.4.3.1. Shear Modulus Determination

One parameter that can be recovered from the Torque-Rotation tests is the shear modulus of the material. The curves obtained with the Torque-Rotation tests can be used to determine it as it is graphically represented by the slope of the tangents to the curves in their linear region. As expected, the shear modulus of the material in austenitic state is higher with respect to the one the material exhibits in martensitic state, confirming that the stiffness of austenite is higher with respect to martensite.

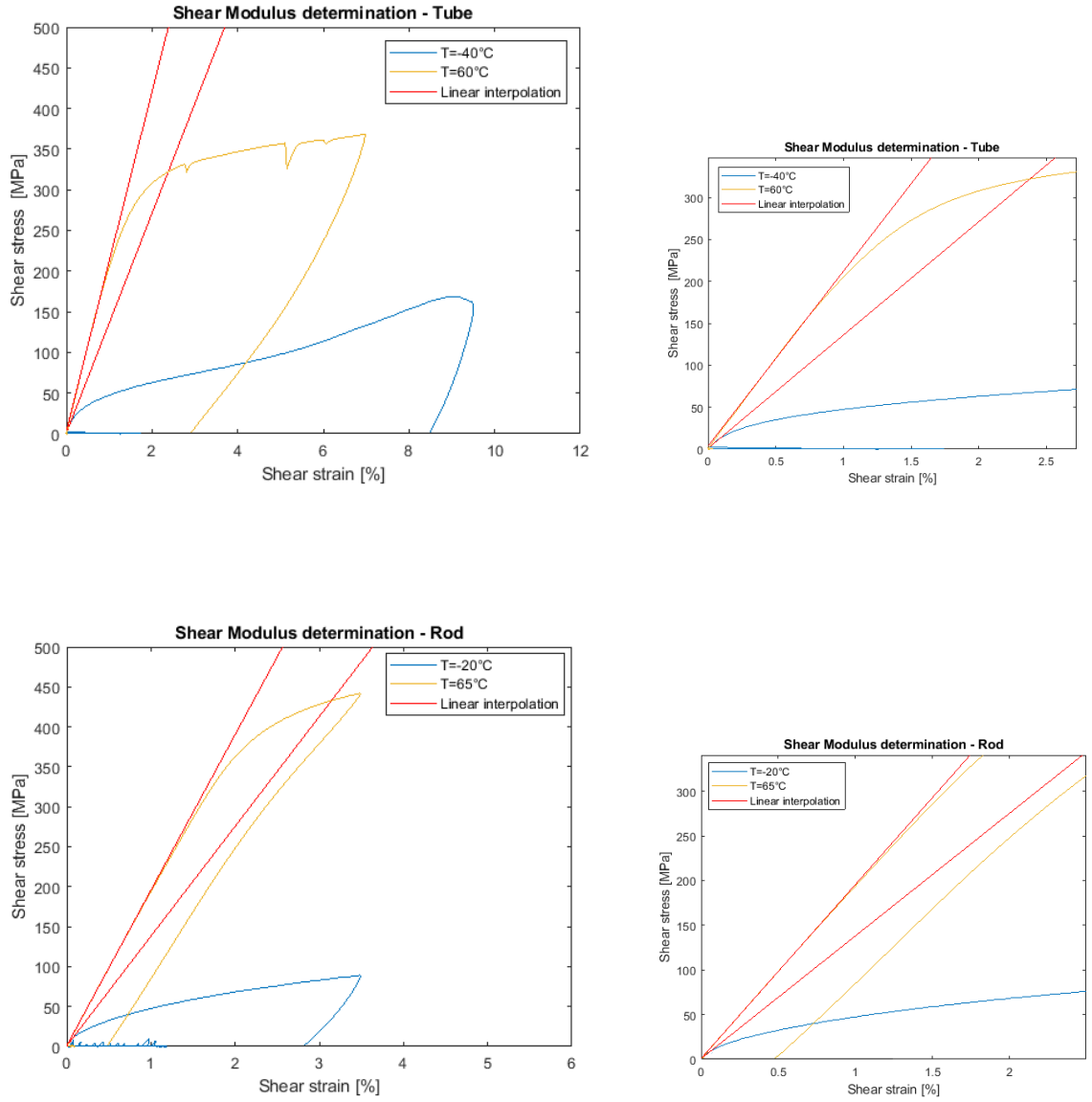

Figure 2.13 Shear modulus graphical representation through linear interpolation of stress-strain curve linear segment

The red lines, obtained through linear interpolation, highlight the different inclination of the linear segments of the curves obtained in austenitic and martensitic phases: computing their inclination, the shear modulus is obtained.
This graph is obtained by converting respectively the applied torque into shear stress and the rotation into shear strain according to the following relationships:

$$\text{Shear Stress} = \text{Torque} \cdot \frac{r}{J};$$

$$\text{Shear Strain} = \text{Rotation} \cdot \frac{r}{L};$$

Where r is the outer radius of the tube, J is the polar area moment of inertia, and L is the length of the tube.

Shear Modulus [GPa]	**Tube**	**Rod**	**SMA tube**	**SE tube**
$\mathbf{G}_{martensite}$	12.8	12.4	6.8	18.7
$\mathbf{G}_{austenite}$	19.9	15	16.9	18.7

Table 2.2 Shear modulus values

The fact that the shear modulus is slightly different between the two geometries, despite having performed the same thermal treatment on the same material, can be due to the different distribution of precipitates in the two samples, meaning that the same thermal treatment, even though performed on the same material, can result in different crystallographic structures depending on the geometry. Anyway, the tube's values are in agreement with shear modulus values found in literature about a shape memory tube and a superelastic tube [27], especially as regards austenite. The difference found for martensite can be due to the fact that the samples used in this thesis are superelastic tubes thermal treated to exibit a shape memory behavior at the temperature of interest, and so, the high presence of the precipitates may be the cause for such intermediate value of the shear modulus in the martensitic state.

2.5. Strain-Recovery test

During the Strain-Recovery test the sample is subjected to a thermal cycle between two limiting temperatures chosen according to the transformation temperatures Austenite Finish and Martensite Finish. The range of temperature reached in this test will be bigger than the difference of the two (T_{Af}-T_{Mf}) in order to guarantee complete transition from complete austenite to complete martensite. The sample is stabilized in complete austenite reaching T = 90°C and then, after having applied a constant torque, the temperature is reduced until reaching a value of T = -50°C. Once this temperature is reached, it can be seen the angle at which the equilibrium between the applied torque and the resistance of the material (martensite phase) occurs. The cycle is completed by making the temperature increase again to the initial one, allowing the recovery of the rotation through shape memory effect. At the end of the test a residual deformation can be identified thanks to the gap between the starting point and the ending point of the curve: this is the rotation the material is not able to recover, and it increases with increasing torque applied.

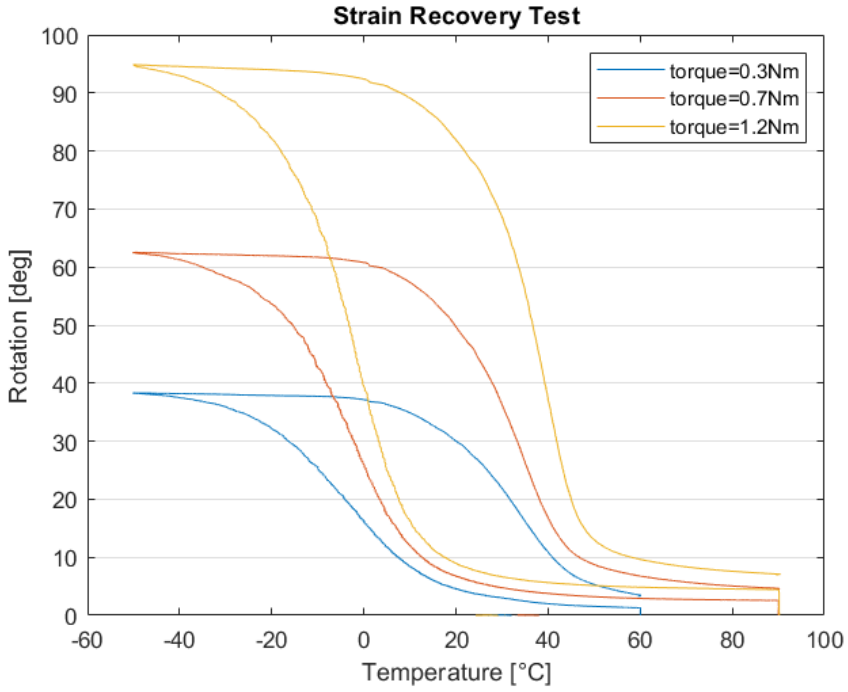

Figure 2.14 Strain-Recovery test of the 6mm-tube

2.5.1. Clausius-Clapeyron coefficients determination

The curves obtained through the Strain-Recovery test can be exploited to find the value of the transformation temperatures, which are identified by the intersection points of the tangents to the linear segments.

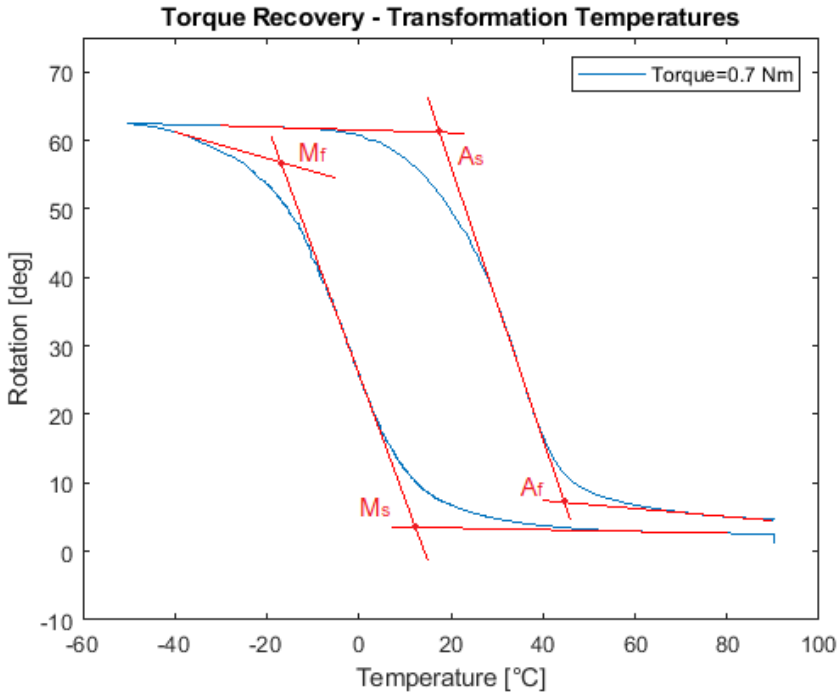

Figure 2.15 Graphical method to find transformation temperatures

Once the transformation temperatures for each test are obtained, the Clausius-Clapeyron coefficients can be determined by computing the slope of the curves obtained with the just-mentioned temperatures.

Applied Torque [Nm]	**M_f [°C]**	**M_s [°C]**	**A_s [°C]**	**A_f [°C]**
0.3	-20	10.9	16	44
0.7	-18.7	11.8	17	45
1.2	-17	12.5	25.4	47.6

Table 2.3 Transformation temperatures for each torque

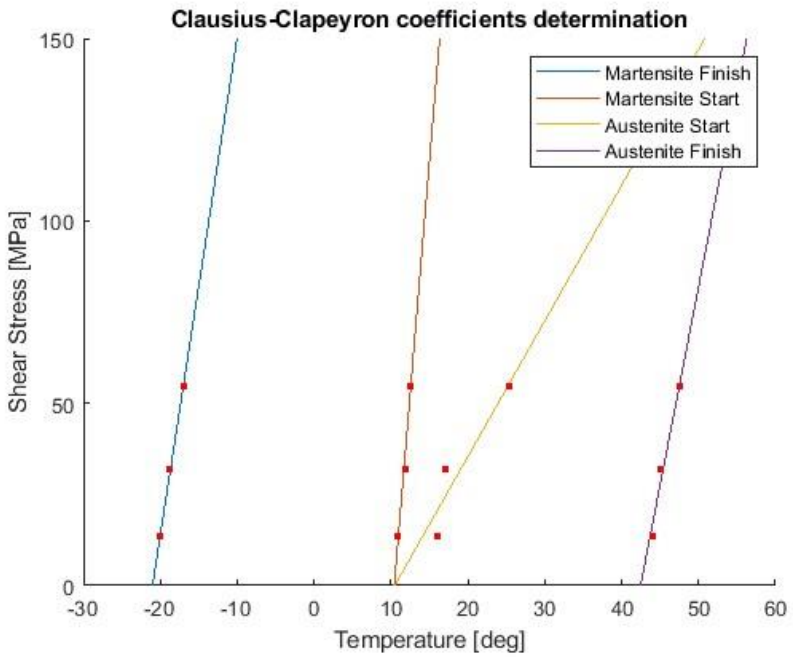

Figure 2.16 Interpolation of transformation temperatures for the determination of Clausius-Clapeyron coefficients

From this graph it should be evident that, by increasing the applied load, the transformation temperatures increase as well, making the interpolating lines characterized by a positive slope. In general, the expectations are meet by the results, even though the orange line, the one representing the M_s transformation temperatures is almost vertical. This is due in particular to the first point of the line, corresponding to the transformation temperature when the torque is equal to 0.3N: the value, indeed, is particularly high. The reason behind this anomalous high temperature can be found in the fact that in the strain recovery test with 0.3N torque the sample was heated only to 60°C, so maybe it was not completely in austenite yet, when the torque was applied. As a consequence, when cooling, the transformation started earlier, or, in other words, at higher temperatures.

In general, it must be remembered that in the torsional configuration the behavior of the SMA material is not as predictable as when it is exploited in the traction

configuration: in the former case the associated stresses vary depending on the location, while in the latter case a uniform deformation is experienced by the section. The values obtained for the Clausius-Clapeyron coefficients are here reported.

Clausius-Clapeyroncoefficients	**[MPa/°C]**
$\mathbf{C_{M_f}}$	13.6
$\mathbf{C_{M_s}}$	25.4
$\mathbf{C_{A_s}}$	3.7
$\mathbf{C_{A_f}}$	10.9

Table 2.4 Clausius-Clapeyron coefficients for each phase

2.6. Outcomes and consequences

The results obtained with the Torque-Rotation test revealed, as seen, that not a perfect rotation recovery was present at almost every temperature, although some good results are still obtained for higher temperature. It must be noticed that the material used is a treated superelastic material, which undoubtedly exhibits a worse behavior than a shape memory material. Indeed, for a real application it is recommended to use dedicated materials produced with the most suited composition, limiting the thermal treatments, which produce defects making the behavior and prediction of the behavior more difficult. Furthermore, the test conducted on the 3mm-bar revealed that it is worth thinking about a compact configuration with an external tube and an internal coaxial bar, both working in torsional antagonism. It is true that the torques developed by the 3mm-rod are not enough to rearm the 6mm-tube, but considering that by slightly increasing the diameter of the rod higher torque would be reachable, we can deduce that a bar of

3.5 mm diameter would be able to arm the 6-mm tube bar (3.5 mm diameter already corresponds to a section of 9.62 mm^2, bigger than the tube's one). The DSC performed after the thermal treatment revealed that for the thesis' aim of studying a torsional antagonistic behavior of the tubes, there is the need of starting from very low temperatures in order to obtain martensite. The Strain-Recovery curves show that temperatures between 0°C and 45°C are the best ones to perform cycling, as they correspond to the flex points of the curve, which represent the medium temperatures of the transformation and thus the maximum strain variation. Anyway, to better monitor the material's behavior, a temperature range of -20°C/60°C has been selected to perform the experiment.

After this preliminary characterization, which also highlights the need of characterizing the tubes' torsional behaviour exploiting such a wide temperature range, the idea of starting from a characterization of the tubes arranged in series, as anticipated in the previous chapter, is confirmed to be the most suitable starting point.

3 Experimental setup

The interest in designing a SMA torsional actuator and choosing antagonism as the rearm mechanism has led to the desire of creating a real demonstrator for characterizing antagonism and validating the fundamental concepts of this thesis. When designing the experimental setup for building the demonstrator, the theoretical aspects behind SMA behavior and the experience derived from characterizing it at the CNR have been taken into consideration. This was done to replicate the optimum conditions necessary for the actuator to function.

Each tube must be clamped to the support structure at one edge, while at the other edge they need to be connected in series to each other. For clarity's sake, we will refer to one tube as "Tube1" and the other as "Tube2". When Tube1 is actuated, its unclamped edge, which is free to rotate, transmits the torque to Tube2, effectively arming it. Once an equilibrium configuration is reached, meaning Tube1 has completed its transformation to austenite, some time is waited in order for the temperature to decrease. Then Tube2 is actuated, generating an opposite rotation that returns Tube1 to its original configuration, arming it as well.

The waiting time for cooling is necessary because otherwise Tube1 would still be in austenite phase, and this would not allow the exploitation of the Shape Memory Effect, which requires the transformation towards austenite to happen in order to recover the deformation, and thus the original shape. To initiate this sequence, Tube1 must undergo a pre-torsion before being mounted on the experimental setup. Imparting this rotation shifts the tube from a martensite structure to a martensite

detwinned structure. To actuate Tube1, the temperature will be increased until it surpasses A_f, thus promoting the transition to austenite. During this transformation, as said, the generated torsional strain corresponds to a rotation, which is transmitted to Tube2, equal and opposite with respect to the pre-imposed one on Tube1. The rotation imposed on Tube1 as a starting point of the sequence is recovered, and now multiple actuation can be performed without disassembling the setup.

Considering that certain interface components will be required to connect the tubes to the structure and to each other, the experimental setup has been develop vertically. This approach eliminates the bending moment generated by the weight of the components, that would otherwise affect the tubes if everything were horizontal. A first representation of the setup is here reported, while many components will be described later on in this chapter.

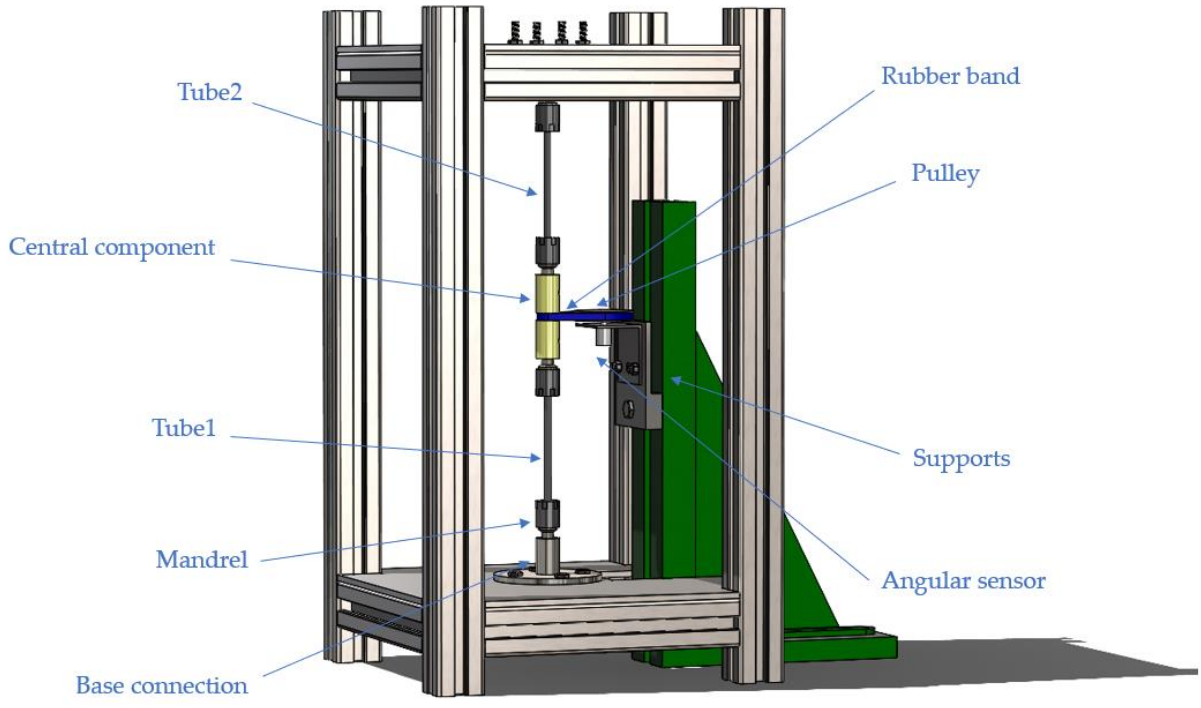

Figure 3.1 Graphical representation of the experimental setup

The four mandrels used has been bought together with the 6mm collet chuck springs, which allow for a correct grasping of the tubes. The mandrels have been cut and leveled in two areas orthogonal one to the other to assure a better interaction with

the set screws that are used to fasten the mandrel with the rest of the chain. Two aluminum interface components have been designed to allow the clamping of the first and last mandrel to the structure, while the central mandrels are connected through an apposite shaped aluminum component. The structure is composed by Bosch tubes and completed by two aluminum plates designed to fit the structure and to allow the correct positioning of the pulley's support structure. Overall, the vertical distance between the two plates is 45 cm, and their squared shape has a side of 30cm.

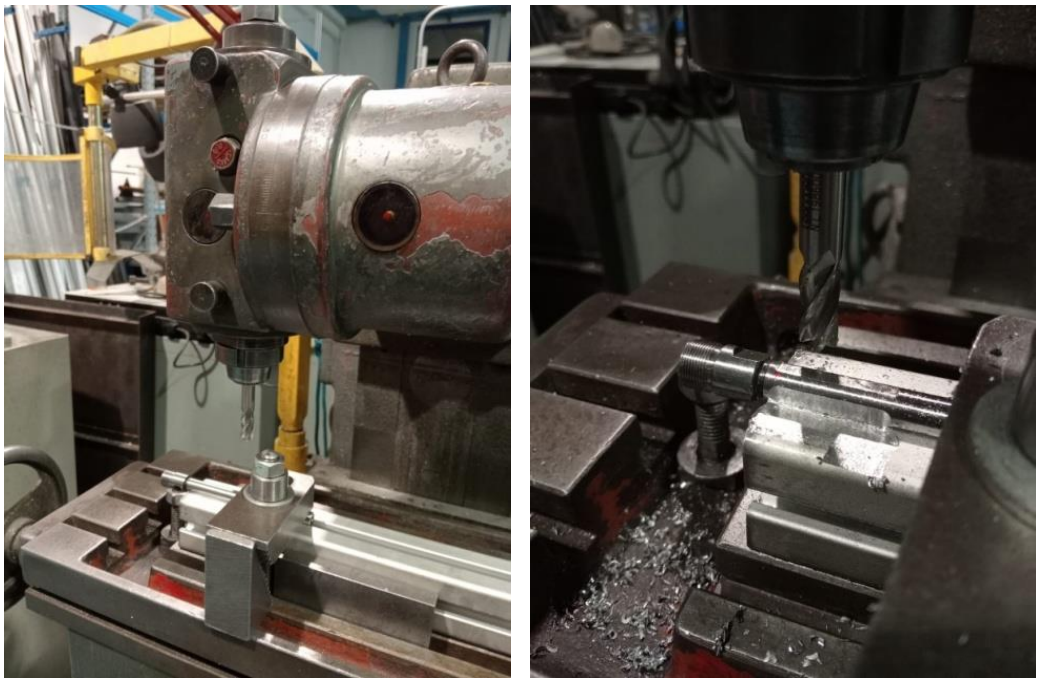

Figure 3.2 Mandrel's milling

The first step before starting the experiment is pre-deforming one tube in order to pass from matensite twinned to martensite detwinned. The transformation temperatures that can be deduced from the DSC are not perfectly clear as regard the martensite start and martensite finish in particular. For this reason, a temperature of -50°C has been chosen as the initial temperature to which both the tubes must be brought, to assure a completely martensitic crystallographic structure. This will be the temperature at which the thermal camera will be open to give the pretorsion to the tube. Choosing such a low temperature allows to have more time to perform this operation: it is indeed foundamental that the tubes do not start the austenitic

transformation. It is of great importance that the tube is kept at a temperature below A_s in that moment: otherwise, a lower part of material would be in martensite detwinned once the setup's chain is closed, causing a decreased rotation recovery to take place. Another reason why this operation must be performed as quikly as possible is that even if the pretorsion is given while the tube is in martensite, if too much time passes before blocking the chain through the set screws and closing the camera, causing the temperature to rise above A_s, part of the rotation will be recovered without being transmitted to the other tube.

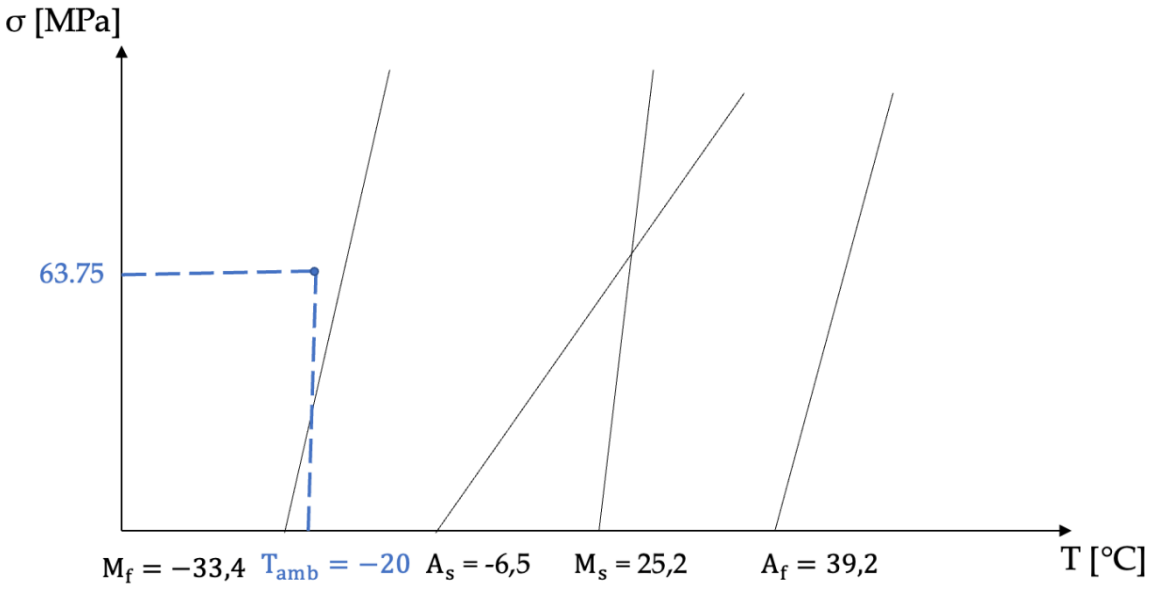

Figure 3.3 Effect of the applied pretorsion

The value on the vertical axis is an estimation of the stress applied when imposing a rotation of 100° while the material is at -20°C: it is obtained from the Torque-Rotation test's graph in Figure 2.8. A value around 100° for the applyied rotation has been considered even though a pretorsion of about 120° has been given: this slightly higher pretorsion is given in order to take into consideration also the elastic return of the material. Moreover, the pretorsion is manually applyied, so there is not a very precise measurement of the actual angle of rotation. In any case, Figure 3.3 is a good approximation of the effect the pretorsion on the material. The inclination of the

transformation lines is obtained considering the values of the Clausius-Clapeyron coefficients summarized in Table 2.4 Clausius-Clapeyron coefficients for each phase
Once the setup is completed with the predeformed tube in martensite detwinned and the other one in martensite, the temperature can be set to -20°C to start the first cycle. This is considered a safe value considering the the austenite start temperature is at -6°C with no load applyied, as the DSC reveals.
At this point the activation sequence can start: the first tube is activated heating it through the constantan wire (the choice of using a constantan wire will be justified and explained later in the chapter) until a temperature well above A_s, chosen to be 60°C, is reached. After the rotation recovery has taken place the current circulation in the wire is interrupted, allowing the components to cool down to -20°C again. At this point the other tube is activated in the same way, it will recover the rotation, arming the first tube as well.

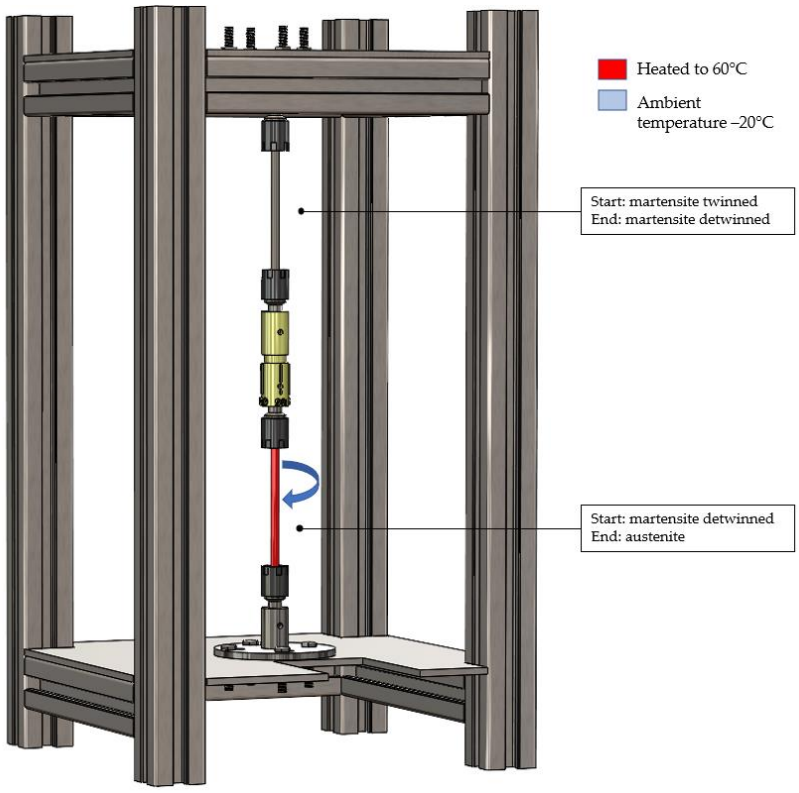

Figure 3.4 First step of the actuation sequence: heating the predeformed tube

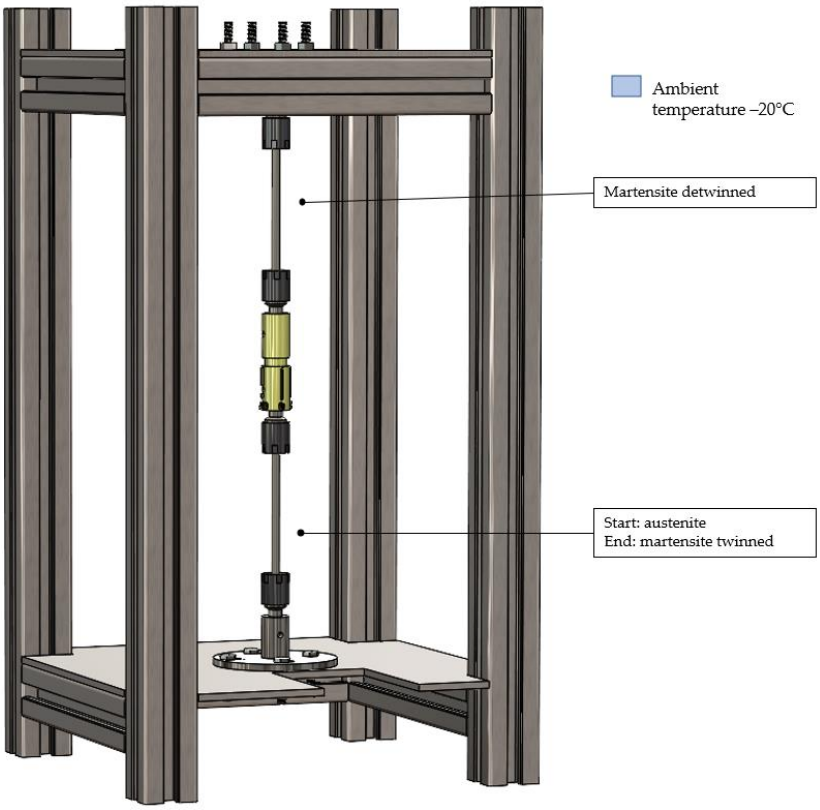

Figure 3.5 Second step of the actuation sequence: cooling of the tubes

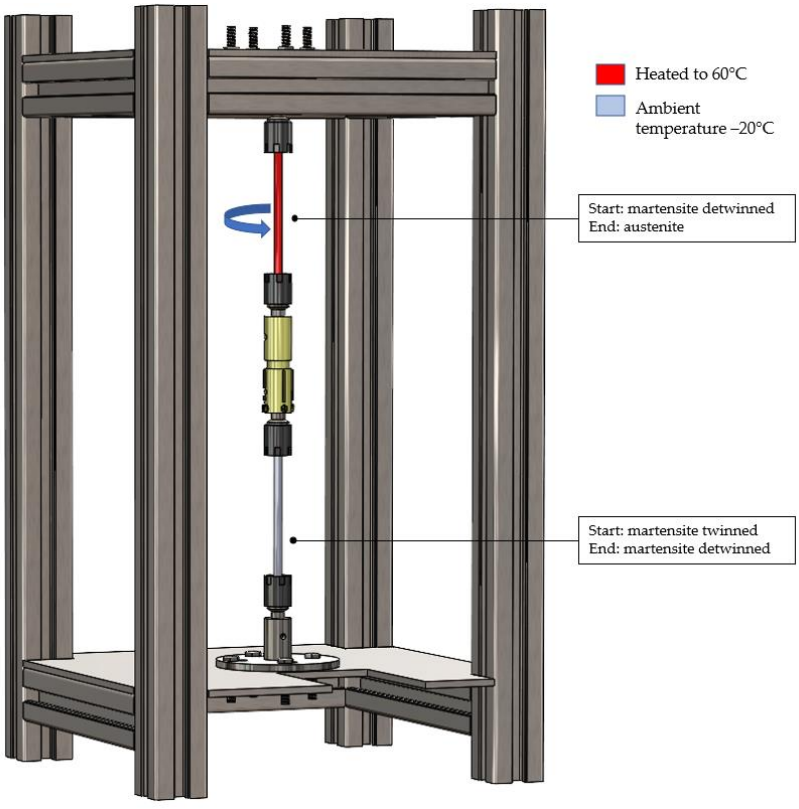

Figure 3.6 Third step of the actuation sequence: heating of the previously armed tube

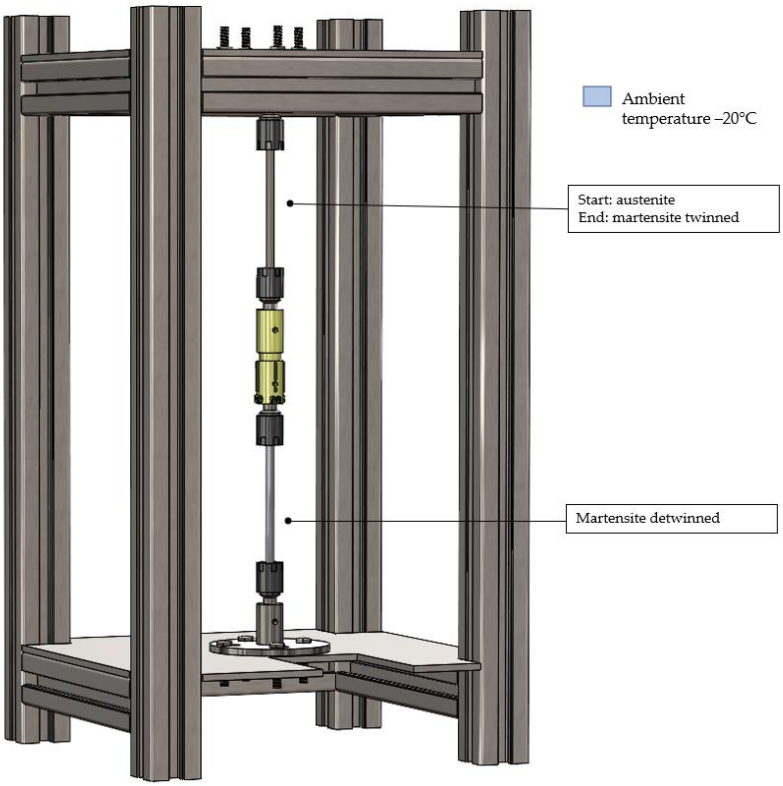

Figure 3.7 Fouth step of the activation sequence: cooling of the tubes

3.1. Cooling strategy

The cooling phase turned out to be foundamental for the functioning of the demonstrator, since it is necessary to bring the material back to the starting martensitic condition: in order to reach such temperature, the environmental chamber of the MTS present in the university's laboratory has been used. Another possibility has also been explored: two small cameras can be built around the tubes, leaving the central 3D-printed components outside, at room temperature. The two cameras will serve as cold room for the tubes thanks to the use of liquid nitrogen pumped into them. In this way, following a sequence of cooling and heating, respectively activating the passage of liquid nitrogen and providing current through the power generator, the experiment could take place in every laboratory room. The practical realization of this adjusted setup has been left as a second viable option worth of developing in case the concept of activation of the tubes via Joule effect and

rearm through antagonism proves to be winning. The first solution, meaning the use of the MTS thermal chamber, allows indeed to go on with the experimental phase without adding further complexity to the setup. Moreover, in this way it is easier to monitor the ambient temperature thanks to integrated thermocouples in the chamber's walls, as well as to set the desired temperature and regulate the nitrogen flux in the chamber thanks to the already installed dedicated software.

3.1.1. Alternative cooling strategy

The possibility of realizing two small cameras only around the tubes allows the central component to work at room temperature, and thus the rotation measurement through the angular sensor. Moreover, having such a low volume to cool down would also reduce the time needed to cool down the SMA samples through nitrogen. The two cameras consist of two cylindrical plastic sleeves containing the tubes, which could be kept separated, allowing, as said, the central component to be kept at room temperature.

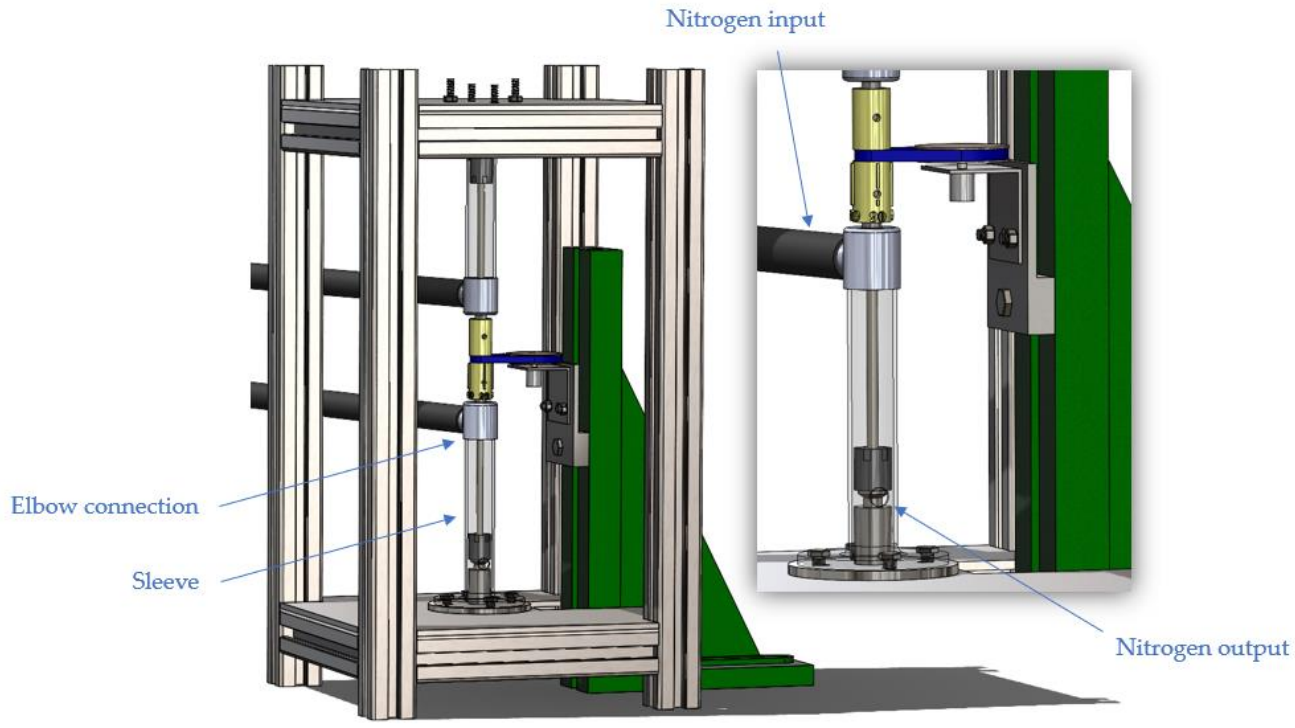

Figure 3.8 Cylindrical sleeves setup configuration

The importance of keeping the central component at room temperature is due to the fact that it allows the interaction of the rotating chain with the angular sensor, which cannot work at low temperatures. The nitrogen will enter and exit the sleeves through two elbow connections, properly drilled to create a passage both for the mandrel, which has to be free to rotate, and for the constantan wire as well as the thermocouples passage. The nitrogen flow will be regulated through solenoid valves in order to keep the temperature constantly at -20°C.

3.1.2. Rotation's measurement

The rotation of the tubes must be accurately measured to understand if all the rotation is recovered, and to check if there is a loss of recovered rotation as the actuation cycles go on. An angular sensor can be used, and in order to integrate it into the experimental setup, apposite components have been designed and produced.

A specific component has been designed to connect the two grabs together, which are blocked to it using two grains. In this way the grab hosting Tube1, the central component, and the grab hosting Tube2, represent a rigid chain of components able to rotate. The central component has been designed to allow also the hosting of a rubber bend, which connect it to an adjacent pulley. The pulley has been mounted on the angular sensor, which is anchored on a metallic support and whose height can be regulated. The chosen angular sensor to be used in the cyclindrical sleeve setup configuration is Model 7280 characterised by 10 turn wirewound and a 7/8'' diameter.

The central component has been initially produced by 3D printing with an ASA filament, in order to make it lighter, reducing its torsional inertia, and because it originated as a temporary solution to allow the first measures and experiments to take place. A torsiometer, indeed, was expected to be used, to measure the torque exchanged between the tubes. Given the long supply times, the alternative solution just described has been adopted, and the experimental setup has been adjusted. The

selected torsiometer was the Futek TFF400 model, with a full-scale of 11 Nm, and an operating temperature between -50°C and +93°C. When the central component turned out to be the final solution it has been produced in aluminum as well, because the threads were not strong enough for being used multiple times and because the low temperatures expected to be reached in the experiment were not suitable for the proper working of the initially chosen material.

The problem of keeping the whole setup at temperatures, is that all the electronic devices cannot be used. That is the case of the angular sensor or of a videocamera to register the experiment, as well as the power generator. With appropriate extension cords the power generator can be taken outside the cold volume, but for the measurements of the rotation a more qualitative measurement technique is the only possibility. For this aim, a graduated scale marking the rotation angle every 10° has been integrated in the setup attaching it on a wheel solidly anchored to the central component.

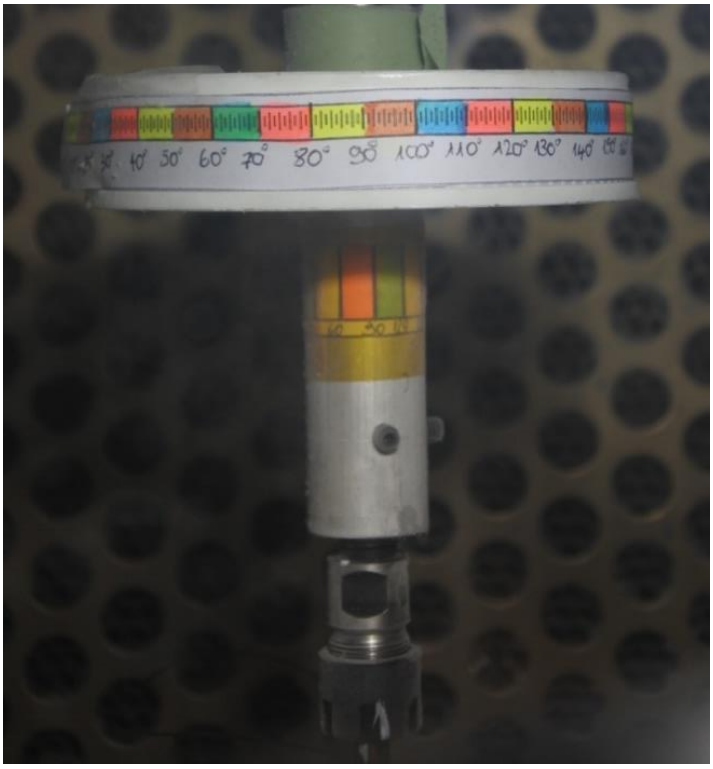

Figure 3.9 Rotation measurements through a graduated scale

3.2. Rotation and length's value determination

The pre-rotation imposed to the first tube will be recovered during the actuation, and it will be transmitted between the tubes during their actuations, according to the sequence previously described. The rotation to be given to Tube1 must be chosen according to the capacity of the tube to recover it. If a rotation is too high the material could enter in the plastic domain, and the deformation would not be totally recovered regardless the transition to austenite takes place. Given that for Shape Memory Alloys the maximum reachable strain to guarantee a recover is 7% a simple Abaqus simulation has been carried out in order to check the torsional strains generated in a tube undergoing different rotations.

The simulations have been carried out on a tube with a geometry characterized by a diameter of 6mm and with diffent lengths, and the material has been described using the values coming from the Torque-Rotation curve at T = -20°C, which are summarized in the following table.

Shear modulus	10.66GPa
Critical stress	16 MPa
Plastic strain	0.06
Poisson's ratio	0.3

Table 3.1 Parameters used in Abaqus simulation

One edge of the tube has been clamped,while a rotation has been applied to the other one. The objective of these simulations was to check which torsional strain levels are obtained in the tubes, considering as a limit value the 7% strains which are the maximum that the tube would be able to recover with the austenite transformation [13]. Obviously, by increasing the length, or by reducing the rotation, a lower and safer level of strain is obtained. Nevertheless, the intrest in studying and validating

through an experiment a significant rotation, guided the choice of the length to obtain the higher rotation possible. Multiple simulations have been carried out, with lengths of 50mm, 90mm and 180mm tested with rotation of 90° and 180°. Here only the most significative oneis presented, obtained for tubes of length equal to 90 mm and applied rotation of 90°.

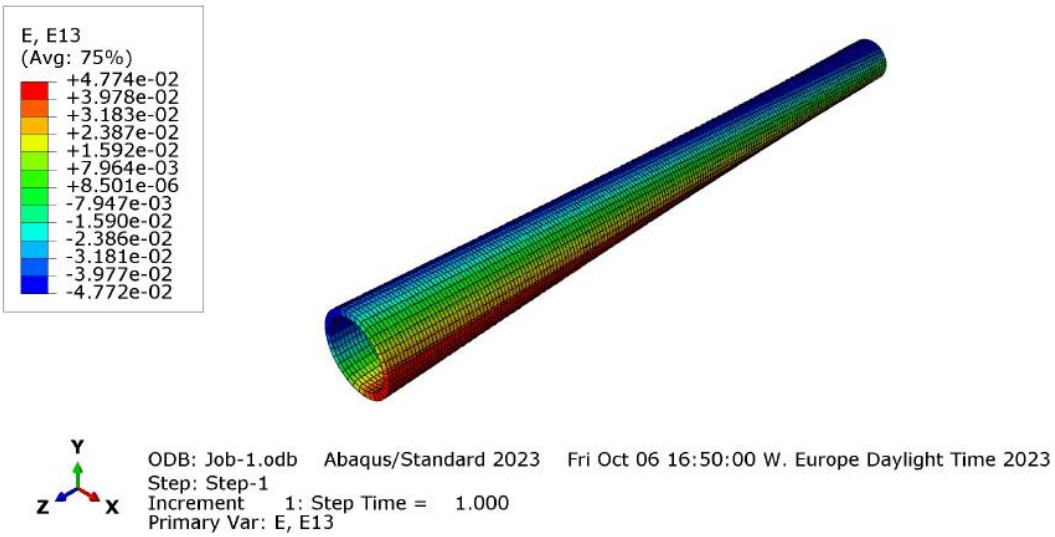

Figure 3.10 Strain ε_{13} generated with a 90° rotation

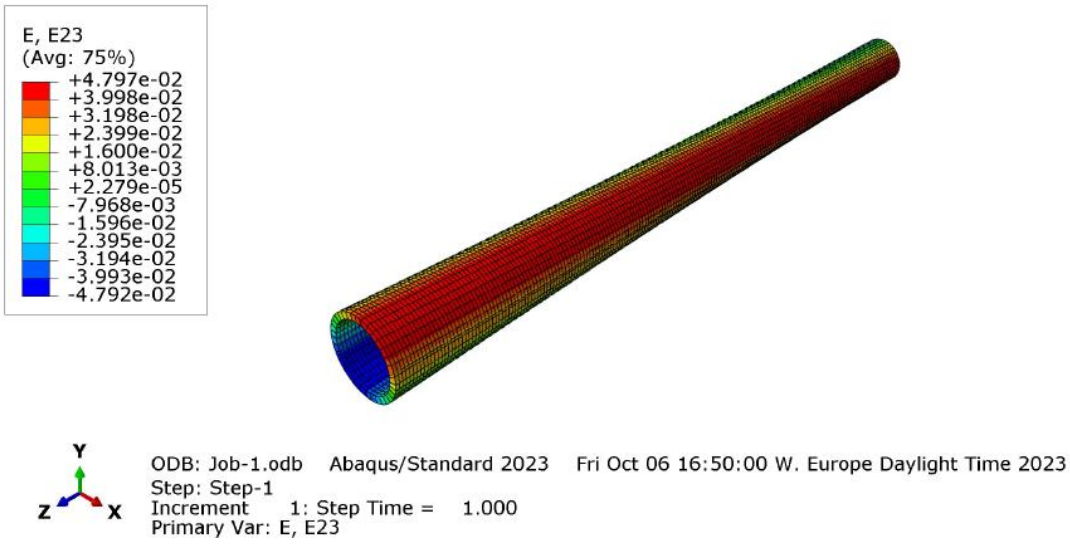

Figure 3.11 Strain ε_{23} generated with a 90° rotation

The torsional strain ε_{13} and ε_{23} are represented in Figure 3.10 and Figure 3.11: as it can be seen the values approach 5%. It wouldn't be safe to overcome this strain level because being the material thermally treated, a plastic deformation could also occur before the theorical value of 7% strain. Moreover, a rotation of 90° is satisfactory also because it allows to simulate the behaviour the tube would have in the space application presented in Chapter 1, where the actuator is responsible for the opening and closing of a CubeSat panel thanks to the rotation of the hinge.

3.3. Temperature's measurement

Since the temperature is a determinant factor in the experimental phase, an accurate monitoring of it has been foreseen. Two preliminary tests have been conducted in order to compare two strategy for measuring temperature: one using thermocouples and one using a thermocamera. The aim of the test was comparing the capability of the two strategies to measure the actual temperature of the tube, in particular it has been checked that the thermocamera results were in agreement with the ones provided by the thermocouples. Moreover, it was useful to relate the value of current required to reach the desired temperature.Testing the thermocamera-registered temperatures allows to have an alternative option in case the use of thermocouples turnes out to be impossible due to the rotation of the tube. Indeed, the thermocouples must stay attached on the surfaceof the tubes, with the risk that during torsion they will no longer be capable of being in contact with the surface due to relative motion. The possibility of placing the thermocouples inside the tubes was also taken into consideration, but due to the presence of the grabs and of strengthening plugs it is not possible.

3.3.1. Thermocouples and thermocamera's measurements

Four thermocouples have been placed on the surface of the tube, at a distance of almost 2 cm one to the other, and fixed to the tube using Kapton scotch tape, which

also provide electrical insulation from the tube itself. The tube,which is kept at a room temperature of 29°C on a table, has been connected to the 10A generator through two crocoldile clips, allowing current to flow. The value of the set current and voltage are respectively 10.4 A and 1.8 V, while the time needed to heat up the tube to a temperature of 60°C and the time needed for cooling it to room temperature are respectively 7 minutes and 11 minutes. This last value is almost in agreement with what was expected after a simple Matlab simulation, where the convection coefficient has been chosen as $15\frac{\mathrm{W}}{\mathrm{m^2K}}$ as an intermediate value between the range of values it can assume in case of natural convection (5-25 $\frac{\mathrm{W}}{\mathrm{m^2K}}$).

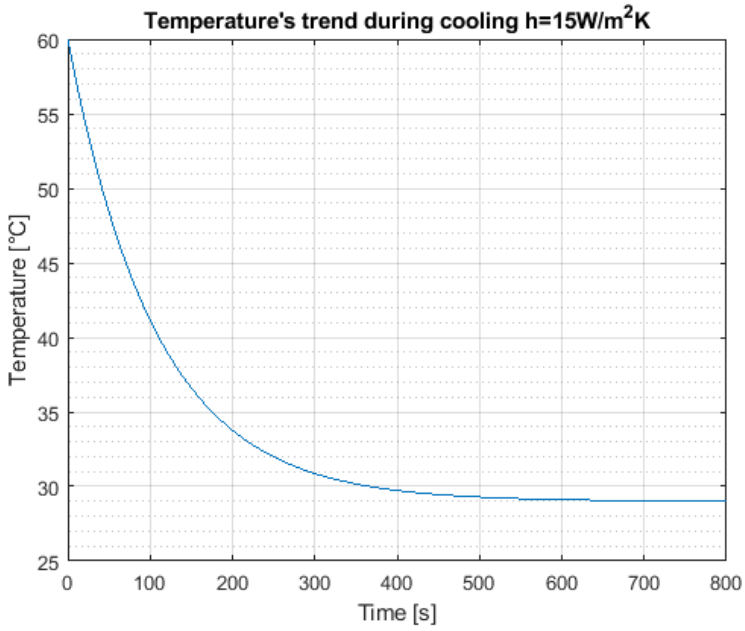

Figure 3.12 Temperature's trend according Matlab model in horizontal configuration

In the model, the time needed by the tube to cool down from its initial temperature T_i (the temperature it reaches after being heated) to the ambient temperature T_{amb}, has been computed exploiting the Newton's Law for cooling, which has been iterated until the condition $T_{tube} \leq T_{amb}$ has been verified:

$$T_{tube=} T_{amb} + \Delta T \cdot e^{-\frac{t_{cooling}}{\tau}} \qquad 3.1$$

Where $\Delta T = T_i - T_{amb}$, and τ is the cooling time constant, computed as:

$$\tau = \frac{m \cdot c_p}{h \cdot A_{ext}} \qquad 3.2$$

Where m is the tube's mass, c_p is the NiTiNOL thermal capacity, h is the convection coefficient, and A_{ext} is the external surface of the tube.

The small difference can be due to the fact that the convection coefficient could be slightly different, or it could be also caused by the fact that lying on the table does not allow the convection to act on the whole tube's surface, and part of the heat is transmitted to the table through conduction.

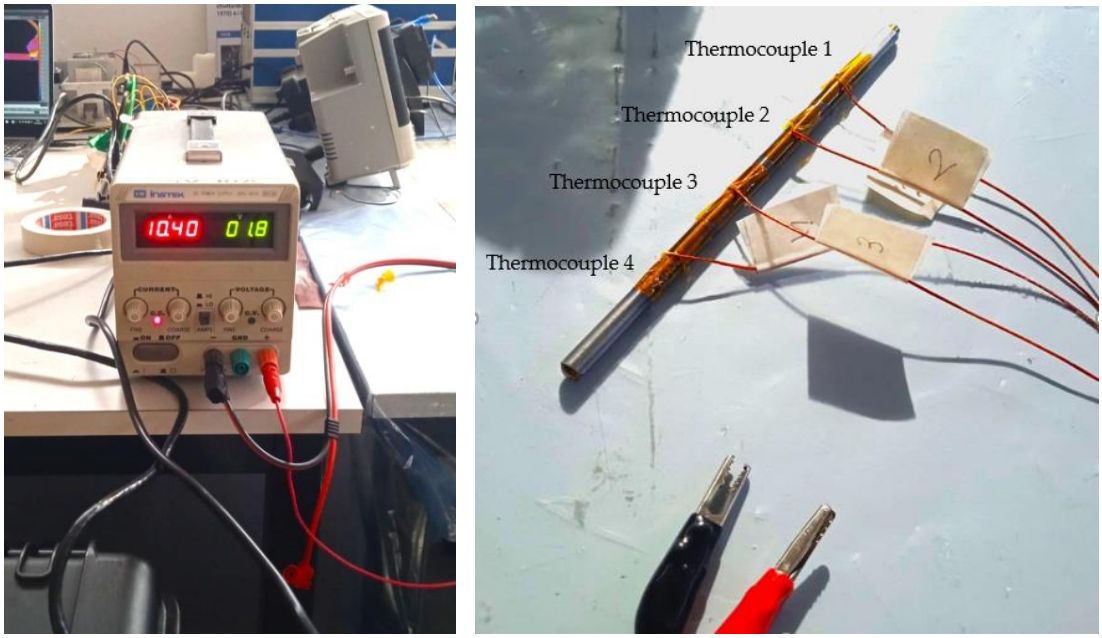

Figure 3.13 Power generator and thermocouples on SMA tube

It must be noted that actually not all the thermocouples measured 60°C, as this temperature was reached by one which was nearer to the electrical clips and which was taken as a reference. This fact can be due to the fact that the insulation made with kapton scotch tape was perfect here, ad no air remained trapped in it, so no alteration of the measurement occurred. LabView is the software used for the acquisition of the thermocouples' temperature, and the result obtained for one thermocouple is here presented. The tests conducted with the thermocamera showed slightly different results, despite the same power generator setup.

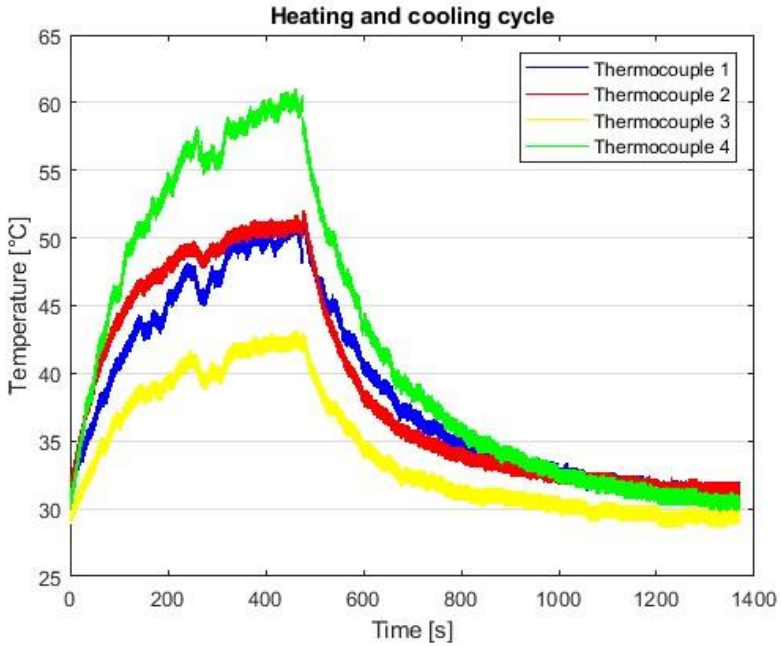

Figure 3.14 Temperatures registered by thermocouples during experimental test

The test has been conducted both with the tube in an horizontal configuration (as done in the thermocouples' test) and in a vertical configuration. In the first case, with the tube lying on the table, it became evident that only the areas of the tube nearer to the electrical terminals actually reached temperatures of about 60°C, while the central region did not go above 45°C. The area where the higer temperatures are reached corresponds with the edges of the tube.

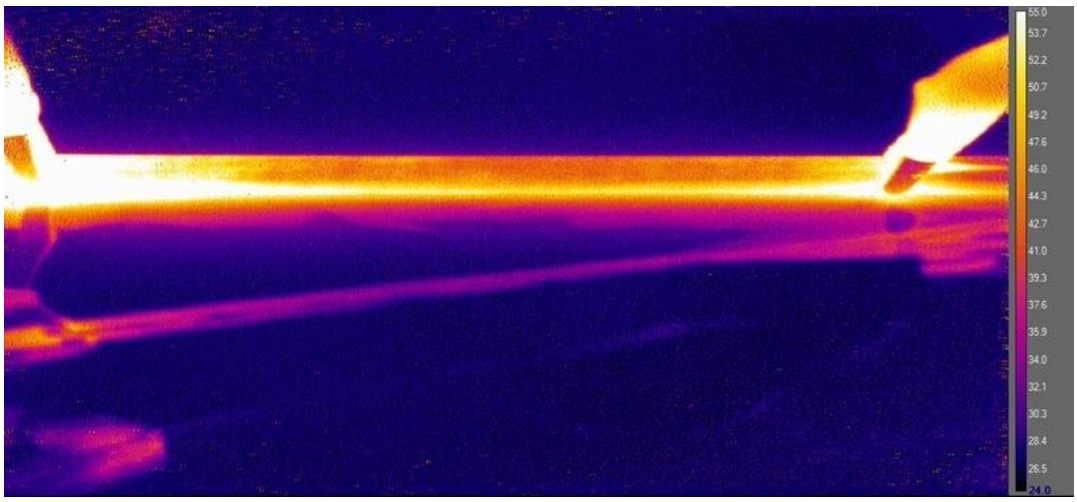

Figure 3.15 Thermocamera registered temperatures in the horizontal configuration

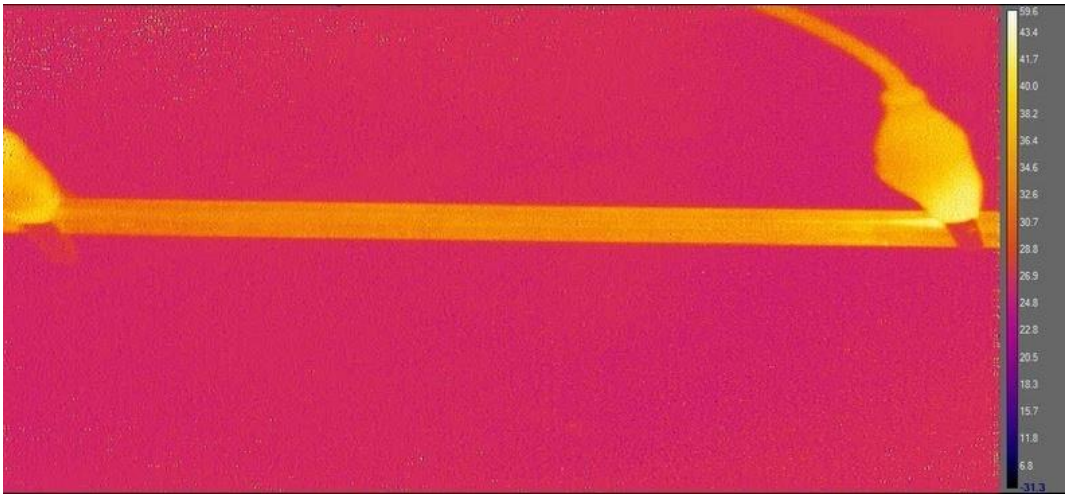

Figure 3.16 Thermocamera registered temperatures in the vertical configuration

What is observed in the tube's vertical configuration is that the temperature is more uniform, although it is visible that higher temperatures are reached on the right end. This is due to the fact that that edge was free, while the other was clamped in the grab, which probably caused part of the heat to be dissipated through conduction. The effect of convection all around the tube is also visible since a lower temperature in general is reached, equal to about 40°C. The time needed for the temperature to reach the highest value is about 15 minutes, while for cooling back to room temperature a time of 3.5 minutes is required. This value meets the model's results considering a convection coefficient of about 35 $\frac{W}{m^2K}$, which is reasonable if we consider that the limit value for natural convection is considered to be 25 $\frac{W}{m^2K}$, while the forced convection is generally represented by a range of the convection coefficient going from 25 $\frac{W}{m^2K}$ to 250 $\frac{W}{m^2K}$. Since the test was conducted in the laboratory but with no particular protection from air movement caused by air circulation and by people movement inside the room, the value extrapolated from the Matlab simulation was considered reasonable both in the horizontal and in the vertical configuration [28].

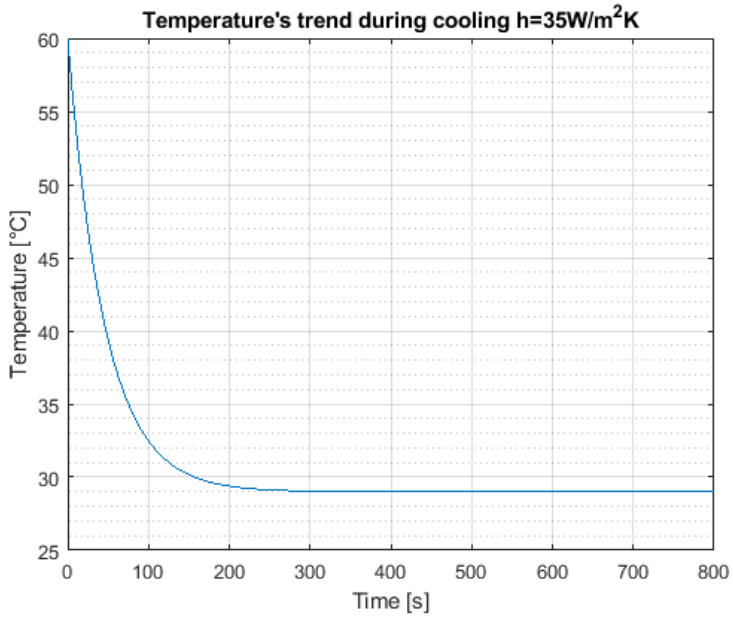

Figure 3.17 Temperature's trend according Matlab model in vertical configuration

The results obtained from the Matlab model is summarized and compared with the tests' outputs in the following table, where h is the convection coefficient and t_c is the cooling time.

Configuration	**h** $\left[\frac{W}{m^2K}\right]$	t_c **model**	t_c **test**
Horizontal	15	10 minutes	11 minutes
Vertical	35	4.5 minutes	3.5 minutes

Table 3.2 Comparison from experimental and simulation's results

The difference in the tests performed with the thermocouples and the thermocamera can be due to the fact that in the former case the thermocouple is directly attached to the surface, and part of the tube is "protected" by the effect of convection thanks to the presence of the kapton scotch tape, while in the latter case the thermocamera is mounted distant from the tube, thus it is able to capture the effect of convection. Given the necessity of performing the experiment inside the thermal camera, thermocouples have been considered as the most adequate solution.

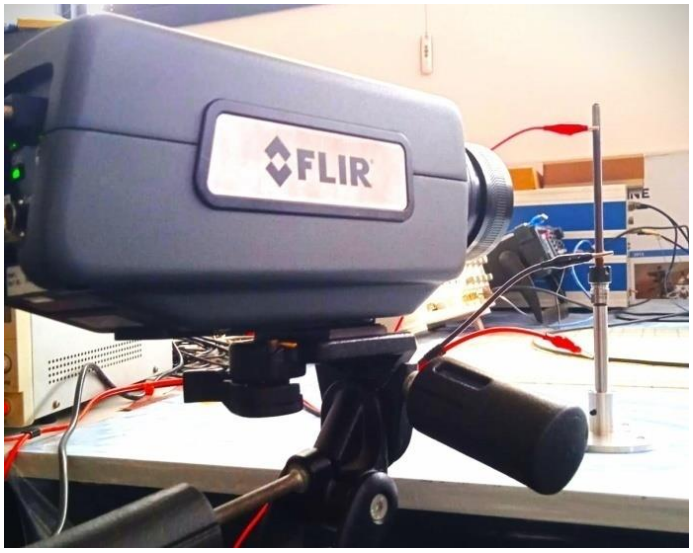

Figure 3.18 Thermocamera and tube in vertical configuration

A solution to obtain higher temperature can be of using another power generator, able to provide a higher level of current, or using another way to distribute current in the tube. This last option was investigated and the idea of using a constantan wire wound on the tube and then connected to the power generator, was tested.

3.4. Heating strategy

Different strategies can be used to provide the tubes with the heat necessary to produce the increment of temperature that promotes the phase change. Being the SMA elements two tubes, this initially suggested the idea of exploiting the passage of anhot fluid able to dissipate its thermal energy to the tubes themselves. Nevertheless, this would add great difficulties in designing a circuit which should be integrated in the experimental setup without compromising the tube's tightening with dedicated grips. The presence of non-hollow grips and the need for a reinforcing plug dissuaded from the use of this solution. Another aspect to consideris that the heat should be transferred to the tubes in the most uniform way possible, in order for the tube to transform simultaneously from martensite to austenite: for this reason, the possibility of using a dedicated hairdryer has been discarded, given the impossibility

of directing the hot air on the whole surface at the same moment, and given the fact that the transferred heat could not be properly determined.

Since the objective of this thesis is demonstrating the possibility of exploiting tubular SMA elements as a torsional actuator, studying in particular the antagonism as a rearm mechanism, the heating strategy has been chosen to guarantee the simplest experimental configuration together with the most effective heat transfer, to achieve the declared goals, without adding unnecessary complexity to the setup. For this reason, heating by exploiting the Joule effect has been selected as the best solution.

The first attempt to heat up the tube through Joule effect has been made by exploiting two crocodile clips positioned at the edges of the tube. As outlined in the previous paragraph this solution allows for a quite slow heating, with temperatures below 45°C. Even considering that convection could be strongly reduced if protections are placed around the tubes, allowing for sligthly higher temperatures to be reached, the long heating time and the fact that the clips are not perfectly stable around the tubes, discouraged from choosing this solution for the experimental phase, when the tubes will actually rotate. To address the issue of ensuring a stable heat source on the surface of the tube, the possibility of soldering wires has been considered as well. Nevertheless, welding is a challenging process due to the high sensitivity of NiTiNOL to heat, atmospheric gases, and the instability of the NiTi phase. Various welding techniques have been explored in research studies, including microplasma arc, electron beam, resistance, capacitor discharge, and laser welding, which has obtained the better results among the others [29]. The general results, however, is that welding can result in a loss of mechanical properties in the welded joint due to recrystallization and an increased presence of brittle intermetallic phases even though optimal shielding conditions and minimal heat input are guaranteed. Moreover, specific soldering alloys are often required, and post-weld thermal treatments are sometimes necessary to restore the properties of NiTiNOL[30]. For these reasons, another option has been finally chosen: a 0.5mm diameter constantan

wire has been wrapped around the tube, and has been electrically powered to ensure Joule heating-based thermal power generation. In between the tube and the ten windings of the wire a thin layer of Kapton film ensures electrical insulation. Two tests have been carried out in order to verify if this technique allows for the desired temperature increment of the tube: the first test consists in heating the tube starting from room temperature, while the other simulates the actual conditions that will be encoutered in the actual experiment, so the tube was taken to approximately -20°C and then heated. What is expected with thesetests is the heating process to be faster with respect to the one conducted using crocodile clips, since a bigger amount of conductor is in contact with the tube's surface. Moreover, this technique would assure a more uniform heating of the tube. The first test shows that heating happens in slightly more than one minute, while cooling back to room temperature takes approximately 4 minutes. For the second test the heating process takes between 8 and 9 minutes, while the cooling one takes almost 3 minutes. Before conducting the tests, two thermocouples have been placed on the tube's surface in two different positions: the first one has been placed near the edge of the tube, while the second one has been placed equally spaced from the edges, approximately in the center of the sample.

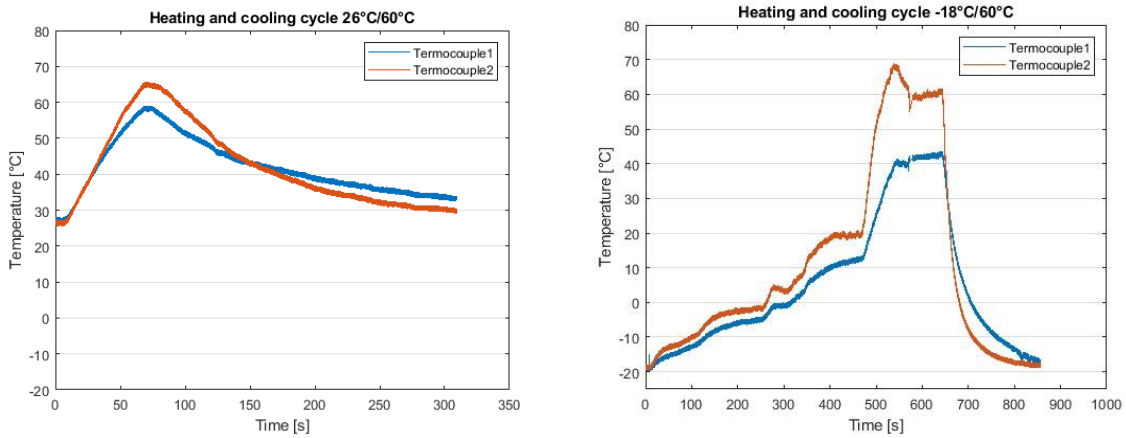

Figure 3.19 Thermocouples' results after heating by constantan wire

As it can be noticed from the graphs, in both the tests the temperature measured by the thermocouples rises almost in the same way at the beginning, but gradually the gap between the curves increases, revealing that the edges of the tube heat up more slowly than the central region. This is due to the presence of the reinforcing metal plug, which represents a thermal inertia. To allow a more uniform heating of the tube, the number of windings can be increased near the ends, reducing the spacing between one and the other. As regards the parameters of the generator, for the first test a current of 3A and a voltage of 10V was set, while in the second test the values were adjust in order to obtain a higher heating rate. This results in the different slopes of the heating segment when passing from -18°C to 60°C: the starting values of current and voltage were the same of the first test, but since the process was quite slow, these values were raised to 4A and 14V, then 7A and 32V, and finally were set to 6.5A and 30V. If these final values are set since the beginning, the heating time is expected to be further reduced. Since these tests were conducted to validate the heating strategy to be used in the experiment, an easier way of cooling was used: the furnace Thermaltest is also able to cool down till -20°C and has the dimensions big enough to host one tube in the vertical configuration.

Figure 3.20 Furnace Thermaltest used for heating strategy validation

3.5. Final setup

In the final setup one thermocouple for each tube has been placed on the tubes' surface, in order to monitor the temperature of the samples. The position has been chosen reaching a compromise between the section which experiences the lowest torsion, meaning the tube's clamped edge, and the one less affected by the thermal inertia of the other components, meaning the tube's central section. For these reasons the thermocouple has been placed in the halfway section between this two.

The constantan wire has been winded around the tube with a total of 10 winding, and in correspondence of the edges of the tube the distance between one winding and the other has been reduced, in order to compensate for the amount of heat dissipated through conduction to the rest of the chain.

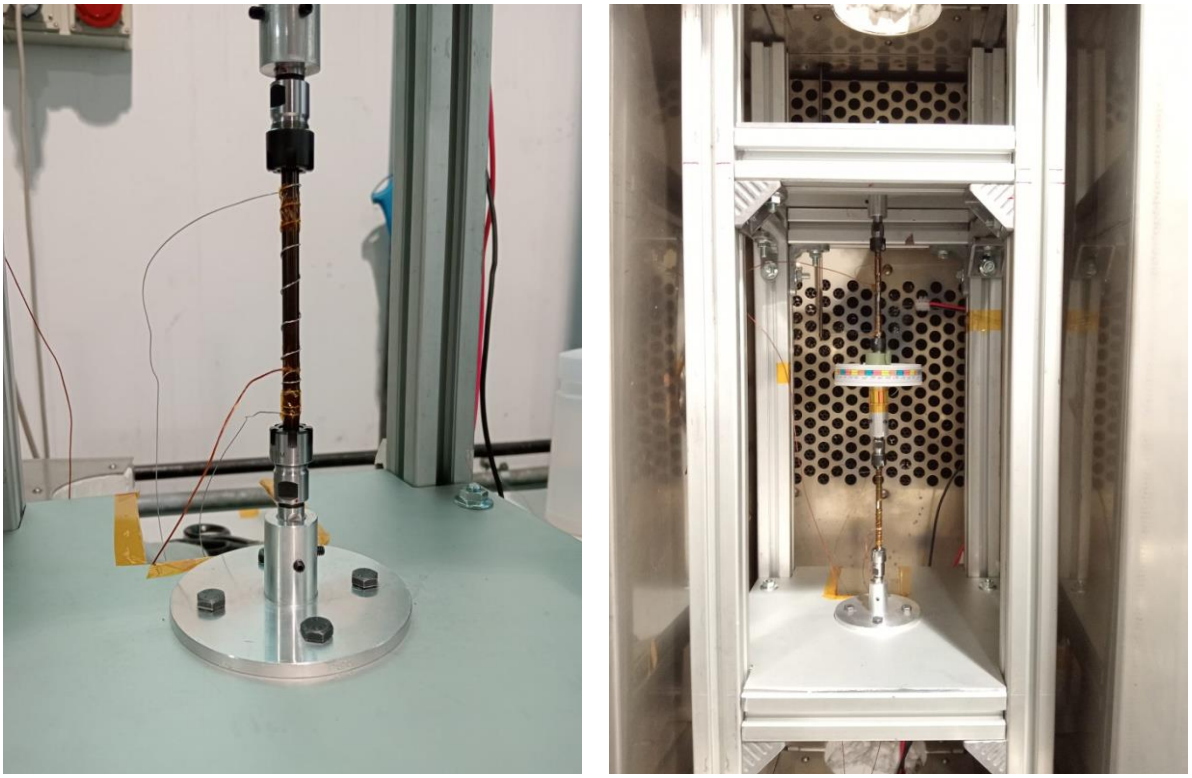

Figure 3.21 Final setup configuration

Once all the components have been mounted in the final setup configuration, the whole structure has been placed inside the MTS environmental chamber, ensuring a

proper insulation between the structure and the chamber's bottom. Even though with the Strain-Recovery test a temperature range between 0°C and 45°C was identified to perform the cycling, a broader range from -20°C to 60°C has been selected for better monitoring the material's behavior since we do not know exactly the new transformation temparatures when the load is applied to the tubes. This is necessary also because, differently from the Strain-Recovery test, when we apply the pretorsion we do not know exactly the value of the rotation we are imposing.

The constantan wires used to heat up the tubes and the thermocouples' wires have been constrained separately to the structure to avoid their contact: the hot temperatures reached by the constantan wires could indeed damage the thermocouples if they happen to be in contact.

The setup is fully prepared except for the two set screws responsible for securing the central component to the lower mandrel. It is crucial for the mandrel to be free to rotate, as the pretorsion is applied to the lower tube only, exploiting the flat areas on the mandrel, facilitating a secure grip with a spanner. This pretorsion process is carried out after that the setup has been brought to -50°C, in order to be sure that the tubes are both in martensitic conditions. Such a low temperature also allows for opening of the camera, applying the pretorsion, and securing the set screws before the tube reaches -6°C, the austenite start temperature.

Another important consideration is that at such low temperatures the collet chuck springs of the mandrels are not as tightly secured as they were at room temperature, compromising the constraints of the tubes. To address this issue, the only solution is to tighten the mandrels again at low temperatures. This step must precede the imposition of pretorsion: otherwise, there is the risk of the tube slipping inside the chuck spring. This process, however, adds a few extra seconds, causing the temperature to rise above the austenite start temperature.

Consequently, the initial procedure aimed at arming one tube, has been divided into two parts:

I. Once the temperature reaches -50°C, the chamber is opened for mandrel tightening and then closed to allow the temperature to decrease again.
II. Subsequently, the chamber is reopened to apply pretorsion and secure the set screws.

Finally, the temperature is stabilized at -20°C, a condition maintained throughout the entire experiment, and the first cycle can start.

The pretorsion to be applied in the step II has been chosen as approximately 120°: the reason is that 120° for a 90mm long tube corresponds to a 7% strain which, as previously seen, is the maximum recoverable strain for SMA tubes [13].

When the arming load was removed, Tube1 exibited a slight elastic return, resulting in an effective deformation of about 100° (5.8% strain), which suggested that also a slightly higher value of pretorsion could actually have been chosen. Nevertheless, since the tube has undergone a thermal treatment which created an high number of precipitates, imposing an higher rotation risking an high plasticization of the material was not considered worthy.

For the sake of clarity it is worth reporting an accurate description of a cycle, first in terms of sequence, and then in terms of angle configurations. As stated before, the lower tube will be referred to as Tube1 and the upper tube as Tube2:

1. Tube1 is heated through the activation of the power supply, which has been configured to 13.3V and 4A;
2. Once Tube1 temperature reaches 60°C, the power supply is turned off;
3. The entire setup stabilizes at -20°C;
4. Tube2 is activated by heating it using a second power supply set to 9.9V and 4.5A:
5. Once Tube2 temperature of 60°C is achieved, the power supply is switched off;
6. The entire setup stabilizes at -20°C;

7. The cycle is completed, and the process is initiated again from step 1 for subsequent cycles.

The first set of cycles, which is referred to as "Test 1" (Figure 3.23), is here considered as the tubes are at the beginning of the cycling, so they are not stabilized yet: this offers a more evident change of behavior as the cycles goes on. Overall, however, the cycling counts 100 cycles, which have been carried out in four phases, and referred to as "Test 1", "Test 2"(Figure 3.24), "Test 3" (Figure 3.25), "Test 4" (Figure 3.26). It is important to assure that whenever one set of tests is finished, the following sequence is performed: this allows to end up in a known tubes' crystallographic structure, in this case austenitic conditions, avoiding residual deformations and stresses which would be impossible to evaluate.

III. Open the chamber to release the set screws, and close it again;

IV. Heat up the whole setup to 60°C;

V. Let the setup cool down to room temperature.

Step IV allows to make both the tubes completely transform towards austenite, recovering their deformations, and in step V, when the ambient temperature is reached, the tubes are still in austenite. Whenever a new set of tests has to begin, step I and step II has to be performed again.

The first cycle (Table 3.3, Figure 3.22) will be now described in terms of angle configurations as it is representative of the behavior exhibited also by all the other cycles. For sake of clarity, also the first activation of the second cycle is reported in the figure. During the first actuation, the armed tube undergoes a recovery of 90°, settling into a 10° configuration at 60°C. When the power supply is deactivated, letting temperature to decrease, an additional rotation of almost 15° becomes visible in the opposite direction. This leads to the final configuration corresponding to an angle of 25° when the temperature reaches -20°C. This is the starting point of Tube2 activation sequence. The actual deformation that this tube has undergone

corresponds then to 75°, considering that a rotation of 15° (25°-10°) has been experienced during the cooling process, as just described.

First cycle's steps	Description	Temperature		Configuration	Additional rotation
		Tube1	Tube2		
1	Tube1 has been armed	-20°C	-20°C	100°	
2	Tube1 has been activated	60°C	-20°C	10°	
3	Tube1 has been cooled down	-20°C	-20°C	25°	15°
4	Tube2 has been activated	-20°C	60°C	95°	
5	Tube2 has been cooled down	-20°C	-20°C	85°	10°

Table 3.3 First cycle's steps and outputs

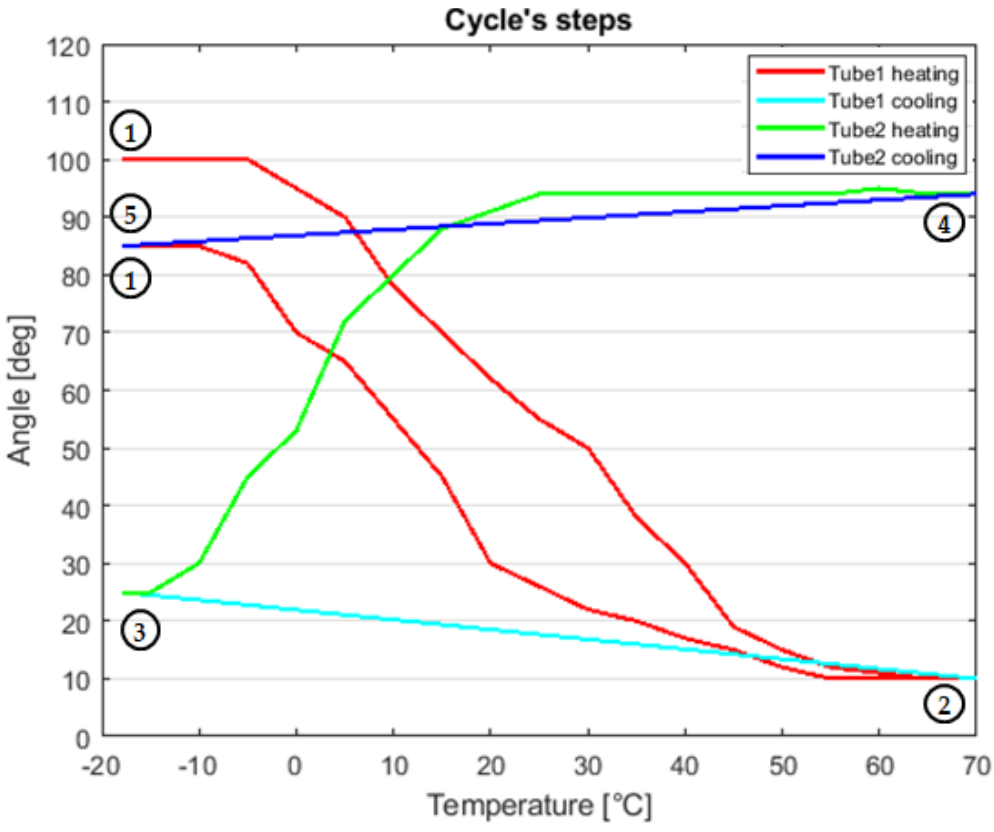

Figure 3.22 Cycle's steps

From the 25° configuration at the beginning of the activation sequence of Tube2, a final configuration of about 95° is reached at the end of the heating process. Again the power supply is turned off allowing the tube to cool down to -20°C, and again a further rotation, this time of 10°, is experienced, settling the final configuration to 85°. From the second cycle on, point 5 is coincident with point 1, and the additional rotation is experienced at every cycle but its value remain constantly equal to 10°. This rotation has been hypothesized to result from the combination of two different contributions: one is the two-way effect that is experienced during cooling, the other one is the elastic return of the martensite. Indeed, after an actuation, one tube is in austenite while the other one is in martensite, so their stiffness is different, being that of austenite higher. As soon as the heating of the activated tube is interrupted and its temperature starts to decrease, its austenite fraction decreases as the transformation towards martensite starts. This means that also the stiffness decreases, making the other tube, which has always been in martensite, capable of recovering part of the deformation. To verify this hypothesis a further test has been conducted: Tube1 has been activated twice, and the two activations have been divided only by the time needed to cool down the whole setup. During the second activation, indeed, Tube1 recovered again only the 10° that it lost during the cooling, meaning that it is able to recover that amount of rotation only when its stiffness increases. Cooling again after this additional actuation showed that, as expected, the 10° are recovered again by Tube2.

Overall, the recovered rotations experienced during the two activations of the first cycle can be summarized as follows:

Cycle 1	**First activation**	**Second activation**
Tube1	90°	-
Tube2	-	70°

Table 3.4 First cycle recovered rotations

This difference is probably due to the fact that Tube1 has been manually armed, experiencing a considerable deformation. When it has been connected to Tube2 and activated, it has been capable of transmitting a good amount of rotation, but not completely, as Tube2 exerts a resistance. The same happens when Tube2, which has been armed of 90°, is activated: it experiences the resistance offered by Tube1, so it recovers 70°. At this point a sort of equilibrium has probably been reached: the hypothesis made is that this value of 70° is maintained during the following cycles as it corresponds to the rotations the tubes are capable of recovering considering the reciprocal resistance they experience. This has been verified by applying a pretorsion of 120°C to Tube1, and then heating it while maintaining it disconnected with respect to Tube2: without the resistence of Tube2, it indeed fully recovers the given pretorsion. What has been described until now is graphically represented in Figure 3.23, where the first 12 cycles are reported.

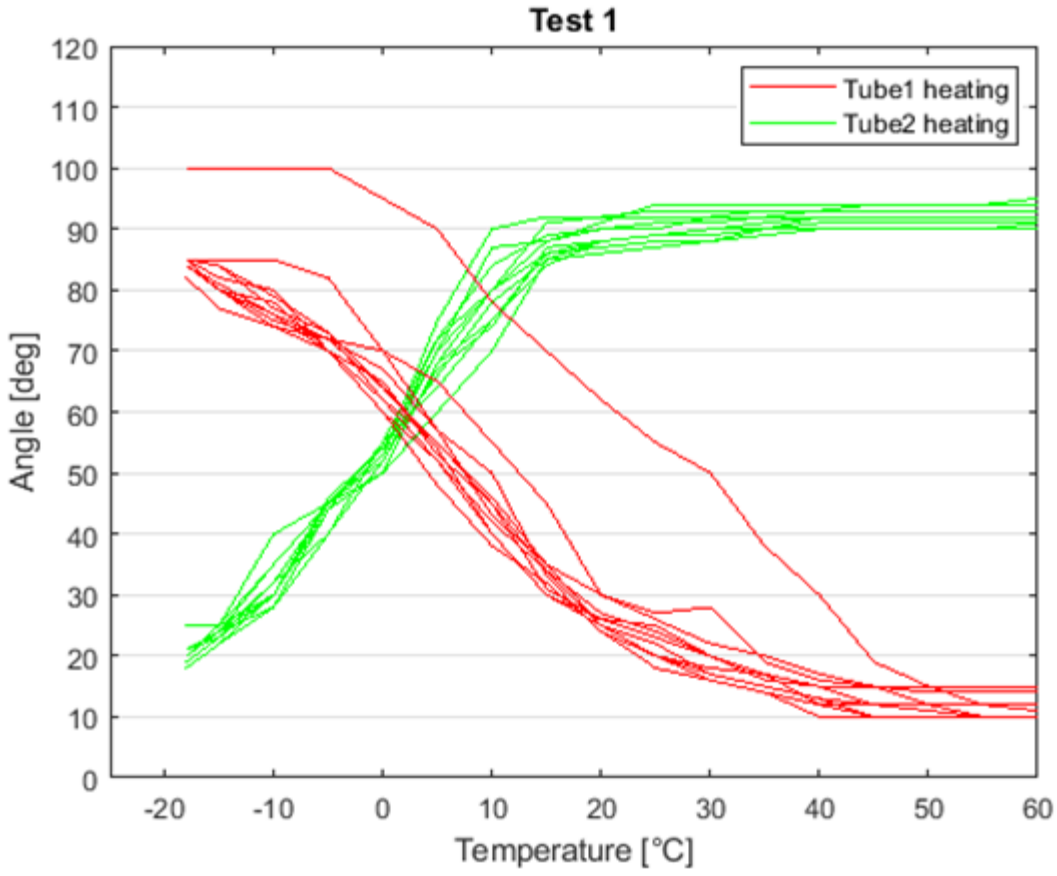

Figure 3.23 Test 1: Cycles from 1 to 12

the activation of the lower tube, meaning Tube1, corresponds to red curves, while the activation of the upper tube, meaning Tube2, corresponds to green curves, which as anticipated are shifted upwards of about 10° because of the additional rotation which makes the ending point (in terms of angle configuration) of Tube1's activation and the starting point of Tube2's activation not coincident.

The first cycle is clearly visible from the graph as it is represented by the red curve which starts from 100° angle configuration, which results from a 120° pretorsion and 20° of elastic return. All the following curves, already from the second cycle, stabilize to a starting angle configuration of about 85° when Tube1 is activated, and about 20° when Tube2 is activated. Considering only the recover experienced while passing from martensite to austenite, meaning during the heating process, it has a mean constant value of 70°. Even more interesting and valuable is looking at the evolution of the values as the cycles goes on. Indeed, it can be noticed that the recovered rotation slightly decreases as the number of cycles goes on (Table 3.5). This behavior has different contributions that in part are due to the limits the experimental setup unavoidably has: for example, it is possible that part of the movement is lost due to the internal setup frictions. Moreover, the impossibility of accurately measuring the initial pretorsion does not allow to perfectly define the starting point of the cycling process. The reduction of the recovered rotation, anyway, could be also compatible with causes related with the material itself: for example, a stabilization of the material to such lower rotations as well as a stress reduction as the cycling goes on. It can also be the case that residual strains are generated at any cycle due to plastic deformation, and their accumulation leads to the reduced recover experienced by the tubes.

The reduction of recovered rotation is clearly visible in the first set of test, as Table 3.5 shows, but it gradually stabilizes as the number of cycles increases, as it is evident looking at the overall trend of the 100 cycles (Figure 3.24, Figure 3.25, Figure 3.26).

	Activated tube	Initial Configuration	Final Configuration	Rotation recovered
Cycle1-Cycle4	Tube1	85°	10°	**75°**
	Tube2	20°	94°	**74°**
Cycle9-Cycle12	Tube1	85°	14°	**71°**
	Tube2	21°	92°	**71°**

Table 3.5 Rotation recovered's trend during the cycling

An ambient temperature of -35°C has been imposed from the second set of tests, so that the tubes reach a temperature comprised between -30°C and -33°C: in this way it is possible to better verify the symmetric trend exhibited by the curves on the left side and on the right side of the graph. To heat up the tubes a slight increment of current has proven to be necessary, settling to 5A for Tube1 and to 5.15A for Tube2. Overall, a whole cycle has a duration of about 12 minutes: 1 minute to heat up Tube1, 5 minutes to allow the temperature to stabilize to -20°C, 1 minute to heat up Tube2, 5 minutes to allow the temperature to stabilize to -20°C again. The hypotheses made to provide a justification to the behavior exhibited by the tubes in Figure 3.23 are valid also to describe the behavior exhibited in the other tests, which are characterized by the same aspects, in particular: the bigger recover characterizing the first activation, the shift of 10° between tubes' activations, the light decrease of rotation recovered as the cycles go on. What can be noticed is that the actual deformation resulting from the initial pretorsion of 120° is slightly higher for Test 3, being 110° instead of 100°, as in that case a lower elastic return has been noticed. In Figure 3.25 it can also be noticed that a slightly lower recover has been experienced: this is probably due to the different loading condition Tube1 undergone, both in terms of pretorsion and in

terms of temperature at which pretorsion has been applied. Overall, a mean 70° rotation recovery has been registered throughout the performed 100-cycles cycling.

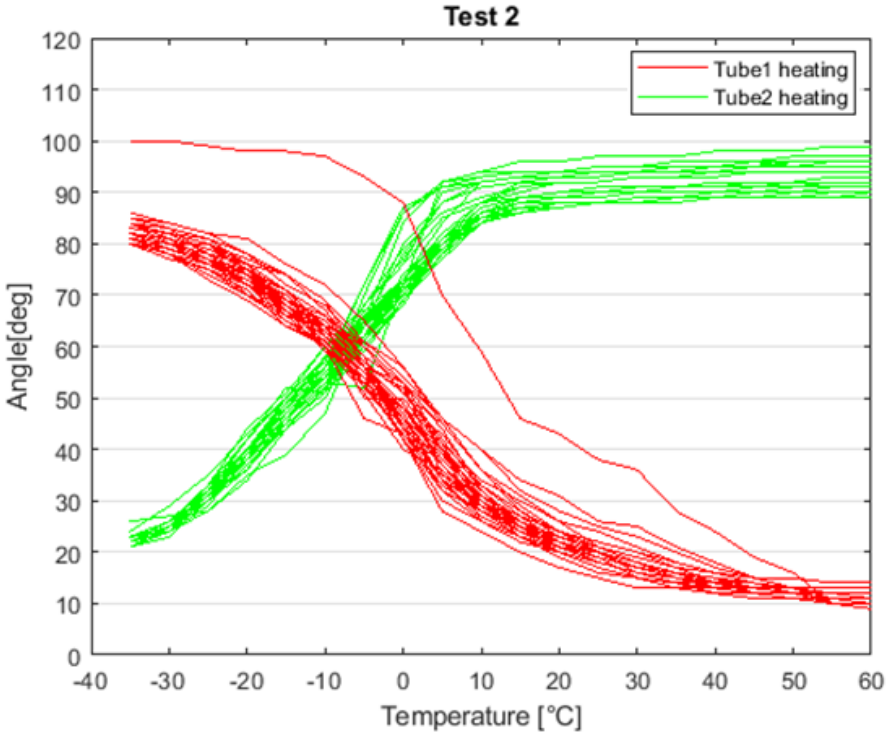

Figure 3.24 Test 2: Cycles form 13 to 52

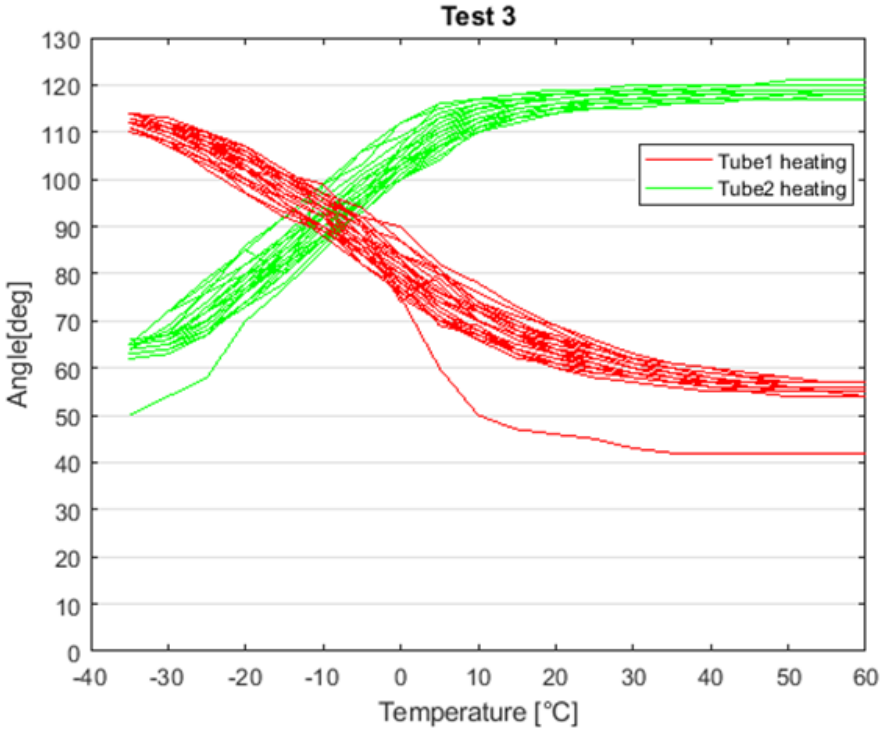

Figure 3.25 Test 3: Cycles from 53 to 80

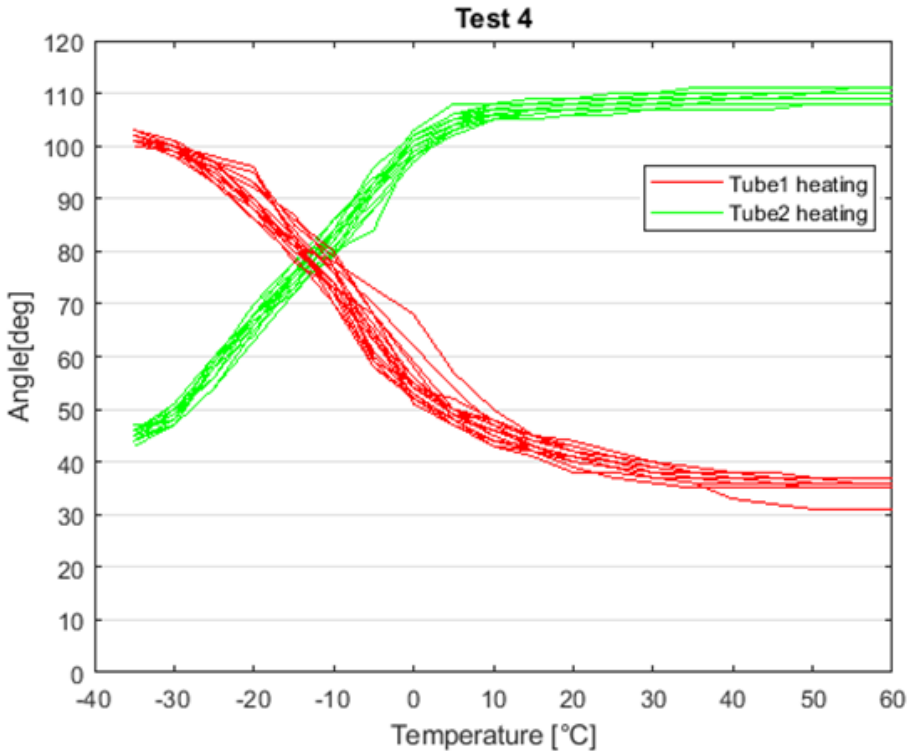

Figure 3.26 Test 4: Cycles from 81 to 100

An alternative way to represent what happens during the cycling is also reported in Figure 3.27, where a complete cycle taken from Figure 3.26 has been reinterpreted to demonstrate what happens to Tube1 and to Tube2 separately, but in such a way that it is evident how a tube influences the other. The starting point of the cycling is identified by number "1" and for the red graph, representing Tube1 cycling, it is in correspondence of a rotation of 100°. Point "1" in the green graph, which represent the cycling of Tube2, represents the initial condition of Tube2, correspondent to a 0° rotation because it has not been armed yet. The transition from "1" to "2" represents the activation of Tube1: in the red graph it corresponds to a rotation recover of 65° during heating, while in the green graph it corresponds to Tube2 arming process, which occur while the tube is in martensite, at -35°C, and is represented by a vertical green line from 0° to 65°. The segment between "2" and "3" is the cooling of Tube1: the red line goes from 60°C to -35°C to represent what happens to Tube1, while the green line brings Tube2 from the angle configuration of 65° to 55°, which is the starting point of Tube2's activation. Indeed, from "3" to "4" the activation of Tube2

happens and it recovers a rotation of 55° , arming Tube1 by the same amount. Again this is represented by a vertical line for Tube1, since the arming process occurs when the temperature of the armed tube is -35°C. Finally, by cooling Tube2, point "5" is reached, bringing everything back to the initial conditions. As it can be seen in the graph, the cycling is aimed at bringing Tube1 in the initial configuration after its actuation, in order to allow for multiple actuations. This is done through an arming process which consists of two steps: first, Tube1 must transforms towards martensite (2-3), then it must be armed by imposing it a deformation (3-4-5). This is possible thanks to the antagonistic action performed by Tube2, which in turn is also armed by Tube1 while it is activated.

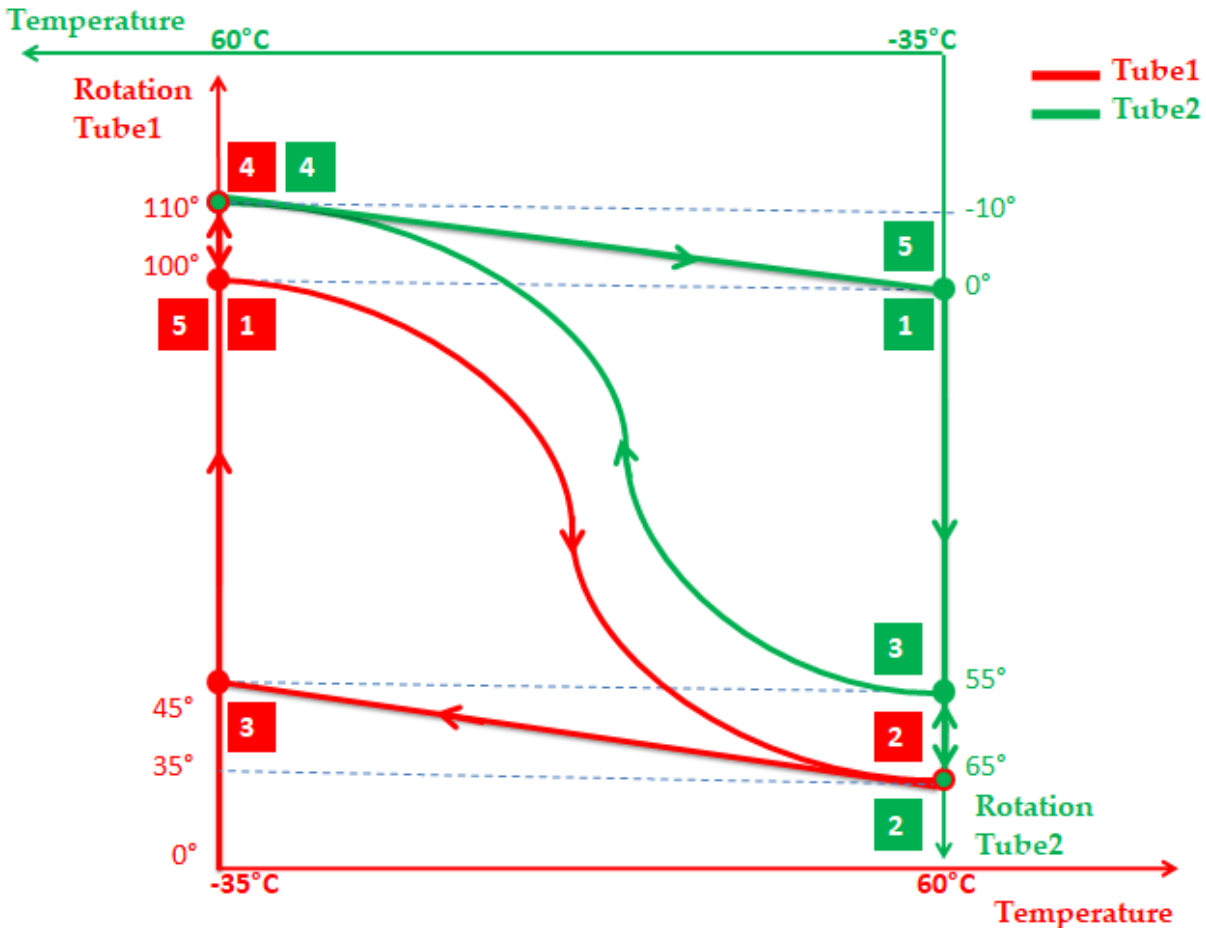

Figure 3.27 Antagonistic behavior of the tubes

A further test has been carried out imposing an actual predeformation of 120°. The aim was to check if by increasing the predeformation also the rotation recovery

increases as well. To do so, Tube1 has been deformed of at least 140° to take in account the elastic return, which was about 20°. By performing two cycles it was immediately evident that the recovered rotation settles around 70°, so that 50° are not recovered at all. This is a huge difference with respect to the results obtained with 80°, 90°, 100° of predeformation: in all that cases, from the second cycle it is evident that the "lost" rotation is only abut 15°-20°(Table 3.6).

Imposed predeformation	**1 cycle recovered rotation**		**2 cycle recovered rotation**	
	Tube1	Tube2	Tube1	Tube2
80°	73°	60°	62°	63°
90°	85°	72°	75°	75°
100°	98°	83°	85°	80°
120°	83°	68°	71°	70°

Table 3.6 Recovered rotations with different predeformations

When tying to explain this behavior it has been considered probable that by applying a rotation of 140° to the tube, it entered the plastic domain. The amount of rotation associated to the plastic deformation can be therefore not recoverable, and this would explain the lost of 50°: in part this is probably due to the fact that the tubes do not recover the whole rotation because of the resistance they mutually exerts, in part it can be due to the material plastization.This hypothesis has been based also on the Torque-Rotation test descrbed in Figure 2.8, where in the curve representing the test at T=-40°C (so very near to the -35°C registered during the tests) exhibits a plastic deformation for angles above 140°. This confirms, for the material used in this thesis, an actual predeformation of 100° to be the best choice.

4 Conclusions and future developments

The present study aimed at characterizing the torsional behavior of SMA tubes samples, in particular, exploiting an antagonistic configuration. This investigation is justified by the desire of designing a SMA actuator for a space application completed by a rearm mechanism. The proposed application consists in using the torsional actuator as a hinge of a CubeSat radiative panel, in order to open and close it: for this reason, an existing CubeSat's orbit and geometry have been taken into consideration to simulate a hot case scenario and check if the activation frequency of the SMA actuator meets the heat dissipation necessities of this type of satellite. A material characterization follows this initial phase, with the aim of determining the properties of a 6mm tube and modifing the material to allow the tube's actuation. A DSC analysis, indeed, revealed the necessity to perform a thermal treatment; then, a mechanical characterization to relate the torque's trend as a function of the rotation has been carried out at different temperatures; finally a test has been performed to study the behavior of the tube during a temperature's cycle under a constant loading condition. All these preliminary tests guided the following decisionof using two equal 6mm tubes to deepen the characterization of their torsional behavior inside an antagonistic configuration. To do that, an experimental setup has been designed choosing among different solutions the ones that allowed a better characterization of the material. Great attention has been made in designing ad hoc components to allow the practical realization of the boudary conditions needed for the proper functioning

of the experiment. Some compromises have been accepted, given the extremely low temperatures at which the tubes need to be taken, like the renunciation to the rotation's accurate measurent through an angular sensor because of the low temperatures reached in the environmental chamber, the inability of defining in a precise way the exact value of manually imposed pretorsion, as well as the temperature at which this is done. Despite this difficulties, the experimental setup proved to work as expected and allowed a particularly noteworthy characterization, even more significant considering the limited or nonexistent presence of such studies in the literature. The tubes, after predeformation of one of them by 100°, have been alternatively heated through Joule effect, recovering a considerable amount of rotation of about 70° at every activation, demonstrating that the antagonistic configuration is a good option for actuators' design. Also different predeformations have been tested, proving the one chosen for the cycling to be the most suitable one. Moreover, the performed cycling consists of 100 cycles, so 100 activations for each tube, which give a encouraging and reliable basis from which future developements can start. This is true especially if considering that the material used is a treated pseudoelastic tube, while better results could surely be obtained with a material already exibiting shape memory effect at the temperatures of interest. For a real application of SMA materials, indeed, the best composition should be selected already from the fabrication process, to avoid the behavior worsening due to the presence of precipitates formed during thermal treatments.

Considering the results achieved, future developments could surely be expected, as they should aim at realizing and testing the proposed advanced experimental setup. This would allow for a correct measurement of imposed rotation as well as recovered rotation at every cycle. Moreover, a torsiometer could also be integrated in the chain in order to gather additional information about the exchanged torque. A step forward needs to be taken also in the design of the actual actuator itself: the conceptual functioning demonstrated with this thesis allows great freedom in

deciding the actuator geometrical characteristics and activation strategies. The suggestion of testing a 3.5 mm bar could lead to the possibility of realizing a compact geometry, exploiting the coaxial configuration of the bar inside the tube. The heating process exploiting the Joule effect could be maintained, or other of the suggested possibilities could be explored, such as the tube's activation through an hot fluid circulation. The decision process defining the actuator characteristics cannot avoid considering the specific application to which it is destinated: an adequate connection must, indeed, be designed between the two antagonistic samples providing, if needed, a proper thermal insulation between the two. Finally, the interface between the actuator and the structure on which it will be mounted must be designed, to allow the correct torque exchange during the operations.

Bibliography

[1] D.C.Lagoudas, Shape Memory Alloys modeling and engineering applications, Springer Science+Business Media, 2008.

[2] G. R. Vladimir Buljak, Constitutive Modeling of Engineering Materials, Academic Press, 2021.

[3] P. P. D.Schryvers, "R-Phase Structure Refinement Using Electron Diffraction Data," in *Materials Transactions*, The Japan Institute of Metals, 2002, pp. 774-779.

[4] C. E. W. Brett Huettl, "Design and Development of Miniature Mechanisms for Small Spacecraft," *CORE*, 2000.

[5] J. W. J. J. H. L. K.-W. K. D.-S. H. Young Ik Yoo, "Development of a non-explosive release actuator using shape memory," *Review of scientific instruments*, 22 Gennaio 2013.

[6] G. C. S. C. G. P. F. Bovesecchi, "Deployment of Solar Sails by Joule Effect: Thermal Analysis and Experimental Results," *Aerospace*, 2020.

[7] "A 4D printed active compliant hinge for potential space application using shape memory alloys and polymers," *Smart materials and structures*, vol. 30(8), no. 085004, 2021.

[8] L. D. Carpenter, "Validation Report for the EO-1 Lightweight Flexible Solar Array Experiment," NASA, 2001.

[9] B. W. e. a. Walgren, "Development and Testing of a Shape Memory Alloy-drive composite morphing radiator," *Shape memory and superelasticity*, 2017.

[10] P. &. L. G. Jenkins, "A rotating arm using shape-memory alloy," 1995.

[11] T. H. Donghyun Hwang, "A Rotary Actuator Using Shape Memory Alloy Wires," *Transaction on Mechatronics*, vol. 9, no. 5, pp. 1625-1635, October 2014.

[12] L. F. U. Icardi, "Preliminary study of an adaptive wing with shape memory alloy torsion actuators," *Materials and design,* no. 30, p. 4200–4210, 2009.

[13] R. e. a. Mehrabi, "Experimental study of Niti thin-walled tubes," *Experimental Mechanics,* 2015.

[14] F. C. B. Yuan, "A review of rotary actuators based on shape memory alloys," *Journal of Intelligent Material Systems and Structures,* 2017.

[15] "ISISPACE," [Online]. Available: https://www.isispace.nl/cubesat-information/. [Accessed 25 July 2023].

[16] NASA, "LEO economy," [Online]. Available: https://www.nasa.gov/leo-economy/faqs. [Accessed 30 July 2023].

[17] S. e. al., "Impact of solar activity on Low Earth Orbiting," *Journal of Physics: Conference Series,* 2020.

[18] K. Stewart, "Low Earth Orbit," 2023. [Online]. Available: https://www.britannica.com/technology/low-Earth-orbit.

[19] W. J. R. Larson W. J., Space Mission Analysis and Design, Space Technology Library, 1991.

[20] I. P.-G. A. S.-A. J. Meseguer, Spacecraft Thermal Control, Woodhead Publishing in Mechanical Engineering, 2012.

[21] NASA, "Goddard Earth Sciences Division Projects," [Online]. Available: https://earth.gsfc.nasa.gov/climate/projects/icecube-0. [Accessed 03 11 2023].

[22] M. K. Choi, "Paraffin Phase Change Material for Maintaining Temperature Stability of IceCube Type of CubeSats in LEO," *American Institute of Aeronautics and Astronautics,* 2015.

[23] A. e. al., "Calculation of environmental loads for a CubeSat," *Journal of Physics: Conference Series,* 2023.

[24] L.-Y. F. e. al., "Mechanism for Entrapment of Debris Using Shape memory alloys," in *Research Gate*, 2017.

[25] D. H.Stroud, "Shape memory alloy torsional actuators," *Smart Materials and Structures,* vol. 29, 2020.

[26] D. Carnier, "Deployment of a CubeSat radiative surface through an autonomous torsional SMA actuator," Politecnico di Milano, 2022/23.

[27] C. e. a. Chapman, "Torsional Behaviour of Niti wires and tubes," *Journal of Intelligent Material Systems and Structures,* 2011.

[28] I. e. al., Fundamentals of Heat and Mass Transfer, Wiley, 2007.

[29] A. S. S.M.Russell, "Laser processing of nitinol materials," in *Proceedings of the international conference on SMA*.

[30] T. T. J. P. Kramár, "Welding of nitinol by selected technologies," *Acta polytechnica,* pp. 42-50.

[31] L. Rapp, "SATELLITE MINIATURIZATION ARE NEW SPACE ENTRANTS ABOUT TO THREATEN EXISTING SPACE INDUSTRY? SIRIUS (Space Institute for Research on Innovative Uses of Satellites," SIRIUS, Toulouse.

[32] D. C. Lagoudlas, Memory Alloys: Moding and Engineering, Springer, 2008.

[33] X. R. Kazuhiro Otsuka, "Physical metallurgy of ti–ni-based shape memory alloys," *Progress in material science,* pp. 516-669, 2005.

[34] R. B. [. al.l], "Thermo-mechanical Response and Damping Behavior of Shape Memory Alloy–MAX Phase Composites," *Metallurgical and Materials Transactions,* May 2014.

A Appendix A: Designed components

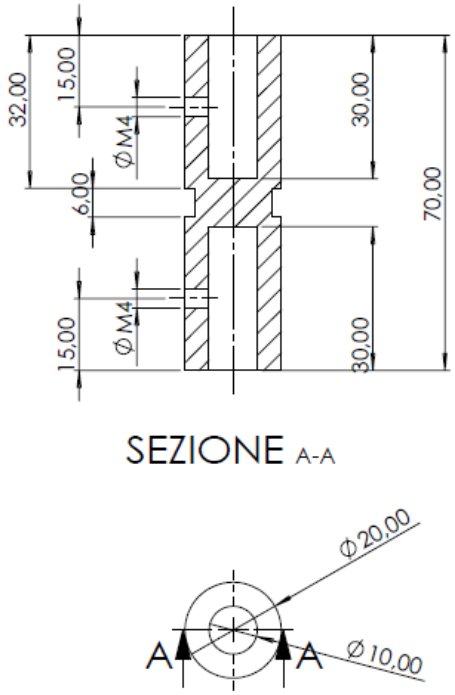

Figure A. 1 Central component

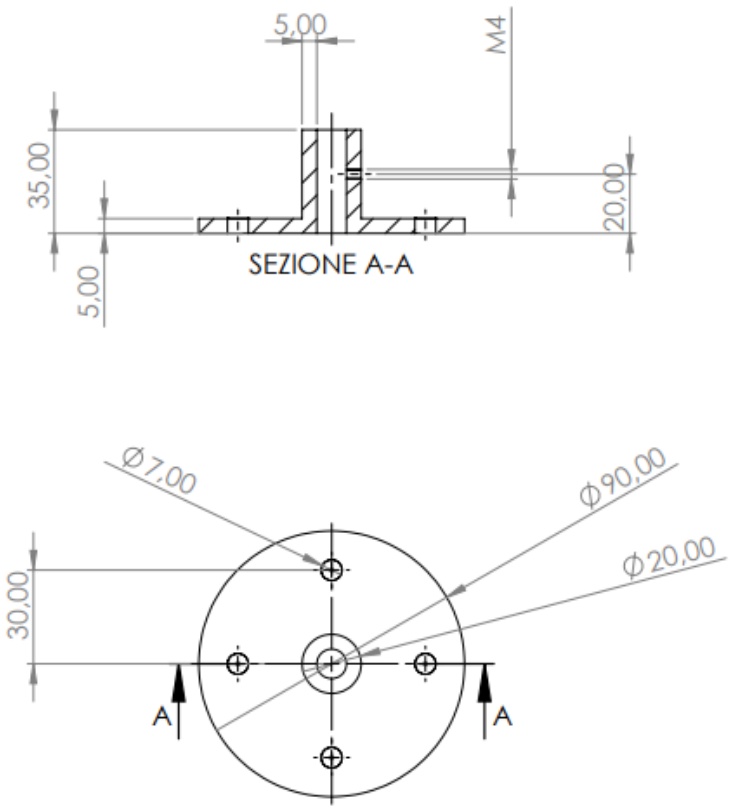

Figure A. 2 Mandrels' housing connecting them to the structure's plates

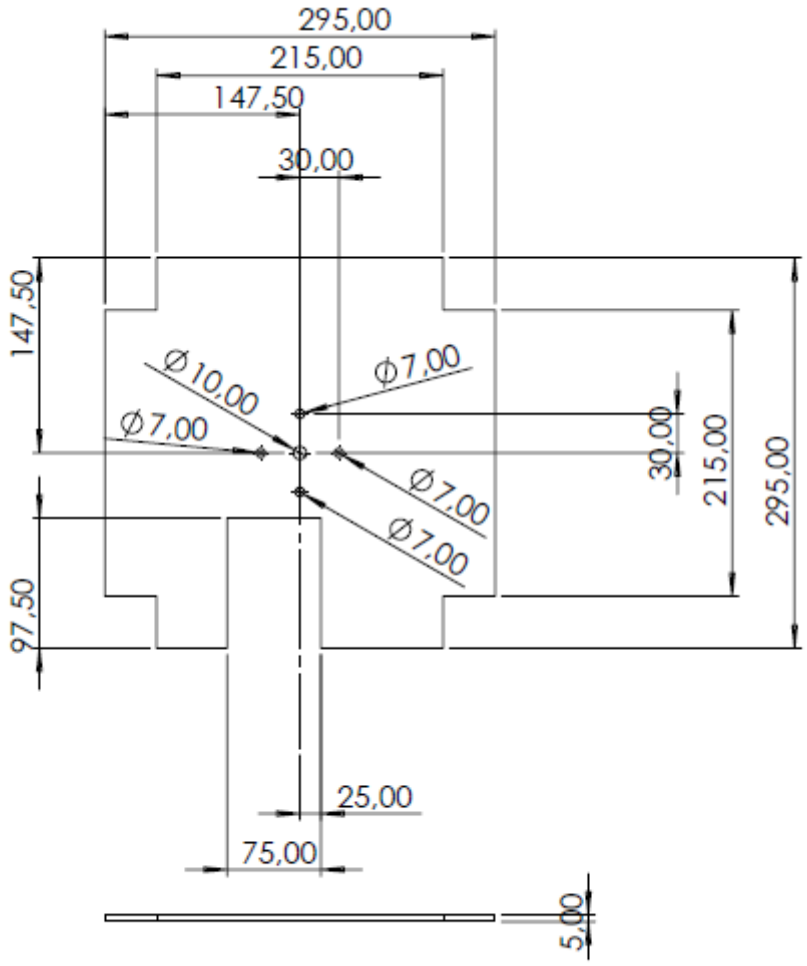

Figure A. 3 Lower plate

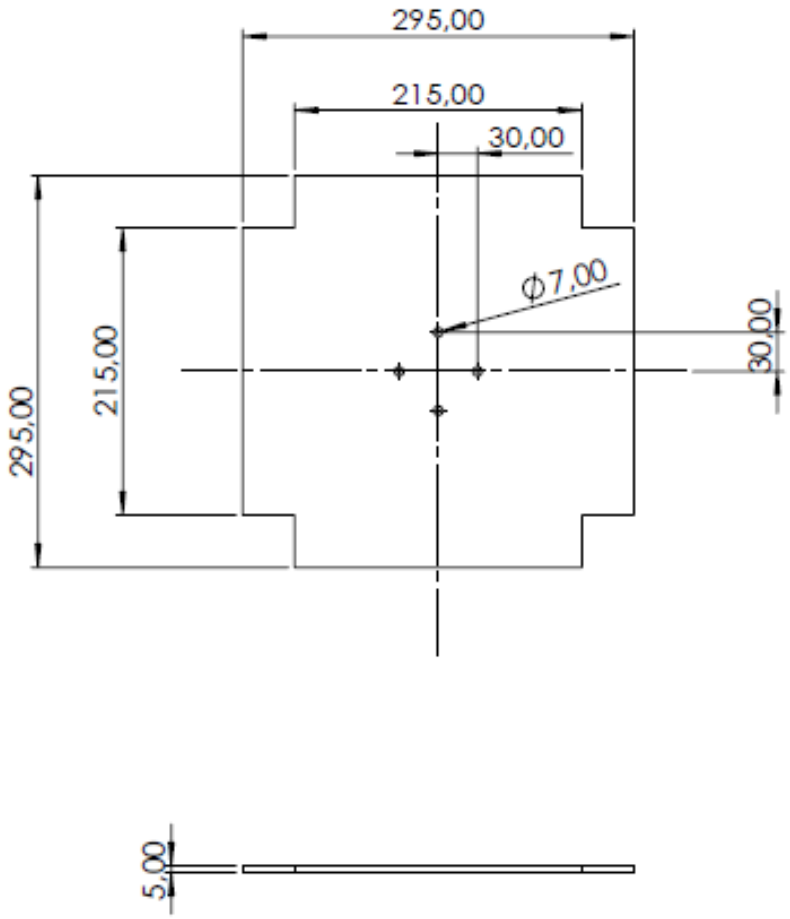

Figure A. 4 Upper plate

B Appendix B: Purchased components

Figure B. 1 Mandrel ER-11

Figure B. 2 Collet spring

List of Figures

List of Tables